Max-Planck-Institut für Biochemie
Abteilung Membran- und Neurophysik

Towards Defined Networks: Guided Growth, Cable Transmission and Electrical Synapses of Cultured Snail Neurons

Astrid A. Prinz

Vollständiger Abdruck der von der Fakultät für Physik der Technischen Universität München zur Erlangung des akademischen Grades eines

Doktors der Naturwissenschaften

genehmigten Dissertation.

Vorsitzender:		Univ.-Prof. Dr. Erich Sackmann
Prüfer der Dissertation:	1.	Hon.-Prof. Dr. Peter Fromherz
	2.	Univ.-Prof. Dr. Paul Tavan, Ludwig-Maximilians-Universität München

Die Dissertation wurde am 11.05.2000 bei der Technischen Universität München eingereicht und durch die Fakultät für Physik am 04.07.2000 angenommen.

Table of contents

1
Introduction

This introductory chapter discusses the motivation for designing geometrically simple neural networks in cell culture and states why nerve cells from the snail *Lymnaea stagnalis* are suitable for this purpose. It also briefly outlines the contents of the other chapters.

1.1 Why design networks of nerve cells?

Brains are very complex structures: They contain, depending on the species, from a few hundred up to 10^{10} nerve cells that can each be connected to as many as 10^3 other neurons via synapses located on different parts of their often extensively arborized cell surface [97]. This highly entangled mesh of cells, together with incoming information about the environment conveyed by sensory cells, gives rise to an ever changing pattern of electrical activity that is thought to be the basis of all brain function, from the processing of sensory information and the activation of muscles to higher functions such as storing and retrieval of memories, planning, emotions and consciousness.

This enormous complexity, while making brains such fascinating organs, also complicates their study on all levels of investigation. Especially on the level of small groups of neurons, the way in which intracellular and intercellular signal processing combine to transform incoming spike trains into outgoing spatiotemporal patterns of activity is difficult to study in the tissue itself. This is because

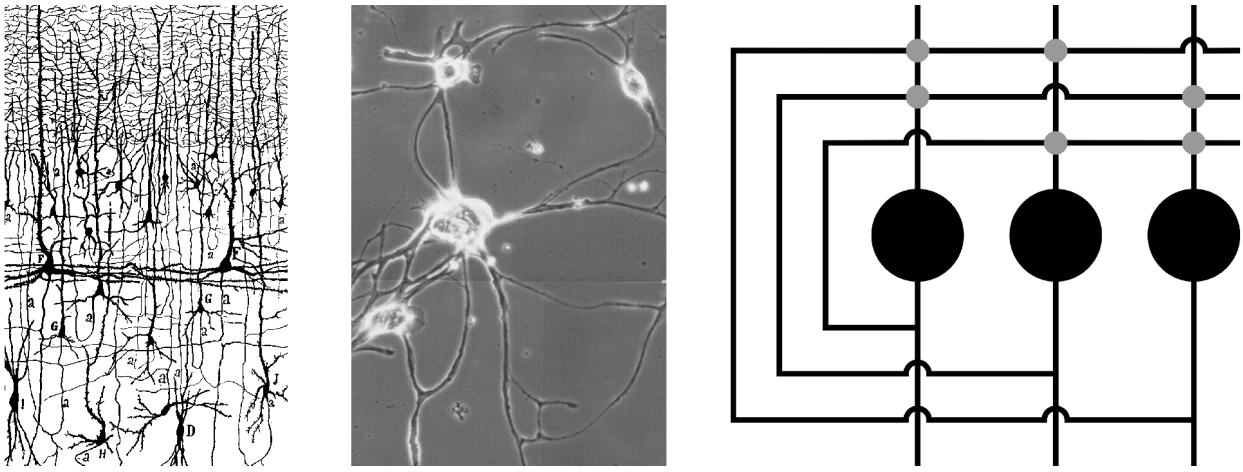

Figure 1.1: ***Neural networks of different complexity.*** *(**Left**) This drawing of a piece of human visual cortex shows only a small percentage of the cells in the tissue. The neurons are not well accessible and highly branched. From* [13]. *(**Middle**) Snail neurons in conventional cell culture. On the 2D-surface of the culture dish, all neurons are accessible, but the network still is rather complex. (**Right**) Schema of an ideal designed network with highly ordered neurites and synapses (indicated by grey dots) at known and predefined locations.*

Figure 1.2: ***The pond snail Lymnaea stagnalis*** *is a freshwater-snail found in ponds all over Europe. The shells can get as long as 7cm, but snails used here mostly had shell lengths of around 3cm. From* [17].

- most cells are not readily accessible for recordings of electrical activity
- if they are, the membrane voltage can often be monitored only at the soma, but not in the neurites
- interactions with neurons not belonging to the group in question interfere with the in-group processes to be studied
- the cells have complex morphologies that are often not known in detail
- the location and the properties of synapses between the cells are not known
- synapses can be very numerous

The first three problems can be (and have been) overcome using conventional cell culture techniques that make the neurons in a network more accessible simply by forcing them to adhere to the two-dimensional culture substrate and that can limit the interactions with surrounding cells by reducing the cell density as compared to brain tissue. These techniques have been used to study single cells or groups of cells that often can reestablish synaptic contacts *in vitro* – if cells can be identified and isolated from the donor brain individually, one can even reconstruct functional units like central pattern generators in cell culture [7][84]. But neurons cultured with conventional techniques still suffer from the last three complications listed above: They, too, display complex and often unknown morphology and connectivity (see fig. 1.1).

The aim of neural network design is to further reduce this complexity by assembling networks of simple geometry from nerve cells with well-known biophysical properties, connected at specific points by synapses of known strength. By reducing the number of unknown variables on the subcellular as well as on the intercellular level, such networks will allow a better understanding of the way in which intrinsic properties of neurons combine with their connectivity to perform the complex processing that even small networks can accomplish.

1.2 Why *Lymnaea* neurons?

While functional units in vertebrate brains can sometimes consist of many nerve cells, the brains

of invertebrates often perform rather difficult tasks with only a few neurons. **Simple networks of neurons from invertebrates are therefore likely to reveal some of the principles of signal processing in smaller brains.**

A more pragmatic reason for choosing invertebrate neurons for the assembly of defined networks is their size: The **cell diameters of sometimes more than 100μm** (as compared to about 10μm for many vertebrate neurons) facilitate the identification, isolation and positioning of individual nerve cells at specific locations in the culture dish and make the cells easy to contact electrically.

The pond snail *Lymnaea stagnalis* (see fig. 1.2) was chosen as the donor for the neurons used in this study because conventional cell culture techniques already exist for this species [76][83][96] and because *Lymnaea* neurons that are connected *in vivo* are known to reestablish their synaptic connections *in vitro* quite reliably [18][61][62][81][84]. In addition, the A-clusters (see fig. 2.1) in the paired pedal ganglia of *Lymnaea* – two groups of motoneurons innervating the cilia on the snail's foot – together contain about 60 electrophysiologically similar cells [79] that are connected *in vivo* by electrical synapses [56] and that therefore allow the reconstruction of synaptic connections *in vitro* with a **high yield of synapses per snail preparation.**

1.3 Outline of this work

For the design of neural networks in cell culture (as motivated in this chapter) and the determination of the biophysical properties of their components, one needs a **cell culture technique** that allows the guidance of neurites along specified lanes on the substrate and a **way to monitor the membrane potential** at the cell soma as well as in the neurites. These methods are introduced in chapters 2 and 3.

If we want to characterize the electrical properties of the neurons that make up designed networks, we first need a **theoretical model for a single neuron** that allows us to specify what we mean by 'electrical properties'. Two such models – a passive and an active one – are discussed in chapter 4; for the passive model (which will be predominantly used here), expressions for the electrical responses of a neuron to different stimuli are derived in the same chapter.

These expressions are then, in chapter 5, used to extract the **electrical parameters describing single neurons** from experimental data.

Once the properties of the neurons themselves are known, we can proceed to the electrical synapses connecting them: Two **theoretical models for electrically coupled cell pairs** are introduced in chapter 6, and for both models, equations are derived that allow the determination of **synapse strengths** from current step experiments. Such experiments on pairs of neurons are then described in chapter 7, and the implications of the results for the design of simple neural networks are discussed.

Finally, chapter 8 summarizes all results.

Several experimental recipes and lengthy theoretical derivations have been outsourced to appendices.

2
Cell culture

The first two sections of this chapter describe the isolation and conventional cell culture of nerve cells from *Lymnaea stagnalis*. Section 2.3 then introduces a method for guiding the outgrowth of neurons *in vitro*, and the last section discusses synapse formation of snail neurons in the culture dish.

2.1 Isolation of neurons from *Lymnaea stagnalis*

Neural network design in culture crucially depends on the vitality of the cells used as raw material and on their ability to grow new processes *in vitro*. Therefore, the aim of the neuron isolation procedure is the separation of the neural cell bodies from their *in vivo* processes and from other surrounding tissue with a minimum of cell damage and under sterile conditions. The technique used to achieve this for *Lymnaea* neurons was developed by Ridgway et al. [76] and was applied here with only minor variations. While the most important steps of the preparation are listed below, details such as recipes for salines and culture media are described in appendix A.

The first part of the preparation is the **isolation of the central ganglionic ring from the snail**:

- A snail (see fig. 1.2) is selected from a laboratory stock (derived from a local pond, kept in tap water at room temperature and fed on lettuce). The snails used in this study mostly had shells of about 3cm length, corresponding to an age of roughly four months [76].
- After deshelling, the snail is soaked for 5min in an antibacterial solution[1] to remove contaminations from the body surface and achieve a slight anesthesia.
- The animal is then pinned to the silicone rubber (RTV615, General Electric) base of a dissection dish containing antibiotic saline[1], an incision is made along the dorsal surface and the body walls and internal organs are pinned aside to expose the brain. Fig. 2.1 shows the snail at this stage of the preparation.
- The now accessible brain is opened by cutting the cerebral commissure and is separated from the esophagus. After cutting all nerves connecting the ganglia to the body, the central ganglionic ring is removed from the animal.

In the second part of the procedure, **individual cells are isolated from the brain**:

- The ganglionic ring is pinned to a small rubber-coated dish in antibiotic saline[1], again with the dorsal side up.
- The outer connective tissue surrounding the ganglia is removed with forceps and the brain is incubated in antibiotic saline[1] for 15min to reduce contaminations. A drawing of the brain at this stage is shown in fig. 2.1.
- Then, the saline is replaced by an enzyme cocktail[1] to partly dissolve the extracellular matrix between the cells and thus facilitate the isolation of individual cells from the ganglia. The

[1] See appendix A for details.

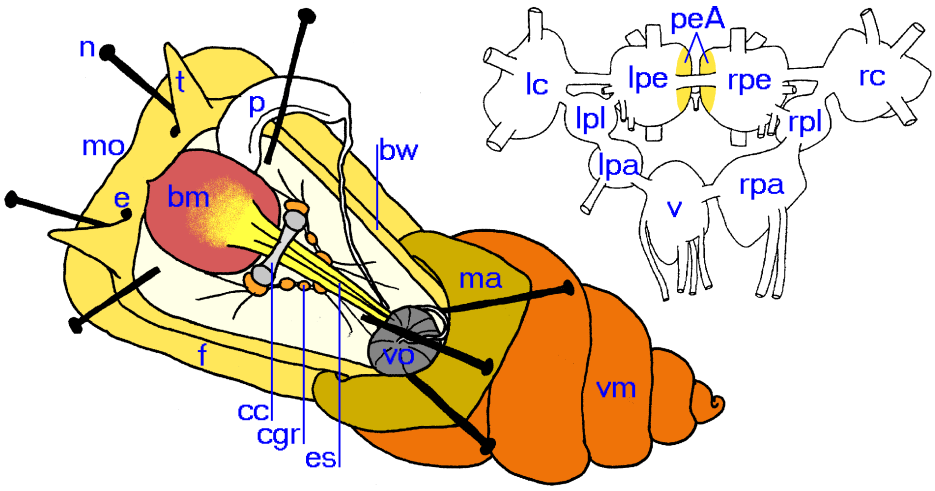

Figure 2.1: ***Anatomy of Lymnaea stagnalis.*** *(**Left**) Dorsal view of the snail during preparation. Body wall and visceral organs are pinned aside to gain access to the brain. n = needle. t = tentacle. p = penis. bw = body wall. ma = mantle. vm = visceral mass (deshelled). vo = visceral organs (pinned aside). es = esophagus. cgr = central ganglionic ring. cc = cerebral commissure. f = foot. bm = buccal mass. e = eye. mo = mouth. The buccal and pedal ganglia are hidden below the esophagus at this stage of the preparation. (**Right**) Dorsal view of the central ganglionic ring with the buccal ganglia omitted. Anterior is up. peA = A-clusters of the pedal ganglia (shown in yellow). lpe and rpe = left and right pedal ganglia. lc and rc = left and right cerebral ganglia. lpl and rpl = left and right pleural ganglia. lpa and rpa = left and right parietal ganglia. v = visceral ganglion. Adapted from* [84].

brains are incubated in this cocktail for 30-35min.

- After enzyme treatment, the ganglionic ring is washed three times with defined medium[1] and incubated for 15min with trypsin inhibitor[1], then washed again three times with defined medium[1].
- The defined medium is replaced by high osmolarity medium[1] and the connective tissue covering the paired pedal ganglia is opened with microneedles.
- Individual neurons are removed from the A-clusters in the pedal ganglia (that can be identified based on their position in the ganglion and yellow cell color) by aspiration through a firepolished and siliconized micro-pipette[1].

Immediately after isolation from the ganglion, the neurons are transferred to the culture dish and placed in their destined position on the substrate.

With some practice, this procedure allows the extraction of around 20 viable cells from each ganglionic ring, so usually several brains were processed in parallel to achieve higher cell numbers per preparation.

2.2 Conventional cell culture

To grow neurites in the culture dish, cells isolated from *Lymnaea* brains need an adhesive substrate, a cell culture medium that supplies them with all the substances necessary for survival and additional growth promoting factors [76][83][96].

The adhesive substrate is provided by cleaned glass coverslips coated with polylysine, a coating that is adhesive for cell membranes presumably because of its high charge density [51] – for the cleaning and coating procedures see appendix A. The coated coverslips are attached to specially

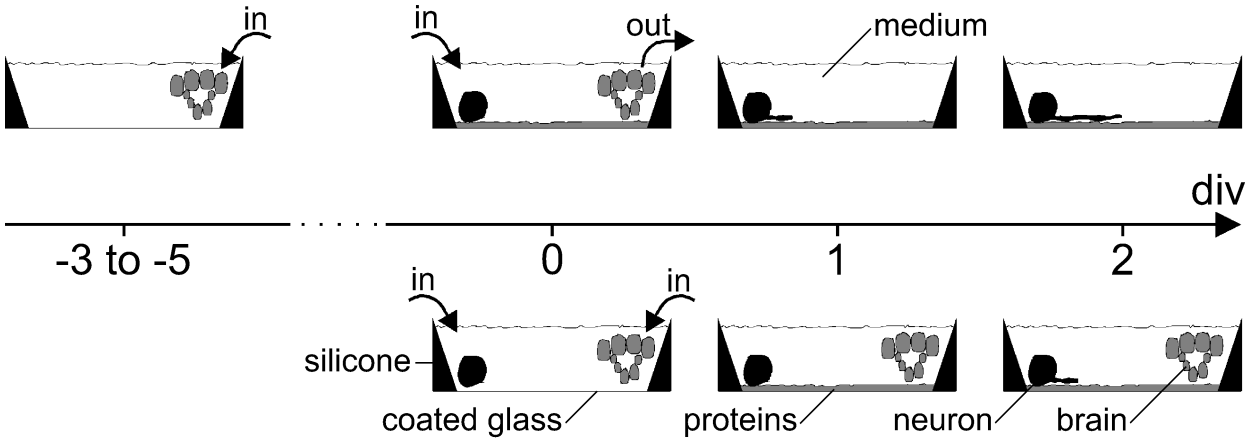

Figure 2.2: ***Pre-conditioned chamber versus co-culture.*** *This diagram compares cell culture in a pre-conditioned chamber (**top**) and in co-culture (**bottom**). In both cases, the chamber consists of a polylysine-coated glass coverslip attached to a silicone chamber and filled with defined medium. For pre-conditioning, brains are added to the chamber 3-5 days before the cells are positioned - the cells encountered a layer of conditioning factors when they are placed in the dish. In contrast, for a co-culture the cells and brains are added to the dish at the same time. Under co-culture conditions, neurite outgrowth is delayed by about a day with respect to cells growing in pre-conditioned chambers and the protein layer can not be patterned as described in section 2.3 because it is not there when the cell culture is started. div = days in vitro. Not drawn to scale.*

manufactured silicone chambers (flexiPERM, In Vitro Systems & Services, Osterode) to complete the culture dishes.

The defined medium, which is used during cell isolation and described in appendix A, is sufficient to keep the snail neurons alive for several days, and cells cultured in this medium exhibit normal resting potentials and action potentials, but they do not extend new processes [76]. To promote outgrowth, the culture medium has to be supplemented with nerve growth factor [76] or conditioned with *Lymnaea* brain tissue [96] either before or during the culture period. The exact nature of the **growth promoting factors** secreted by *Lymnaea* brain tissue during conditioning has not been determined, but similar conditioning factors secreted by brains of the closely related snail species *Helisoma* are of proteinaceous nature [94]. In view of the fact that the two species are so similar that *Lymnaea* conditioning factors can promote the outgrowth of *Helisoma* neurites [96] and that neurons from the two species can form trans-species synapses in mixed cultures [85], this is likely to be true for *Lymnaea* conditioning factors, too.

In addition, most of these growth promoting factors are known to adhere to the polylysine-coated bottom of the culture dish [95]. Modifying an existing protocol for the conditioning of culture medium with snail brains [95], this was exploited to **pre-condition the whole culture dish** (see fig. 2.2) in the following manner:

- Central ganglionic rings were isolated from pond snails as described in section 2.1.
- The brains were incubated in antibiotic saline (see appendix A) for ten times ten minutes to reduce contaminations.
- Cell culture dishes consisting of polylysine-coated glass coverslips attached to silicone chambers were filled with 1ml of defined medium and three of the washed brains, each.

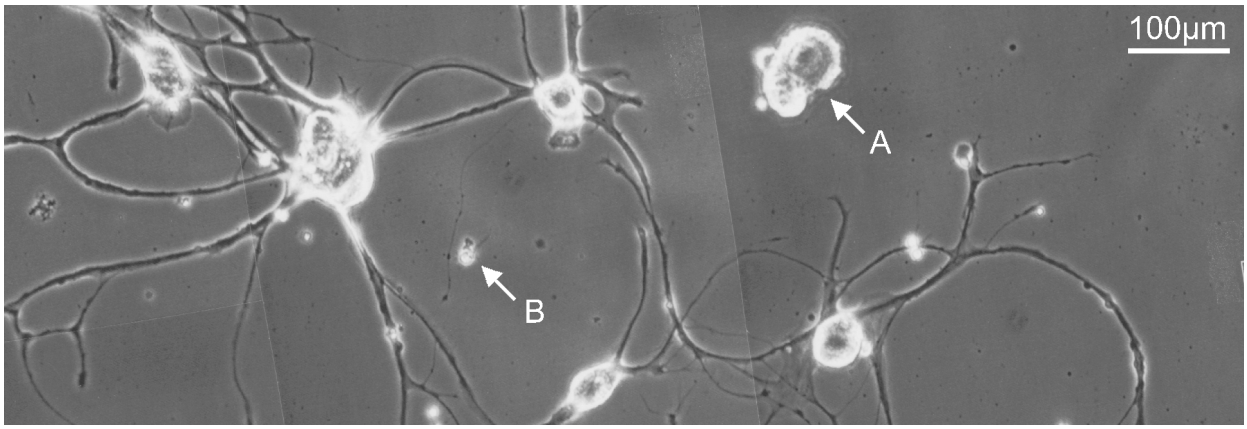

Figure 2.3: ***Neuronal outgrowth in conventional cell culture.*** *This micrograph of pedal A-cluster neurons after two days in a co-culture shows some of the typical features of co-cultures and cultures in conditioned chambers: Some cells adhere to the substrate but do not grow (A), small non-neuronal cells* [95] *appear in large amounts in the vicinity of the brains used for conditioning (not shown) and in smaller densities all over the dish (B) and the neurite diameters can be highly variable.*

- The chambers were incubated at 20°C in a humid atmosphere for three to five days.

After this incubation period, the conditioning factors adhering to the bottom of the dish formed a layer of 5-7nm thickness[2]. The ganglionic rings were removed and the medium in the now pre-conditioned chambers was either diluted in a ratio of 1:1 with defined medium or replaced by defined medium; the chambers were then ready to take up freshly isolated cells for cell culture.

Growth results on pre-conditioned substrates

Most of the neurons stably adhering to such pre-conditioned substrates and cultured at 20°C extended new neurites in all directions within a few hours and kept growing for several days until they reached a stable morphology; if neurons with one or more neurites of more than one soma diameter in length were considered to have grown [76], around **80% of the neurons adhering to the dish grew within three days in culture**[3].

Unfortunately, the proteinaceous conditioning factors adhering to the polylysine-coated glass dish – besides enabling the nerve cells to grow new processes – also reduced the adhesiveness of the substrate as compared to polylysine alone: An estimated 20% of the cells initially placed on the substrate failed to stably adhere, got washed away minutes to hours after positioning and eventually died.

An alternative: Co-culture

This loss of cells could be avoided by conditioning the culture chamber not before, but during the cells were cultured, i.e. by adding the brains for conditioning only after the neurons already stably adhered to the polylysine-coated glass [95]. Cells planted in such **co-cultures** (see fig. 2.2) adhered much better than when planted on a pre-conditioned substrate, but their outgrowth was delayed by about a day as compared to the growth in pre-conditioned chambers – presumably because the co-cultured brains require some time to release the growth-promoting factors [95]. Co-cultures like this were prepared for the experiments with randomly growing cells described in

[2] Thickness of the dried layer as measured by Günther Zeck.
[3] The total number of cells in this growth assay was n=399.

chapter 7.2, but they can not be used for guided outgrowth and network design, because growth promoting factors can only be patterned with the method introduced in section 2.3 if they are already present on the substrate *before* the cells are added. For an example of outgrowth on a homogeneous substrate, see fig. 2.3.

2.3 Simple geometry through guided outgrowth

When placed in an environment as described in the previous section, neurons grow new processes isotropically and branch or contact other cells at seemingly random positions on the dish. This outgrowth is very different from the simple geometry and defined connectivity desired for simple networks. Several approaches have been used in the past to get neurites to grow in a more ordered way and with fewer branching points, some of them using topographic guidance with pits for cell bodies and grooves for neurites [12], others relying on differential adhesion of cells and growth cones to synthetic substrates [11][51] and still others patterning physiological substrates to provide areas on the culture dish that mimic the natural environment of the cells and are separated by less bioactive areas [9][29][30][34][38].

The method introduced here (and published in [71]) falls into this latter category. It exploits the fact that the majority of the unknown growth-promoting factors secreted by snail brains during conditioning adhere to the polylysine-coated substrate [95] instead of remaining in the supernatant culture medium. This means that they are localized on the culture dish and can be selectively inactivated by lithography based on their position. The basis for this **lithographic technique** is the absorption of UV-light by proteins that can lead to a loss of biological function of the molecules.

The masks used for patterning consisted of silica plates of 1-2mm thickness coated with a thin aluminium layer into which the desired pattern was etched [29]. Because silica is transparent for UV-light and aluminium is not, UV-illumination of the substrate through these masks exposes the growth promoting factors to irradiation only where there is no aluminium, leaving the areas covered by aluminium intact.

Patterning pre-conditioned culture dishes (that were prepared as described in section 2.2) with this technique involved the following steps (see fig. 2.4):

- drying of the culture dish after removal of the conditioning brains and the supernatant medium
- positioning of the mask on the dry dish with the aluminium coating in contact with the substrate (to avoid diffraction)
- illumination of the substrate trough the mask with the full spectrum of a 200W mercury lamp (Osram HBO 200, intensity of the 366nm-line around 170mW/cm^2) for 20min
- removal of the mask and rinsing of the exposed substrate with defined medium to remove protein fragments from the exposed areas
- refilling of the chamber with the supernatant medium and defined medium in a ratio of 1:1 or with defined medium only

Growth results on patterned substrates

Of all neurons initially positioned on such patterned substrates, the percentages of cells that stably adhered and of cells that grew processes were about the same as for homogeneous pre-conditioned

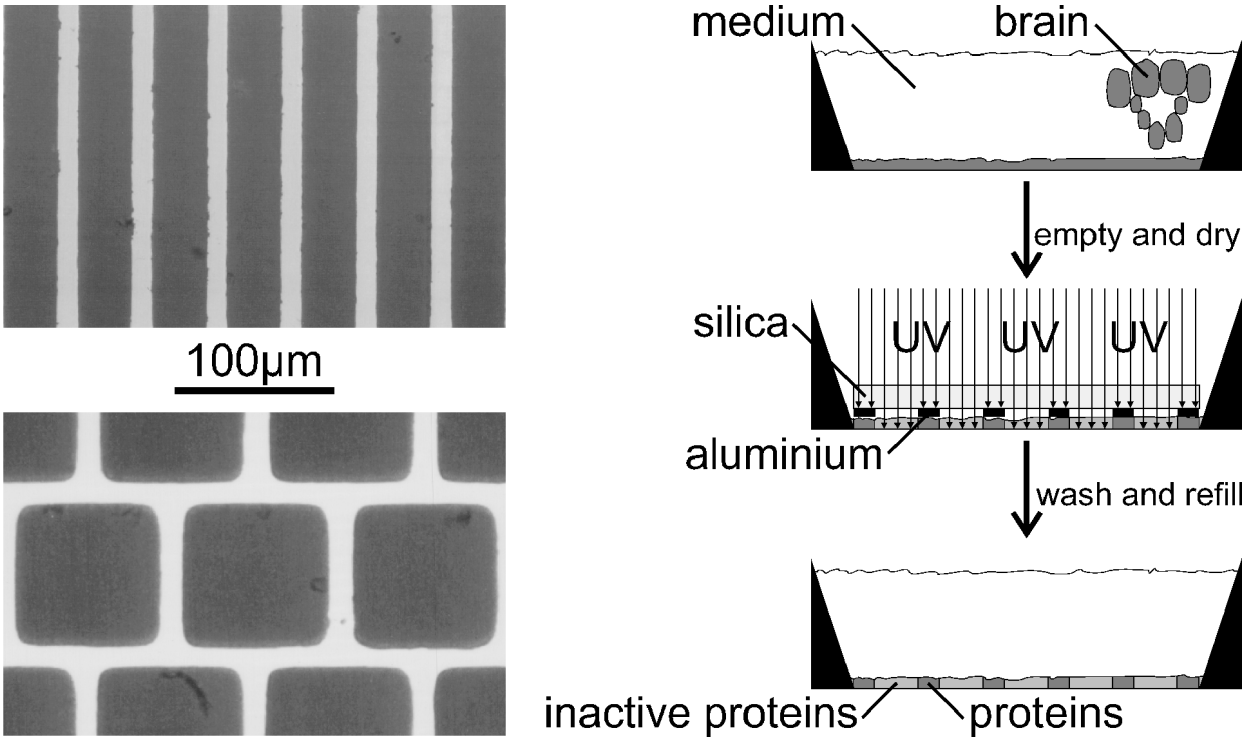

Figure 2.4: ***Substrate patterning.*** *(**Left**) Reflection micrographs of the two masks used for patterning the pre-conditioned chambers. The aluminium lanes appear bright against the dark silica background. Lane widths are 14μm for the linear pattern (**top**) and 16μm for the brick wall pattern (**bottom**). (**Right**) Patterning procedure. Brains and medium are removed from pre-conditioned chambers. The dried dishes are illuminated with UV-light through the mask, then washed with medium and refilled. The conditioning factors become inactivated wherever they are exposed to UV-irradiation.*

substrates (see section 2.2). The newly extended **neurites followed the lanes of undamaged substrate, but guidance was not perfect** (see fig. 2.5): After one day in culture, about 20% of the neurons had at least one neurite that crossed the areas of inactivated substrate, and many of the neurites that faithfully followed the lanes during the first day in culture started to deviate from the desired pattern at later stages of growth – a development that may be due to new growth promoting factors secreted by the cultured neurons themselves during cell culture [40]. Luckily, this dramatic decrease of compliance to the pattern after more than two days in culture is not a problem for the design of simple neural networks, because the growth rate of the neurons is high enough to reach neurite lengths of up to 1mm after the first day in culture, such that simple neural networks can be assembled and studied within one day.

Cells growing on the brick wall pattern shown in fig. 2.4 show an additional kind of deviation from the pattern that is well-known from other attempts to guide neurites around corners [29][30]: While the growth cones stay on the lanes of intact substrates, they seem to pull their neurites from the pattern onto areas of inactivated protein as if to minimize neurite length. fig. 2.6 illustrates this and also shows that the newly extended neurites do not necessarily branch at every branching point of the protein lanes they encounter – another fact that will have to be taken into account when designing masks for neural networks of controlled geometry.

Taken together, these results show that the **outgrowth of *Lymnaea* neurons in cell culture can be guided by patterns of growth promoting factors** produced with photolithography. The

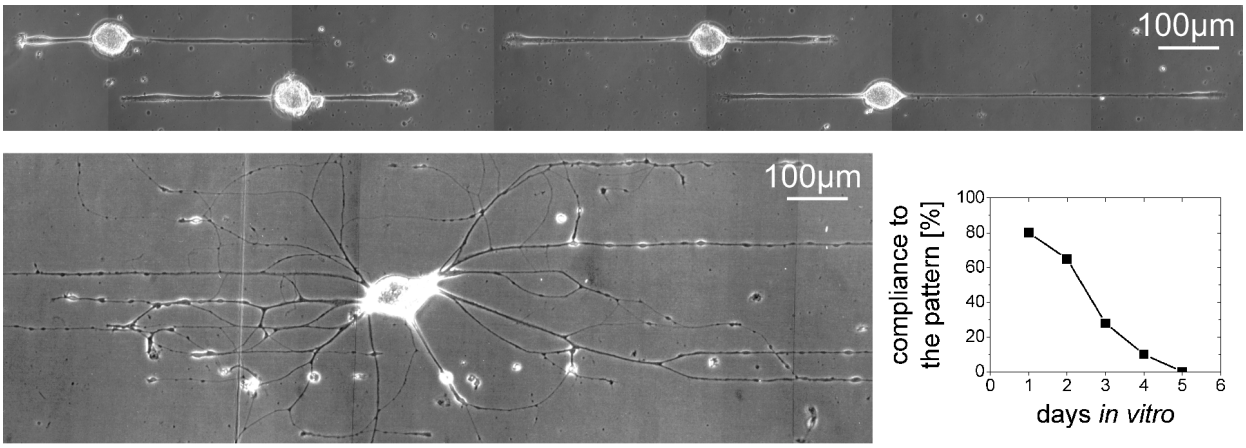

Figure 2.5: ***Outgrowth on linearly patterned substrate.*** *(**Top**) Neurons positioned on a linearly patterned substrate after one day in culture. At this stage, most neurons extended neurites exclusively along the lanes of intact proteins. (**Bottom left**) Cell on the same kind of substrate after three days in culture. While this particular cell was an extreme example of non-compliance, most cells at this stage displayed one or several neurites that deviated from the linear pattern. (**Bottom right**) Percentage of cells without any deviations from the pattern, plotted against the cell culture duration. While most cells faithfully followed the pattern during the first day in vitro, the degree of compliance dropped dramatically after about two days, and after five days in culture all cells deviated from the pattern with at least one of their neurites. The overall cell count in this assay was $n = 312$.*

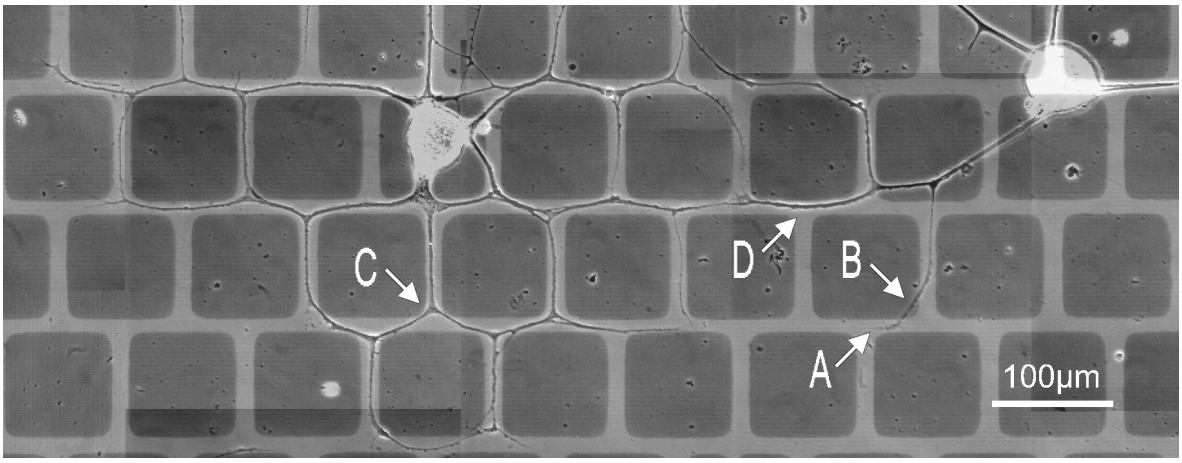

Figure 2.6: ***Guided growth on a brick wall pattern.*** *Pedal A-cluster neurons positioned on a brick wall pattern after one day in culture. To illustrate deviations from the pattern, a micrograph of the cells was superimposed with an image of the mask. While the growth cones mostly follow the lanes of intact protein (A), the neurites are often dislocated from the lanes (B), apparently to minimize neurite length. Similarly, branching points seem to be pulled from their original position (C). Neurite branchings occur at most, but not all of the lane branchings that the growth cones encounter (D).*

guidance is not perfect, but the results presented in chapter 7 suggest that it is good enough for the study of small designed networks with simple geometry in cell culture.

2.4 Synapse formation in cell culture

A culture environment supporting neurite outgrowth is not necessarily sufficient for synapse for-

mation [83], but neurons from the pond snail have been reported to form synapses when cultured in medium conditioned with brain tissue [18][61][62][81][84]. In those studies, a strong **specificity of synapse formation** was found: *Lymnaea* neurons formed synapses in cell culture only with cells they are connected to *in vivo*, and the newly established connections always were of the appropriate kind and transmitter type. This is in contrast to findings from other mollusk species: Neurons from *Helisoma* [36][37] or *Aplysia* [52] can occasionally form connections *in vitro* that are not present in the animal, and the kind of synapse formed between *Aplysia* neurons even depends on the culture substrate [59].

As mentioned in section 1.2, the specificity of synapse formation in culture observed for *Lymnaea stagnalis* was one of the reasons for choosing the A-clusters in the paired pedal ganglia as a source for neurons that can be expected to reestablish synapses in culture with high yield because they are connected *in vivo* by electrical synapses.

Chapter 7 will demonstrate that A-cluster neurons cultured on both homogeneous substrates and patterned substrates as described above fulfil this expectation, thus **information about *in vivo* connectivity can be combined with cell culture techniques to achieve *in vitro* synapse formation** with sufficient yield for neural network design.

3
Measuring voltage with electrodes and dyes

The primary signal in a nerve cell is the membrane voltage, and the standard technique to monitor and manipulate it at the cell body with an intracellular microelectrode is briefly described in section 3.1. As will become apparent in section 4.2, however, electrode measurements at the soma are not sufficient for characterizing the electrical properties of the neuritic cables attached to the cell body. Therefore, we need information about the membrane voltage not only at the cell body, but with **high spatial resolution throughout the nerve cell**. Section 3.2 describes how this information can be obtained by using **voltage-sensitive dyes as molecular probes of membrane voltage**.

3.1 Electrophysiology

A common way to monitor and manipulate the membrane potential of neurons – at least at the cell body – is to **impale the cell with a microelectrode** that allows the measurement of the trans-membrane voltage and the injection of current into the cell. Fig. 3.1 shows a schema of the setup used to simultaneously monitor and manipulate the currents and voltages in two neurons.

The microelectrodes used here consisted of borosilicate glass capillaries (inner ∅ 0.58mm, outer ∅ 1.00mm, Hilgenberg, Malsfeld) that were pulled to sub-micron tip diameters with an electrode puller (DMZ Universal Puller, Zeitz, Augsburg), filled with a saturated solution of potassium sulfate and contacted with a chlorinated silver wire. These electrodes had resistances of 10-40MΩ and were mounted on a micro-manipulator (a 'patchman' from eppendorf, Köln) for exact positioning in the cell body. The surrounding medium was held at ground with a chlorinated silver wire.

The intracellular electrodes were connected to electrode amplifiers (SEC-05L, npi, Tamm) via headstages; these amplifiers (by employing a discontinuous mode of current injection to minimize errors in the voltage measurements due to the high series resistances of the electrodes) allowed the injection of currents into the cells and the monitoring of the membrane potentials and supported current clamp and voltage clamp, meaning that it was possible to hold either the injected current or the membrane potential at a constant value for each cell. For details of the amplifier's circuitry and a discussion of discontinuous current injection see [67].

The command currents or voltages applied to the cells were controlled by a home-made computer program[4] written in LabView (National Instruments, Austin, Texas) via a 12-bit data acquisition interface card (AT-MIO-16E-2, again from National Instruments) that was also used for digitizing the measured membrane currents and voltages supplied by the amplifiers with sampling rates of

[4] Most of the software was written by Martin Jenkner.

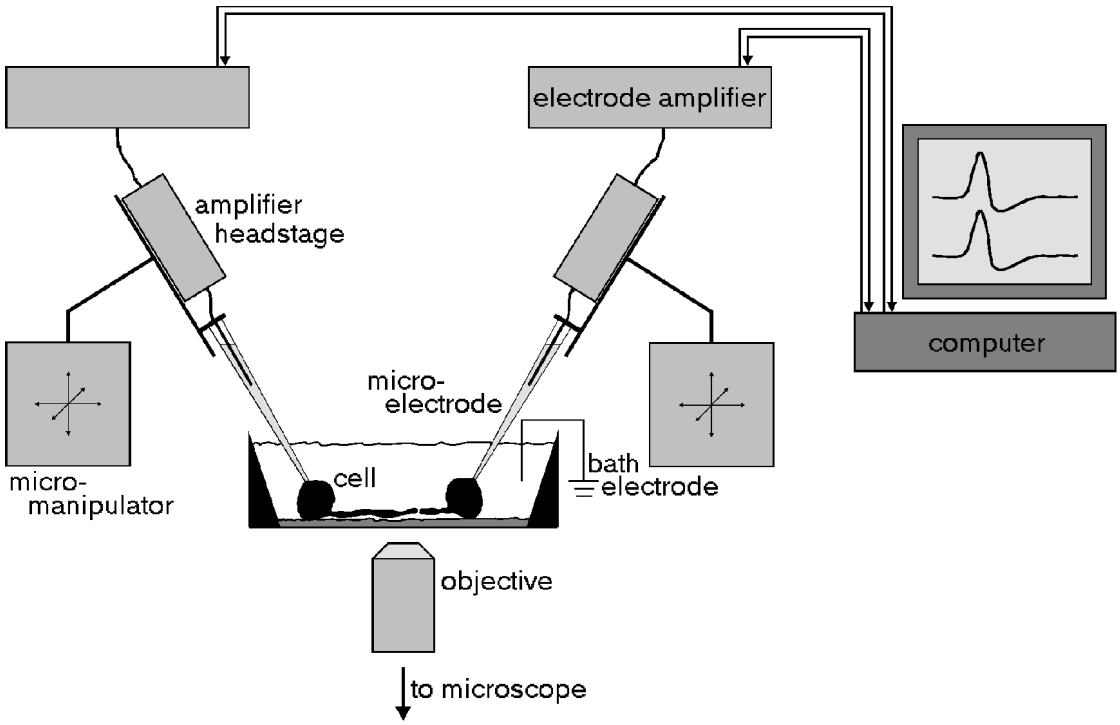

Figure 3.1: ***Schematic drawing of the electrophysiology setup.*** *This schema shows the setup used for manipulating and recording the membrane voltages and currents of two neurons simultaneously. The cells were impaled with micro-electrodes consisting of K_2SO_4-filled glass capillaries that were contacted with chlorinated silver wires. The electrodes were connected to two electrode amplifiers via headstages; electrodes as well as headstages were mounted on micro-manipulators for accurate positioning. A computer was connected to the amplifiers to either current clamp or voltage clamp the cells by controlling the currents injected into the neurons and recording the amplifier outputs. The chamber containing the cells, the electrode holders and the headstages were mounted on the stage of an inverted microscope (not shown).*

10kHz or higher.

3.2 Imaging of signal propagation

3.2.1 Voltage-sensitive dyes as probes of membrane potential

The information provided by electrodes about the voltage distribution in a neuron is limited to the cell body or to (at most) two or three locations in the cell. But neurons, due to their highly elongated processes, are usually not isopotential, and thus much of the signal processing going on in the neurites remains unknown if electrical activity is recorded only from the cell body.

Much higher spatial resolution – in some applications down to 20μm or better [26][31][48][65][70] – can be achieved if **voltage-sensitive dyes** are used as **molecular probes of membrane potential** changes all along the neurites. These fluorescent molecules, upon absorption of a photon of suitable wavelength, make a transition to an excited state that is accompanied by a charge shift in the molecule (see fig. 3.2). The energy required for this charge shift depends on the component of the local electrical field parallel to the direction of the charge translocation and thus

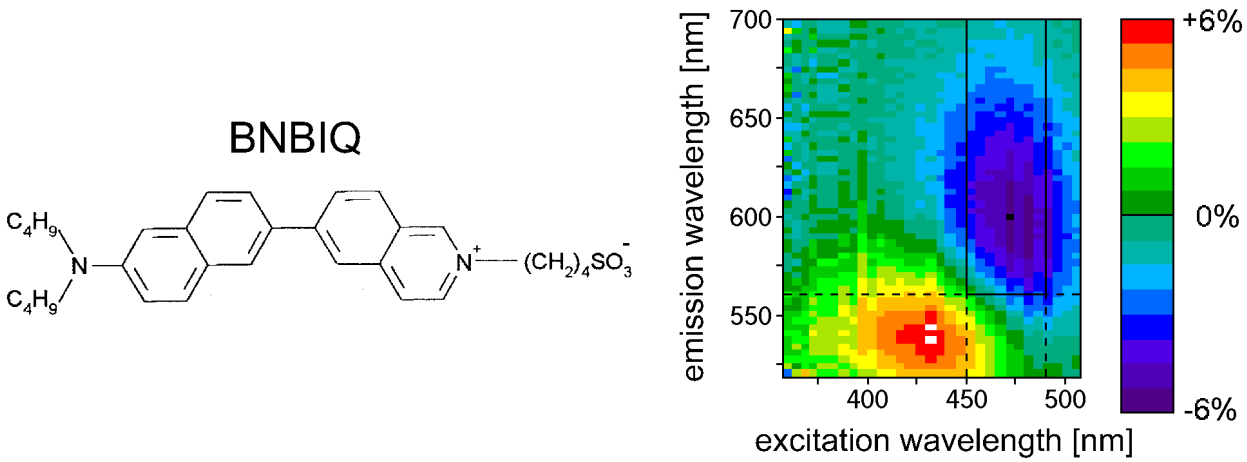

Figure 3.2: ***Structure and fluorescence-change spectrum of the voltage-sensitive dye BNBIQ.*** *(**Left**) The molecular structure of the dye BNBIQ. Upon excitation, positive charge is shifted from pyridinium to aniline (from right to left in the figure)* [16][23]. *(**Right**) Change in fluorescence intensity of BNBIQ in neuronal membrane (of the leech) when the membrane potential is depolarized by 100mV. The color-coded fluorescence change is expressed in % of the maximum fluorescence intensity before depolarization and plotted against excitation and emission wavelength (from* [55]*). With the apparatus described in section 3.2.2, the wavelength ranges used for excitation and detection were limited by a band pass filter (450-490nm) and a long pass filter (560nm); this range is indicated by black lines in the plot.*

couples the absorption spectrum (and by a similar mechanism also the emission spectrum) of the dye molecules located at the cell surface to the momentary membrane voltage. In addition to this electrochromism, the two spectra are shaped by solvatochromic effects: Electrical field changes can influence the polarity of the dye molecule's local environment – and therefore the contribution of solvation energy to the spectrum – by changing the position of the chromophores relative to the membrane [16][23][24].

Due to these two effects, the absorption spectrum and the emission spectrum of dye located at the neural membrane depend on the trans-membrane voltage (see fig. 3.2), and if suitable excitation and detection wavelength ranges are chosen, this dependence results in a fluorescence intensity whose change is directly proportional to any change in membrane potential in the physiologically relevant range [25]. The optical detection of these fluorescence changes with high spatial resolution on a neuron's processes therefore allows the **monitoring of voltage changes as they are occurring during signal propagation along the neurite**.

Staining cells with voltage-sensitive dyes

When voltage-sensitive dyes are to act as probes for neural signaling, they have to be brought into the cell membrane. The amphiphilic nature of the dyes – a hydrophilic head group with hydrophobic tails – favors their localization at the lipid-water interface, but it also makes the dye hard to solubilize in the culture medium that it has to pass through to get to the cell in the first place.

For the particular dye used here, BNBIQ (see fig. 3.2), this was overcome by dissolving the dye in a solution of cholic acid in defined medium[5]. In this solution, the cholic acid forms micelles that can host the dye molecules. When the concentration of the cholic acid drops below a critical

[5] See appendix B for a recipe of the dye solution and the staining procedure.

value – as it does when the solution is added to the culture chamber containing the cells and the medium[5] – the micelles fall apart and the dye molecules are free and can stick to any hydrophilic-hydrophobic interface they encounter in the dish, among others the cell membrane.

Toxicity

The high spatial resolution that can be achieved in measurements with voltage-sensitive dyes is the major advantage of this technique as compared to electrode recordings. But a price has to be paid for this: The **dyes are phototoxic** and – when used in the concentrations necessary to achieve good signal-to-noise ratios in measurements with subcellular resolution and no signal averaging – irreversibly damage the cells within a few seconds of exposure to excitation light [26][31][65]. This damage can be detected electrophysiologically and from changes in the neuron's morphology: The resting potential gradually decreases in magnitude, the action potentials become broader and decrease in amplitude and eventually the membrane produces bubbles and the neurites rupture.

To avoid artifacts in the measurements due to such toxic effects, only data recorded from a cell *before* any of these symptoms appeared can be trusted. Luckily, the measurement durations necessary for the determination of neuritic membrane parameters as described in section 5.2 were significantly shorter than the time scale on which toxic effects first became detectable.

3.2.2 A setup for detecting fast fluorescence changes

Voltage-sensitive dyes, when used with suitable optical filters, transform membrane potential changes into fluorescence intensity changes that are small – usually at most a few percent of the fluorescence intensity – and very fast due to the millisecond-timescale of neural voltage dynamics. Until recently, virtually all setups used for the detection of such fast fluorescence signals were based on photodiodes, and so was the detection device used here (see fig. 3.3). As it has been described in detail before [66][70], the description that follows focuses on the major components:

The chamber containing the stained cells was mounted on the stage of an inverted microscope and the neuron was contacted with an intracellular electrode connected to an electrode amplifier via a headstage just as described in section 3.1, the only difference being that the manipulator in this case was a mechanical 3-axis micromanipulator (Zeitz, Wetzlar).

The microscope was equipped with a xenon lamp whose light was passed through a shutter and a band pass filter, reflected by a beam splitter and projected onto the neuron through an objective. The fluorescent light emitted by the dye molecules in the neural membrane passed trough the same objective and beam splitter, was long pass filtered and projected onto a **linear array of 100 photodiodes** with the aid of an additional lens[6] not shown in fig. 3.3. The band pass filter, beam splitter and long pass filter were chosen to maximize the fluorescence change per voltage change; see fig. 3.2.

The output currents from the 100 diodes (that were proportional to the fluorescence intensity detected by the respective diode) were converted to voltages and preamplified individually with a time-constant of 400μs, then passed on to 100 differential sample-and-hold amplifiers. The voltage signals from those amplifiers were digitized, displayed and stored by a computer that also

[6] This lens caused a slight distortion of the image, resulting in an effective spatial resolution that varied between 5.3μm per diode at the center of the image and 3.9μm per diode at the edges. Unless stated otherwise, this distortion was always corrected for.

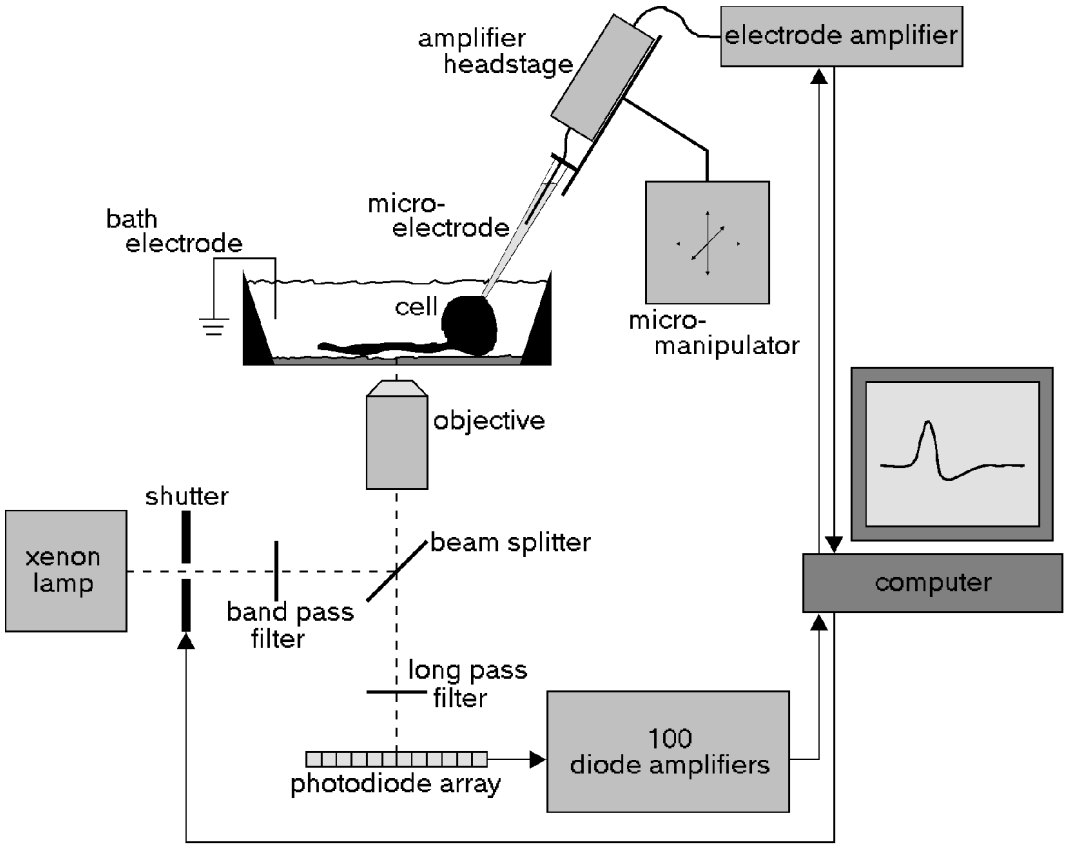

Figure 3.3: ***Setup for measuring fast fluorescence changes.*** *The fluorescence intensity changes caused by voltage transients in neurites stained with BNBIQ were detected with a linear array of 100 photodiodes. For a description of the apparatus, see text or* [66].

opened and closed the shutter and controlled and stored the current and voltage transients of the cell.

In addition to the components shown in fig. 3.3, the inverted microscope was equipped with a halogen lamp for observation of the neuron under white or (with an additional filter) red light and with a CCD-camera. Prior to the experiment, the straight neurite of the stained cell was aligned with the linear photodiode array by superimposing a red-light image of the cell with a pre-adjusted, virtual image of the diode array generated by the computer.

In all measurements, the shutter was opened by the computer only at the times of optical recording to keep the exposure time to excitation light as short as possible.

3.2.3 Signal processing

The 100 amplifier output signals stored by the computer during optical recording contain information about the voltage changes in the neurite, but to retrieve this information, the signals have to undergo some processing:

A complication is that the fluorescence intensity detected by each diode during an experiment not only changes in proportion to the voltage change in the membrane patch ‘seen’ by the diode, but in addition changes due to **dye bleaching**. These two effects have to be separated if the voltage change in the membrane is to be reconstructed. The exact mechanism and dynamics

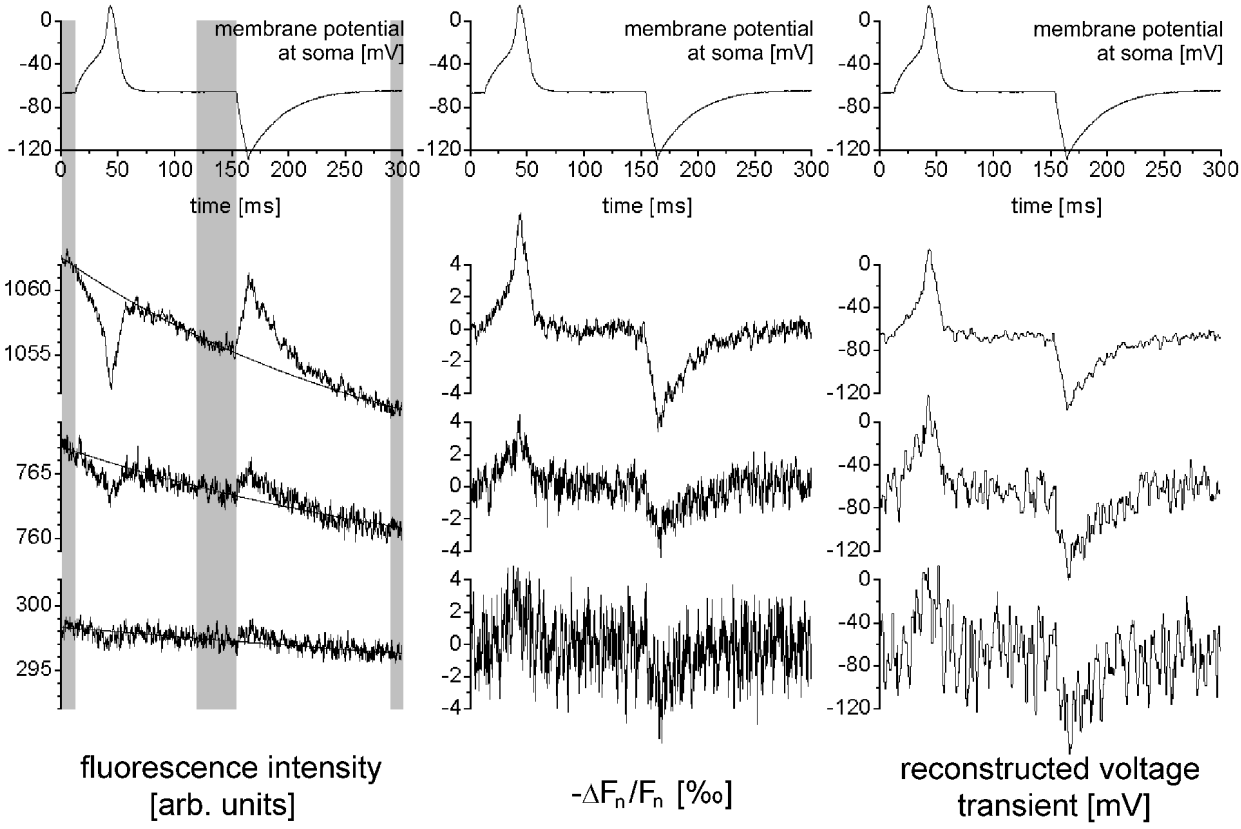

Figure 3.4: ***Reconstruction of voltage transients from measurements with voltage-sensitive dyes.*** *These plots illustrate different steps of signal processing for an exceptionally clear fluorescence signal (**second row**), an average signal (**third row**) and a very noisy signal (**bottom row**), measured at three locations on the same neurite. In the **top row**, the membrane potential at the cell body - recorded with an intracellular electrode - is plotted for comparison at each processing stage. The cell was induced to fire an action potential by depolarizing current injection and was then briefly hyperpolarized. (**Left**) Original signals and intensity baselines. The shaded areas indicate to which parts of the transients the baselines were fit. (**Middle**) Relative fluorescence changes. For these traces, the difference between original signal and baseline was inverted and divided by the baseline. (**Right**) Reconstructed voltage transients, obtained by median-filtering $-\Delta F_n/F_n$ and rescaling the resulting trace according to the assumptions of constant resting potential and action potential amplitude. For details, see text.*

of dye bleaching are not known, but fluorescence intensity transients caused by bleaching alone (without any changes in membrane voltage) can be fit quite well to a curve of the form

$$F_n(t) = F_{n,0} + F_{n,bl} e^{-\frac{t}{\tau_{n,bl}}} \tag{1}$$

where the offset intensity $F_{n,0}$, the bleaching intensity $F_{n,bl}$ and the bleaching time constant $\tau_{n,bl}$ are fit variables and are determined separately for each diode n.

For a fluorescence transient that is influenced by both bleaching *and* voltage changes, the baseline fluorescence intensity due to bleaching *alone* can be found by fitting (1) only to those parts of the transient that were recorded when the cell was at resting potential. To this end, the injection current protocol used for optical measurements was designed such that the cell was at resting potential at the beginning, in the middle, and at the end of the recording period. Three examples of such transients and fits are shown in the left column of fig. 3.4. These examples also show that the fluorescence intensity from different parts of the same neurite can vary; this is due to inhomogeneous illumination of the neurite, different areas of stained membrane in each diode's

field of view and inhomogeneous staining of the membrane. Also note that the noise amplitude is almost the same in the three traces, consistent with the finding that most of it is caused by the pre-amplifier circuitry in this particular setup [66].

The 100 intensity baselines $F_n(t)$ obtained by separately fitting the 100 original traces in this manner were then subtracted from the original signals, resulting in the fluorescence changes $\Delta F_n(t)$ caused by voltage changes alone. Because of the particular choice of optical filters used here (see section 3.2.2 and fig. 3.2), a depolarizing change in membrane voltage caused a decrease in fluorescence intensity, so $\Delta F_n(t)$ had to be inverted to obtain a signal directly comparable to the voltage signal measured by the electrode. The middle column in fig. 3.4 shows these inverted signals after division by their respective baseline $F_n(t)$. While the voltage sensitivity of BNBIQ in neuronal membrane has been found to be higher than 10% per 100mV [55], the amplitudes in these examples are around 0.5% for an action potential amplitude of 80mV – this shows that a large amount of dye contributes to the fluorescence but does not sense the voltage changes in the membrane, quite likely because it is not located at the cell surface but in the protein layer the cells grow on.

As mentioned, the fluorescence change ΔF_n is proportional to the voltage change in the membrane [25] – but the **proportionality factor is unknown** and can be different for each diode [26], so the 100 transients $\Delta F_n(t)$ alone contain no information about the amplitude of the voltage change at their respective site on the neurite. There are two alternative ways to deal with this problem, and both will be used at different points later on in this work:

Alternative I: Forget about the amplitude

Alternative I is to accept the lack of information about the *amplitude* of the transients and just use the information contained in their *shape*. This is precisely what will be done in section 5.2, where the hyperpolarized portion of each transient $-\Delta F_n(t)$ is divided by the absolute value of its minimum and thereby normalized to amplitude -1:

$$S_n^{fluo}(t) = \frac{-\Delta F_n(t)}{|\min\left[-\Delta F_n(t)\right]|} \tag{2}$$

where $\min\left[-\Delta F_n(t)\right]$ is found by averaging over an interval of several ms around the actual minimum to compensate for the relatively large noise of the fluorescence data. If the same normalization is done with the theoretical transients, these can then be fit to the experimentally obtained shapes $S_n^{fluo}(t)$ without making additional assumptions as in alternative II and thus without the risk of introducing errors in the fits due to the assumptions being not exactly fulfilled by snail neurons.

Alternative II: Make additional assumptions

In spite of the unknown factor between voltage change and fluorescence change, the voltage transient for the section of the cell projected onto diode n can be reconstructed if two additional assumptions are made:

- **The action potential propagates along the neurite with constant amplitude.** This is a reasonable approximation if the neuritic membrane has voltage-gated ion channels with dynamics similar to those of the Hodgkin-Huxley-model (see [26][32][65] and section 4.3).
- **The resting potential is the same all along the neurite.** This assumption is made by *all* models of neurons simply because no other information is available.

With these two assumptions made, each diode's transient $-\Delta F_n(t)$ can be rescaled such that its baseline-to-maximum amplitude is the same as the action potential amplitude measured with the intracellular electrode at the soma and can then be shifted such that it starts at the resting potential measured at the soma. The rightmost column in fig. 3.4 shows the three example signals after these transformations. Traces of this sort from all 100 photodiodes, if assembled in a 3D-plot, result in a **spatio-temporal map of signal propagation** along the neurite as presented in section 5.3.

4
Theory, part 1: Models of single cells

If we want to characterize the basic unit of designed networks – the neuron with unbranched neurites – by determining a number of electrophysiological parameters for the cell, we first need a model of the cell that captures its electrical behavior and allows us to specify what the relevant parameters are. This chapter introduces two such models, namely

- a **passive model** that assumes that the membrane conductance of the cell does not depend on trans-membrane voltage and
- an **active model** that includes voltage-dependent conductances.

In section 4.2, theoretical voltage and current transients for passive model cells are used to demonstrate that **it is not possible to determine all of the cell's electrical parameters from measurements at the soma alone**, implying that we need additional information from measurements of neuritic voltage transients.

4.1 Passive model: Cable theory

The development of a mathematical model for an extended neuron with uniform and passive membrane was pioneered by Wilfrid Rall around 1960 [72][73][74], and his by now classical model has been widely used to determine the electrical properties of nerve cells for many years. This section reviews his model, makes a small (but crucial) generalization and then derives expressions for voltage and current transients in cells of different geometry.

4.1.1 The model

To be able to derive differential equations for the distribution of passive electrotonic potentials in the cell, Rall made the following assumptions about the geometric and electrical properties of the neurons [72] (whose respective applicability to the neurons used here are discussed):

1.) **The neurites, between any two branching points, are cylindrical.** The neurite diameter of the cells used here is not perfectly constant along the neurites (see fig. 4.1), so this is an approximation. In principle, variations in neurite diameter could be included in the model, but as they usually are small and as including them would complicate the model a lot, this was not done here.
2.) **The electrical properties are uniform over the entire surface of the neuron.** As will be discussed later, this assumption was dropped in more recent models because of significant differences between the somatic and neuritic membrane parameters.
3.) **The electrical potential is constant over the external surface of the neuron.** This is equivalent to the assumption of infinite conductivity of the medium surrounding the cell. The error introduced by this assumption can be shown to be negligible even for a neuron embedded in tissue [72], and is all the more negligible for a cultured neuron surrounded by

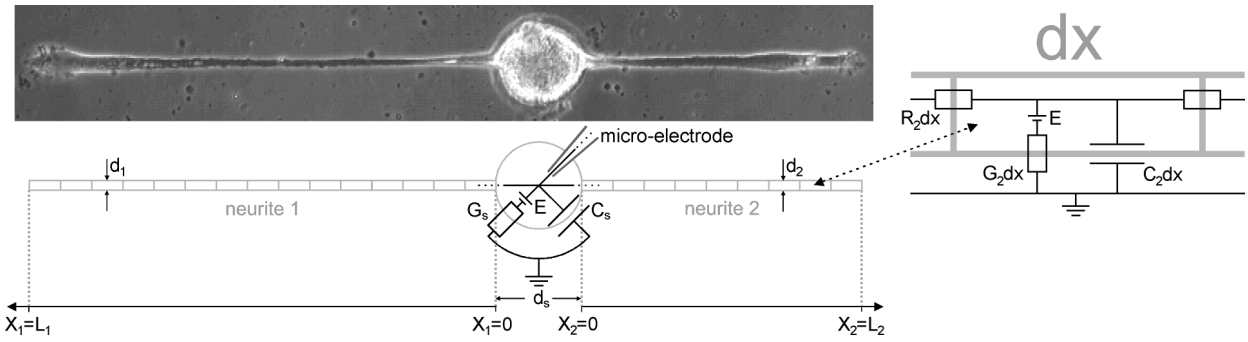

Figure 4.1: ***Equivalent circuit for a cell according to the cable model.*** *This figure shows how the geometry of a cell, together with Rall's assumptions, translates into an equivalent circuit. (**Left**) The micrograph at the top shows the cell to be modelled. The model cell at the bottom consists of a single spherical compartment for the soma (with the same diameter as the original cell body) and two cylindrical neurites with the same average diameter as the real neurites. The neurites are assembled from compartments of length dx; while dx is infinitesimal for analytical calculations, it has a finite value for numerical simulations. In this example, dx=10μm, which also provides a scalebar for the cell at the top. (**Right**) Enlarged version of an element dx. The electrical components of the model cell are explained in the text.*

highly conductive medium.

4.) **The electrical potential is constant over the internal surface of the cell body.** This amounts to the assumption of infinite conductivity of the somatic cytoplasm. For unfavorable conditions, the voltage drop across the cell body can be estimated to be up to 2% of the electrotonic potential at the soma [72] – but as dropping this assumption would mean that the electrical properties of the cell body and the electrode position would have to be modelled in detail, this assumption was unavoidable.

5.) **The internal potential and current are continuous at all points in the neuron.** That's an obvious physical requirement.

6.) **The electrical current inside any cylindrical component flows axially through an ohmic resistance which is inversely proportional to the area of cross section.** This assumes that the interior of the neurite has homogeneous specific conductivity. As the spatial distribution and electrical properties of the different materials within the neurite are not known, this is the simplest assumption one can make.

7.) **The uniformly distributed membrane impedance consists of an ohmic resistance in parallel with a capacity.** The assumption of an ohmic resistance neglects any voltage-dependence of the underlying ion channels and makes Rall's model a 'passive' model. As will be discussed in section 4.3, the neural membrane conductance is clearly *not* independent of the membrane voltage, but passive models can still be a good approximation as long as the membrane potential remains in a range where the voltage-dependence of the conductance is weak. The capacity is included to model the separation of two highly conductive compartments (the cytoplasm and the medium around the cell) by the thin and insulating lipid bilayer of the membrane.

8.) **A membrane electromotive force is in series with the membrane resistance and is constant for all of the membrane.** This 'electromotive force' is the resting potential and arises from the interplay of membrane conductances and ion concentrations (see section 4.3). Again, the assumption of a constant value for the entire membrane is made because more detailed information about the spatial distribution of ion channels and pumps is not available.

For any given neuron, this set of assumptions – together with the geometry of the cell – allows the

prediction of the time-course of voltage distributions in the cell as they arise after perturbations of the system such as current injections into the soma. This involves **four steps**, namely

- the construction of an equivalent circuit for the cell
- the derivation of a differential equation that governs the dynamics of voltage distributions in this equivalent circuit
- the specification of boundary conditions for the voltage distributions
- the solution of the differential equation for a given perturbation under these boundary conditions

and comparing these solutions to electrophysiological measurements from the real neuron can convey information about the electrical properties of the cell's membrane and cytoplasm [73].

A generalization: The somatic shunt cable model

But before we go through the four steps, we drop Rall's assumption (2) and replace it by the more general assumption that the cell body may have different membrane conductance and capacitance than the neurites. This leads to the **'somatic shunt cable model'** [14][49], which contains Rall's original model as a special case.

Initially, this generalization was motivated by the findings of several groups [15][45] that were unable to fit voltage and current transients recorded from some neurons with Rall's classical theory – a problem that could be solved by assuming that the membrane time constant at the cell body is different from that in the neurites. Often, this difference in time constants is attributed to a larger membrane conductance at the soma, thus the name 'somatic shunt cable model' [14].

The **first step** in the translation of this more general set of assumptions into predictions about voltage transients is the construction of an equivalent circuit for the cell as illustrated in fig. 4.1. There, E denotes the electromotive force from assumption (8). The somatic conductance G_s and capacity C_s are the products of the respective values g_s and c_s per unit area[7] and the somatic membrane area:

$$G_s = g_s \pi d_s^2 \qquad \text{and} \qquad C_s = c_s \pi d_s^2 \tag{3}$$

where d_s is the diameter of the cell body. Similarly, the conductance G_j and capacity C_j per unit length of neurite j are the products of the specific values g and c (per unit area) and the neuritic circumference:

$$G_j = g \pi d_j \qquad \text{and} \qquad C_j = c \pi d_j \tag{4}$$

with the neurite diameter d_j of neurite j. And finally, the ohmic resistance R_j per unit length of neurite j is obtained from the specific resistivity r of the internal medium via

$$R_j = \frac{4r}{\pi d_j^2} \tag{5}$$

As explained above, the more general somatic shunt cable model used here allows that $g_s \neq g$ and $c_s \neq c$, whereas the classical Rall model would be the special case in which $g_s = g$ and $c_s = c$ according to Rall's assumption 2.).

In a **second step**, a differential equation – the **'cable equation'** – is derived [10][43] that describes

[7] Note that the use of upper-case and lower-case letters in electrophysiology is often counter-intuitive for physicists. In the present work, specific parameters such as conductance per unit area or cytoplasmic resistivity are always denoted by lower-case letters. Corresponding symbols used by many electrophysiologists are C_M for c, R_M for $1/g$, and R_i or ρ for r.

the dynamics of voltage distributions in the neuritic cables attached to the soma. This equation is

$$\lambda_j^2 \frac{\partial^2 V^e}{\partial x_j^2} = V^e + \tau \frac{\partial V^e}{\partial t} \tag{6}$$

or, in a normalized version,

$$\frac{\partial^2 V^e}{\partial X_j^2} = V^e + \frac{\partial V^e}{\partial T} \tag{7}$$

where the **electrotonic potential**

$$V^e = V - E \tag{8}$$

is the deviation of the membrane potential V from its resting value E and

$$\lambda_j = \sqrt{\frac{d_j}{4gr}} \qquad \text{and} \qquad \tau = \frac{c}{g} \tag{9}$$

are the neuritic **space and time constants** that – in (7) – are used to normalize space x_j and time t via

$$X_j = \frac{x_j}{\lambda_j} \qquad \text{and} \qquad T = \frac{t}{\tau} \tag{10}$$

The normalized distance X_j from the soma is also called the electrotonic distance. Note that the space constant λ_j of neurite j depends on the diameter d_j of the neurite. This means that the space constants can differ between neurites.

According to assumptions (7) and (8) from Rall's model, the **current density** flowing across the membrane of neurite j at location X_j is

$$i_{m,j}(X_j) = c\frac{\partial V^e}{\partial t} + gV^e = g\left(\frac{\partial V^e}{\partial T} + V^e\right) \tag{11}$$

and assumptions (3) and (6) imply [72] that the **axial current** flowing along neurite j at location X_j can be expressed as

$$I_{a,j}(X_j) = -\frac{1}{R_j}\frac{\partial V^e}{\partial x_j} = -\frac{1}{\lambda_j R_j}\frac{\partial V^e}{\partial X_j} \tag{12}$$

The **third step** is the specification of what happens at the terminations of the neurites distal to the cell body. In principle, the resistance encountered by axial currents flowing between the last segment of the neurite and the extracellular medium could have any value between zero (which is called the 'killed end boundary condition') and infinity (the 'sealed end boundary condition') [72]. The killed end condition would require that the trans-membrane voltage at the termination of the neurite be zero at all times [72], a possibility that is clearly ruled out by the optical measurements presented in section 5.2 (which indicate that changes in membrane voltage can in fact be observed at the tip of the neurite). Also, a neuron with highly conductive neurite endings would not be able to transmit much information in the form of voltage changes to its nerve terminals and from there to adjacent cells, so the killed end boundary condition would not make much sense from a functional point of view, either. In contrast, the sealed end boundary condition can be shown to be a very good approximation of a membrane cylinder whose end is sealed with a disk composed of the same membrane [72] – which is the simplest assumption one can make if nothing is known about the conductance of the growth cone's membrane as compared to the rest of the neuritic membrane. Because of these considerations, and for the sake of a simple neuron model, **we make the assumption of sealed neurite endings** instead of introducing an additional unknown parameter in the equivalent circuit to model the resistance of the nerve terminal.

In the **fourth and final step**, solutions of the cable equation for different perturbations of the

system are derived. Most of the calculations necessary for this are done in appendix C; the following three subsections summarize the solutions derived there for different cell geometries, proceeding from the special cases of neuriteless cell bodies and cells with only one neurite to the most general case of a soma with an arbitrary number of unbranched neurites:

4.1.2 Current step solution for cells without neurites

For the determination of the somatic membrane conductance and capacitance in section 5.1, we need an expression for a neuriteless cell body's voltage response to a step in the injection current.

For such an **isolated soma**, the equivalent circuit according to the passive model reduces to a single compartment with a capacitance C_s in parallel to an ohmic conductance G_s and a battery E. The current I_{inj} injected into the cell through the electrode has to be equal to the current leaving the cell via the membrane, so we can immediately write down the differential equation governing the voltage dynamics in this circuit, namely

$$I_{inj} = C_s \frac{dV}{dt} + G_s(V - E) \tag{13}$$

where V is the membrane voltage – this can also be obtained by multiplying (11) for the somatic compartment with the somatic membrane area. This equation is easily solved for a current step from $I_{inj,0}$ to $I_{inj,\infty}$ at time zero, resulting in a **mono-exponential voltage transient** decaying with the somatic membrane time constant $\tau_s = C_s/G_s$, namely

$$V(t) = V_\infty + \frac{I_{inj,0} - I_{inj,\infty}}{G_s} e^{-\frac{t}{\tau_s}} \tag{14}$$

where V_∞ denotes the steady state voltage after the current step.

4.1.3 Solutions for cells with one neurite

Although neurons consisting of a cell body and a single neurite rarely occurred in the cell cultures used here, we consider this special case because the solutions are needed for section 4.2. With only one neurite, our model is identical to the one used in the original literature on the somatic shunt cable model [14][49], but as these publications do not contain all the solutions we require, all desired expressions are derived in appendix C and summarized here for three different types of perturbations suggested by Rall [73], namely:

1.) a voltage step applied at the cell body or
2.) a current step injected into the cell body or
3.) a brief current pulse injected into the cell body.

The model neuron's responses under these different conditions are (note that the index j for different neurites is suppressed here):

1.) **Voltage step applied at the cell body:** Following a somatic voltage step from $V^e_{s,0}$ to $V^e_{s,\infty}$ at time zero, the spatio-temporal voltage distribution in the single neurite is

$$V^e(X,T) = V^e_{s,\infty} \frac{\cosh(L-X)}{\cosh L} + \frac{2}{L}(V^e_{s,0} - V^e_{s,\infty}) \sum_{n=1}^{\infty} \frac{\zeta_n}{\zeta_n^2 + 1} \sin(\zeta_n X)\, e^{-\left(1+\zeta_n^2\right)T} \tag{15}$$

where $L = l/\lambda$ is the normalized length of the neurite and the ζ_n are defined by

$$\zeta_n = \frac{(2n-1)\pi}{2L} \tag{16}$$

The necessary injection current for this voltage clamp is

$$I_{inj}(T) = V^e_{s,\infty}G + (V^e_{s,\infty} - V^e_{s,0})\frac{2}{L\lambda R}\sum_{n=1}^{\infty}\frac{\zeta_n}{\zeta_n^2+1}e^{-\left(1+\zeta_n^2\right)T} \quad (17)$$

$$= V^e_{s,\infty}G + \sum_{n=1}^{\infty} I_n e^{-\frac{t}{\tau_n}} \quad (18)$$

with the amplitudes and time constants

$$I_n = (V^e_{s,\infty} - V^e_{s,0})\frac{2}{L\lambda R}\frac{\zeta_n}{\zeta_n^2+1} \qquad \text{and} \qquad \tau_n = \frac{\tau}{1+\zeta_n^2} \quad (19)$$

and the neuron's input conductance G given by

$$G = G_s + \frac{\tanh L}{\lambda R} \quad (20)$$

2.) **Current step injected into the cell body:** The voltage transient in the single neurite after a step in the injection current is

$$V^e(X,T) = V^e_{s,\infty}\frac{\cosh(L-X)}{\cosh L} + \sum_{n=1}^{\infty} K_n \cos(\eta_n(L-X))e^{-\left(1+\eta_n^2\right)T} \quad (21)$$

where the η_n are solutions of the transcendental equation

$$G_s\left[1 - \frac{\tau_s}{\tau}\left(1+\eta_n^2\right)\right] = \eta_n\frac{\tan\left(\eta_n L\right)}{\lambda R} \quad (22)$$

and the coefficients K_n are defined by

$$K_n = \left(V^e_{s,0} - V^e_{s,\infty}\right)\frac{2\eta_n\left(\tanh L + \lambda R G_s\right)}{(1+\eta_n^2)L + (1-\eta_n^2)\sin(\eta_n L) + 2\eta_n\lambda R G_s\cos(\eta_n L)} \quad (23)$$

with the somatic steady state potentials $V^e_{s,0}$ and $V^e_{s,\infty}$ before and after the current step. Although it is not immediately obvious, this result can be shown to be equivalent to equation (20) in [14], confirming that the calculus in appendix C is consistent with the original somatic shunt cable model for just one neurite.

3.) **Current pulse injected into the cell body:** The complete analytical expression for the voltage transient in the neurite following a brief current pulse injected into the soma is

$$V^e(X,T) = V^e_{s,0}\frac{\cosh(L-X)}{\cosh L} + \sum_{n=1}^{\infty} K_n(1 - e^{-T^{pulse}(1+\eta_n^2)})\cos(\eta_n(L-X))e^{-\left(1+\eta_n^2\right)T} \quad (24)$$

where the η_n and K_n are again given by (22) and (23) and where T^{pulse} is the normalized pulse duration.

4.1.4 Solutions for cells with arbitrarily many neurites

The calculus leading to these most general solutions is again done in appendix C; the derivations follow the same strategies as previously applied to a soma with only one cable attached [14] [73][75], but extend the solutions to a neuron consisting of $J > 1$ neurites attached to a cell body and thus make them applicable to the neurons used in the present study. The results for the same types of perturbations as above are, in summary:

1.) **Voltage step applied at the cell body:** If the somatic voltage is stepped from $V^e_{s,0}$ to $V^e_{s,\infty}$ at time zero, the resulting spatio-temporal voltage distribution in neurite j is

$$V^e(X_j,T) = V^e_{s,\infty}\frac{\cosh(L_j-X_j)}{\cosh L_j} + \frac{2}{L_j}(V^e_{s,0}-V^e_{s,\infty})\sum_{n=1}^{\infty}\frac{\zeta_{j,n}}{\zeta_{j,n}^2+1}\sin\left(\zeta_{j,n}X_j\right)e^{-\left(1+\zeta_{j,n}^2\right)T} \tag{25}$$

where $L_j = l_j/\lambda_j$ is the normalized length of neurite j and the $\zeta_{j,n}$ are defined by

$$\zeta_{j,n} = \frac{(2n-1)\pi}{2L_j} \tag{26}$$

The current that has to be injected into the soma to achieve this voltage clamp is

$$I_{inj}(T) = V^e_{s,\infty}G + (V^e_{s,\infty}-V^e_{s,0})\sum_{j=1}^{J}\frac{2}{L_j\lambda_j R_j}\sum_{n=1}^{\infty}\frac{\zeta_{j,n}}{\zeta_{j,n}^2+1}e^{-\left(1+\zeta_{j,n}^2\right)T} \tag{27}$$

where

$$G = G_s + \sum_{j=1}^{J}\frac{\tanh L_j}{\lambda_j R_j} \tag{28}$$

is the neuron's input conductance. Thus the part of the injection current due to neurite j consists of exponentially decaying currents with time constants

$$\tau_{j,n} = \frac{\tau}{1+\zeta_{j,n}^2} \tag{29}$$

with $\tau_{j,1}$ being the largest time constant, followed by $\tau_{j,2}$, and so on.

2.) **Current step injected into the cell body:** If the injection current at the soma is stepped to a different value at time zero, the voltage transient in neurite j is

$$V^e(X_j,T) = V^e_{s,\infty}\frac{\cosh(L_j-X_j)}{\cosh L_j} + \sum_{n=1}^{\infty}K_{j,n}\cos(\eta_n(L_j-X_j))e^{-\left(1+\eta_n^2\right)T} \tag{30}$$

where $V^e_{s,0}$ is the voltage at the soma before the step and the η_n are solutions of the transcendental equation

$$G_s\left[1-\frac{\tau_s}{\tau}\left(1+\eta_n^2\right)\right] = \eta_n\sum_{j=1}^{J}\frac{\tan\left(\eta_n L_j\right)}{\lambda_j R_j} \tag{31}$$

where τ_s is the time constant of the somatic membrane. If the η_n are numbered in ascending order, the exponentially decaying components of the voltage transients have time constants

$$\tau_n = \frac{\tau}{1+\eta_n^2} \tag{32}$$

with $\tau_n > \tau_{n+1}$. For the coefficients $K_{j,n}$, no analytical expression is known when $J > 1$ – if complete solutions for the voltage transients are needed, they have to be obtained numerically.

3.) **Current pulse injected into the cell body:** If a brief current pulse is injected into the soma and terminates at time zero, the voltage transient in neurite j has the same structure as for a current step (see (30)), namely

$$V^e(X_j,T) = V^e_{s,0}\frac{\cosh(L_j-X_j)}{\cosh L_j} + \sum_{n=1}^{\infty}M_{j,n}\cos(\eta_n(L_j-X_j))e^{-\left(1+\eta_n^2\right)T} \tag{33}$$

where $V^e_{s,0}$ is the voltage at the soma before the pulse and the η_n again are the solutions of (31). Only the coefficients $M_{j,n}$ are different; they are related to the $K_{j,n}$ via

$$M_{j,n} = K_{j,n}(1-e^{-T^{pulse}(1+\eta_n^2)}) \tag{34}$$

where T^{pulse} is the normalized pulse duration. But because the $K_{j,n}$ are not known analytically, complete solutions for a cell with arbitrarily many neurites can – as above – only be obtained by numerical simulation.

4.2 Why do we need imaging data?

The simplest building block of designed neural networks is a cell body with one or several unbranched neurites attached to it. For the passive cable model, five different parameters have to be specified to fully describe the electrical behavior of this basic unit, namely c_s and g_s for the somatic membrane, c and g for the neuritic membrane and r for the cytoplasm. What is the easiest way to measure these parameters?

The two somatic parameters c_s and g_s, one might think, can be measured independently on neural cell bodies without any neurites that are available in the cell cultures. As will be shown in section 5.2, however, this does not work here because **cell bodies of snail cells with neurites have other electrical properties than neuriteless cell bodies**. The number of unknown variables can therefore not be reduced from five to three by independent measurements on neuriteless cell bodies.

For a cell with neurites, any current injected into the soma partly flows into those neurites, and the injection current necessary for a somatic voltage step is partly due to the resulting changes in the neuritic voltage distribution, so under current clamp as well as voltage clamp conditions we expect that the electrical properties of the neurites influence the overall response measured at the soma. This is confirmed by the expressions derived for such responses in section 4.1, namely (27) and (33). Given these equations, it is tempting to think that the electrical properties of soma as well as neuritic cables can be determined from somatic transients in response to voltage or current steps, and the present section describes how exactly this could – in theory – be done for a cell with one neurite.

However, this approach does not work in reality, which is also demonstrated below. **The electrical parameters describing the neuron can thus not be derived from electrophysiological measurements at the soma alone – this is why we need to measure voltage transients directly in the neurites with the aid of voltage-sensitive dyes.**

Electrical parameters from somatic voltage transients ?

A method to derive the electrical parameters of a passive neuron with one neurite from its somatic voltage transient in response to a current step was suggested in the first publications on the somatic shunt cable model [14][49]. This method consists of fitting the two slowest decaying components of the voltage transient to exponentials and of then finding the electrical parameters that best reproduce the amplitudes and time constants of these exponentials.

Specifically, the **method** involves the following steps:

1.) Fitting the somatic voltage transient after the current step to the function

$$V(t) = V_\infty + V_1 e^{-\frac{t}{\tau_1}} + V_2 e^{-\frac{t}{\tau_2}} \tag{35}$$

where V_∞ is obtained from the steady state at the end of the transient and where V_1, V_2, τ_1 and τ_2 are fit variables. Because the transient (according to (21)) theoretically consists of infinitely many exponentially decaying components with different time constants, fitting the transient with only two components is a compromise between fit accuracy and number of free variables. To avoid fit errors due to the faster decaying components, the first 0.5ms after the current pulse should therefore be excluded from the analysis [90].

2.) Choosing a pair of values for τ and L.

3.) Computing η_1 and η_2 from τ_1, τ_2 and τ with (32).

4.) Computing the ratio of the somatic and neuritic time constants (called 'somatic shunt parameter ε' in [14]) with

$$\varepsilon = \frac{\tau_s}{\tau} = \frac{\eta_2 \tan(\eta_2 L) - \eta_1 \tan(\eta_1 L)}{(1+\eta_1^2)\,\eta_2 \tan(\eta_2 L) - (1+\eta_2^2)\,\eta_1 \tan(\eta_1 L)} \tag{36}$$

which is obtained by eliminating $\lambda R G_s$ from the two versions of (22) for $n = 1$ and $n = 2$.

5.) Computing the ratio of the neuritic input conductance and somatic membrane conductance (in [14] called 'dendritic dominance ratio ρ') via

$$\rho = \frac{\frac{\tanh L}{\lambda R}}{G_s} = \frac{\tanh L}{\eta_1 \tan(\eta_1 L)} \left[1 - \varepsilon\left(1+\eta_1^2\right)\right] \tag{37}$$

which is derived from (22) for $n = 1$.

6.) With all these values, calculating the theoretically expected values of V_1 and V_2 according to

$$V_n^{theo} = \frac{\eta_n^2}{1+\eta_n^2} \frac{2(\rho+1)\left(V_{s,0}^e - V_{s,\infty}^e\right)}{(1+\eta_n L \tan(\eta_n L))\left[1-\varepsilon(1+\eta_n^2)\right] + \eta_n^2(2\varepsilon + \rho L \coth L)} \tag{38}$$

which can be obtained from (21) and (23).

7.) Evaluating the squared error function of the two amplitudes, which is defined by

$$SE = (V_1 - V_1^{theo})^2 + (V_2 - V_2^{theo})^2 \tag{39}$$

8.) Repeating steps 2.) through 7.) to find the values of τ and L that minimize the error function.

Together with the input conductance G of the neuron, which is obtained from the steady state voltage and current at the end of the current transient, the parameters τ, L, ε, and ρ in the minimum of the error function describe the electrical behavior of a neuron without requiring any information about the physical dimensions of the cell, which is an advantage if the model is applied to cells whose exact dimensions are unknown. But if, as here, the dimensions of the neuron are known, these five parameters can easily be translated into c_s, g_s, c, g and r with (36), (37) and equations from section 4.1.1, showing that the two sets of parameters are equivalent if the physical dimensions of the neuron are known.

Unfortunately, **the so-called 'inverse' or 'parameter identification' problem for the somatic shunt cable model, namely the determination of all five parameters from somatic voltage transients as described above, is ill-posed**, meaning that very small errors in measured data – for example due to very modest levels of noise – can lead to large and unpredictable errors in parameter estimates. This has been demonstrated in [90] by computing somatic voltage transients for model neurons according to the somatic shunt cable model and by then treating them as if they were experimentally obtained transients, with grossly inaccurate results:

Fig. 4.2 (adapted from [90]) shows a noiseless and a noisy transient computed for such a model neuron and illustrates the shape of the error surface $SE(\tau, L)$ computed for the noiseless transient according to (39). Between the dotted lines, the error surface has a large domain for which the computed error is very small, indicating that **model neurons with very different electrical parameters can respond with almost identical somatic transients** to test current steps. For the noiseless trace, this inherent ill-posedness of the parameter identification problem leads to errors in parameter estimates that range from 4% for L to 77% for ε. For noisy traces (even if the noise level is as small as illustrated in the left part of fig. 4.2), the situation is even worse: The minima of SE found for ten different noisy traces (shown as red dots in the right part of fig. 4.2) correspond to widely varying sets of electrical parameters, with relative errors of sometimes several 100% [90].

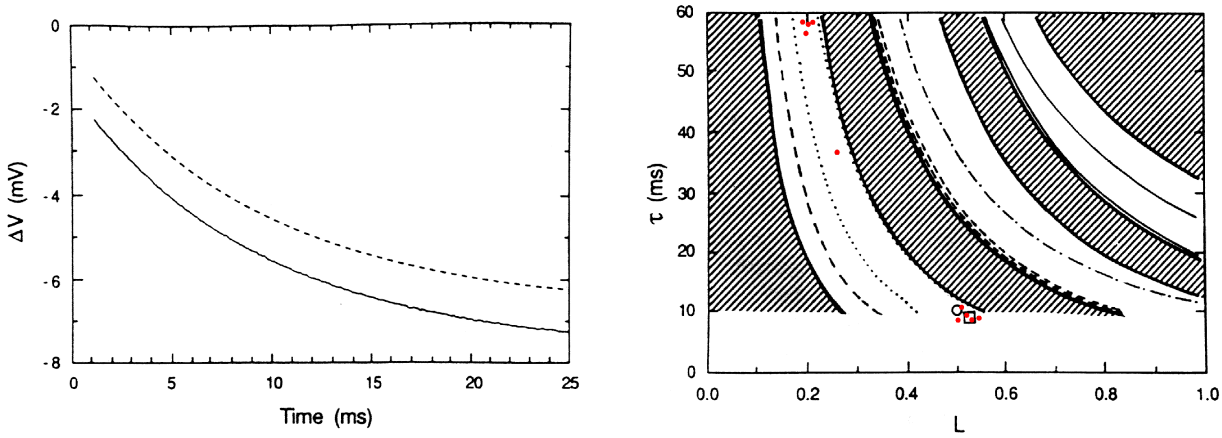

Figure 4.2: ***The electrical parameters of neurons can not be determined from somatic voltage transients.*** *(**Left**) Somatic voltage transients computed for a model neuron with $\tau = 10$ms, $L = 0.5$, $\varepsilon = 0.5$, $\rho = 5$ and $G = 15$nS in response to a current step of -100pA. ΔV is the deviation of the membrane potential from its resting value. The dashed curve is the original, noiseless response; for the solid curve, normally distributed noise with a standard deviation of 10μV was added – the curve was also shifted by -1mV to allow comparison. (**Right**) Error surface $SE(\tau, L)$ for the noiseless trace. Lines on the plot represent contours of constant SE, namely $SE = 0.001$ (dotted), $SE = 0.005$ (dashed), $SE = 0.05$ (dashed and dotted), and $SE = 0.5$ (thin solid). Illegal domains (in which one of the electrical parameters is negative) are hatched and separated from the legal domains by heavy lines. The region with $\tau < \tau_1$ is excluded from the surface because $\tau \geq \tau_1$ according to (20). The correct solution for τ and L is indicated by the open circle, the open square shows the error minimum for the noiseless transient and the red dots are error minima for ten different noisy signals. Adapted from* [90].

Electrical parameters of neurons can hence not be reliably estimated by fitting their somatic voltage response after a current step.

Electrical parameters from somatic current transients ?

The fit strategy suggested in [14] and [49] and described above does not consider voltage clamp data. But one can show that additional information gained from somatic current transients under voltage clamp can not be used to determine the electrical parameters of a neuron, either. To demonstrate this, we first derive **expressions of the electrical parameters in terms of voltage clamp data** and then proceed as in [90], that is, we apply these expressions to artificial data from a model neuron and compare the resulting parameters to the true values.

We can obtain an expression for τ if we compute the amplitude ratio of the two slowest decaying components (for $n = 1$ and $n = 2$) of the current transient (17) with the aid of (19), which gives

$$\left(\frac{I_1}{I_2}\right)^2 = \frac{(\tau - \tau_1)\,\tau_1}{(\tau - \tau_2)\,\tau_2} \qquad \text{or} \qquad \tau = \frac{(\tau_1/I_1)^2 - (\tau_2/I_2)^2}{\tau_1/I_1^2 - \tau_2/I_2^2} \tag{40}$$

Thus if I_1, I_2, τ_1 and τ_2 can be determined from an experimental transient, τ can be computed. With τ known, L can be obtained from

$$L = \frac{\pi}{2\sqrt{\frac{\tau}{\tau_1} - 1}} \tag{41}$$

which is a combination of (26) and (19). The next step is to compute the product λR from

$$\lambda R = \frac{V^e_{s,\infty} - V^e_{s,0}}{I_1} \frac{2}{L} \sqrt{\frac{\tau_1}{\tau} - \left(\frac{\tau_1}{\tau}\right)^2} \tag{42}$$

which was found by solving (19) for λR in the case of $n = 1$. And finally, G_s can be obtained

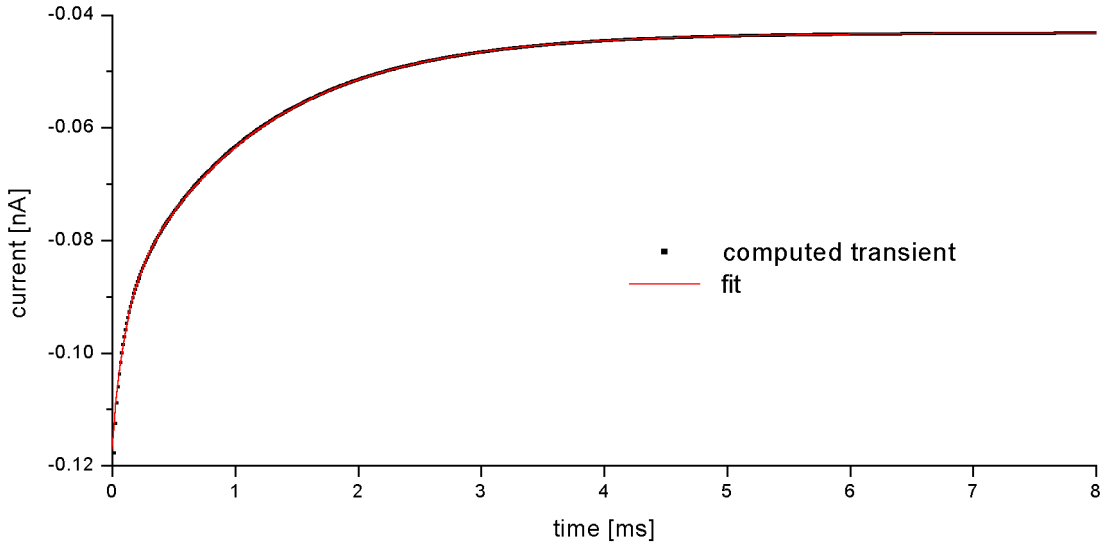

Figure 4.3: ***Somatic current transient and fit for a model neuron in response to a voltage step of −10mV.*** *This graph shows the first 8ms of the current response calculated for the model neuron described in the text (black dots) and the corresponding fit according to (40) (red line). Data and fit agree well for times greater than 50μs.*

from (28) because we know the input conductance G of the neuron from the steady state voltage and current at the end of the current transient (see time-independent part of (17)).

As we also know the physical dimensions of the neuron, the results for τ, L, λR and G_s can then easily be translated into the electrical parameters g, c, r and g_s with equations from section 4.1.1. Note, however, that the somatic capacitance c_s can *not* be derived from the current response to a somatic voltage step. This is because for an ideal voltage step, the charging of the somatic membrane capacitance occurs instantaneously, such that the only contribution of the somatic membrane to the current transient after the step is the current flowing via its conductance – the somatic capacitance does not contribute to the current transient and can therefore not be determined from it.

To test whether these expressions – if applied to somatic current transients – give the correct electrical parameters, a **passive model neuron** with the following geometrical and electrical parameters was constructed: soma diameter $d_s = 60\mu$m, neurite diameter $d = 5\mu$m, neurite length $l = 300\mu$m, somatic conductance $g_s = 0.03$mS/cm^2, somatic capacitance $c_s = 1.1\mu$F/cm^2, neuritic conductance $g = 0.02$mS/cm^2, neuritic capacitance $c = 1.0\mu$F/cm^2, cytoplasmic resistivity $r = 394\Omega$cm. This corresponds to a somatic membrane time constant of $\tau_s = 37$ms, a neuritic time constant of $\tau = 50$ms and a neuritic space constant of $\lambda = 1260\mu$m – the electrical parameters are consistent with the results from chapter 5 for cultured *Lymnaea* neurons and the physical dimensions are typical for such cells.

The response of this model neuron to a voltage step of -10mV applied at the soma was then computed with the aid of (17); it is shown in fig. 4.3. This transient was fit to the function

$$I(t) = I_\infty + I_1 e^{-\frac{t}{\tau_1}} + I_2 e^{-\frac{t}{\tau_2}} \tag{43}$$

where the value of I_∞ was obtained from the steady state at the end of the transient and the amplitudes I_1 and I_2 and the time constants τ_1 and τ_2 were the fit parameters. To avoid fit errors due to faster decaying components, the first 50μs of the transient were excluded from the analysis

– note that for an experimental transient, these initial data would not be reliable, anyway, because of stimulus artifacts [90] and because voltage steps with ramp durations below 50μs are hard to achieve with single-electrode voltage clamp in large cells [21]. The resulting fit is also shown in fig. 4.3; it is virtually identical to the calculated transient for times greater than 50μs.

As we know the exact parameters of the model neuron, we can compute the true values for the two largest time constants in the transient and for the corresponding amplitudes with (26) and (17). The true values, those obtained with the fit and their ratios are

		true value	from fit	$\frac{\text{fit result}}{\text{true value}}$
τ_1	[ms]	1.124	1.118	0.99
I_1	[nA]	−0.049	−0.050	1.02
τ_2	[ms]	0.127	0.100	0.79
I_2	[nA]	−0.017	−0.025	1.47

The agreement between the fit results and the true values is very good for the slowest component, but not so good for the second component. The reason for this is that the second time constant is very small and, in particular, is not much larger than the third time constant (which is $\tau_3 = 0.045$ms according to theory) and also not far above the cut-off time of 50μs chosen to avoid contaminations by higher order components. This already indicates that **current transients in response to voltage steps may be too fast for a reliable determination of electrical cell parameters**, and it is also the reason why using voltage clamp data was avoided in [90].

From I_1, I_2, τ_1 and τ_2, we compute the electrical parameters of the neuron as described above. The results, the true values and the ratios between them are

		true value	from fit	$\frac{\text{fit result}}{\text{true value}}$
g	[mS/cm^2]	0.02	0.59	29.50
c	[μF/cm^2]	1.00	0.97	0.97
r	[Ωcm]	394	1227	3.11
g_s	[mS/cm^2]	0.03	-0.07	-2.33

The ratio of fit result and true value is close to one only for c, and far from one for the other three variables – the electrical cell parameters obtained from the somatic current transient in response to a voltage step hence are grossly inaccurate even for noiseless data from a perfectly passive model neuron. For the more realistic case of a noisy transient with stimulus artifacts obtained from a real neuron, the result will not be better, implying that **a neuron with one neurite can not be characterized by analyzing its current response to a voltage step**, either.

We need measurements of neuritic transients!

In summary, the present section demonstrates that the electrical parameters c_s, g_s, c, g and r of a perfectly passive cell with only one neurite can not be determined from electrophysiological measurements at the soma alone. As more neurites and even weak voltage-dependence of the membrane conductance can only complicate the situation, this **demonstration of ill-posedness for the somatic shunt cable model** implies that we can not characterize cultured *Lymnaea* neurons with several neurites if we lack additional information.

Such additional information can be obtained by **monitoring the voltage dynamics directly in the neurites with the aid of voltage-sensitive dyes** and will, in combination with transients recorded with a microelectrode at the soma, allow the determination of the electrical parameters of snail neurons in chapter 5.

4.3 Active model: Hodgkin-Huxley dynamics

The cable model introduced in section 4.1 – even though it results in quite complicated expressions for the dynamics of voltage distributions in the cell – is a very simplified model for the electrical behavior of a neuron. The most dramatic simplification stems from Rall's assumption (7), which treats the membrane resistance of the neuronal membrane as an ohmic resistance, neglecting any voltage-dependence. This is in stark contrast to reality, because many of the ion channels responsible for the membrane conductance *are* sensitive to the trans-membrane potential difference. In spite of this, **the cable model is a good approximation as long as the membrane voltage is in a range where the voltage-dependence of the conductance is weak**, which usually is the case for potentials more hyperpolarized than the resting potential. For the rest of the physiologically relevant potential range, a more elaborate model has to be used.

The classical parametrization for a neural membrane *with* voltage-sensitive conductances was introduced by Hodgkin and Huxley in 1952 for the squid giant axon [42]. They arrived at a set of differential equations for the membrane voltage (and several conductance variables) that are briefly summarized in this section. These equations describe dynamics on two levels of organization, namely

- the level of ion channels and
- the level of a membrane patch

On the background of the cable model from section 4.1, the Hodgkin-Huxley model is most easily understood if we first consider a membrane patch and proceed to the molecular level later:

The model describes an entire **segment of neural membrane** with an equivalent circuit (fig. 4.4) that is a generalization of the circuit used for the cable model (compare to fig. 4.1). Instead of a single ohmic conductance that allows current flow through the membrane, Hodgkin and Huxley used two separate (and voltage-dependent) conductances for sodium and potassium currents to model the highly ion-selective channel types of the neural membrane and a third, voltage-independent 'leak' conductance for all other ion types. And instead of a single resting potential that drives current through these channels, separate batteries $E_{Na} = E+115\text{mV}$, $E_K = E-12\text{mV}$ and $E_L = E+10.613\text{mV}$ were included for each ion type i – this was necessary because the ion concentrations inside and outside the cell (c_i^{in} and c_i^{out}) are different for each kind of ion, resulting in different reversal potentials E_i according to the **Nernst equation**

$$E_i = -\frac{k_B T}{z_i e_0} \ln \frac{c_i^{in}}{c_i^{out}} \tag{44}$$

where k_B is Boltzmann's constant, T is the temperature and $z_i e_0$ is the charge of ion type i.

The **current density** flowing through the membrane then is (compare to (11))

$$i_m = c\frac{dV}{dt} + g_{Na}(V - E_{Na}) + g_K(V - E_K) + g_L(V - E_L) \tag{45}$$

where g_{Na} and g_K are the voltage-dependent sodium and potassium conductances, g_L is the voltage-independent leak conductance (all per unit area) and $c = 1\mu\text{F/cm}^2$ is the membrane capacitance per unit area.

On the **level of ion channels**, the Hodgkin-Huxley model specifies how the sodium and potassium conductances are influenced by the trans-membrane voltage. It assumes that each voltage-dependent ion channel consists of four independent subunits – so-called **'particles'** – and that

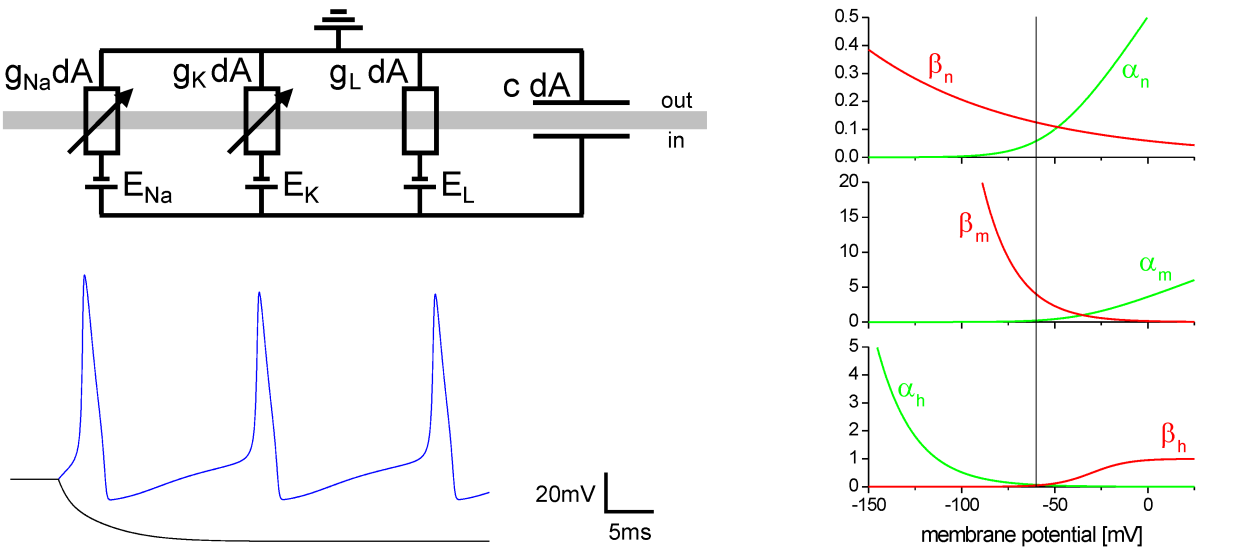

Figure 4.4: ***The Hodgkin-Huxley model.*** *(**Top left**) Equivalent circuit for a patch of membrane according to Hodgkin and Huxley. The area of the patch is dA. The sodium and potassium conductances change depending on the trans-membrane voltage. (**Right**) Voltage dependence of the activation rates α_i (green) and deactivation rates β_i (red) of the three 'particles' n, m and h for a Hodgkin-Huxley membrane with a resting potential of -60mV (indicated by the vertical line). Note the different vertical scales: Between resting potential and zero potential, the activation of m is faster than the deactivation of h, which in turn is faster than the activation of n. In combination, this can lead to an action potential. (**Bottom left**) Voltage responses of a Hodgkin-Huxley neuron with 50μm diameter to the injection of 0.5nA depolarizing current (blue) and -0.1nA hyperpolarizing current (black). At potentials more hyperpolarized than the resting state, the membrane is approximately passive.*

each of these subunits can be in one of two states, namely an activated and a deactivated state, changing from one state to the other at a rate that depends on the momentary membrane voltage:

$$\text{deactivated} \underset{\beta(V)}{\overset{\alpha(V)}{\rightleftharpoons}} \text{activated}$$

According to the model, the channel can only conduct ions if all four of its subunits are in their activated state. Therefore, if n is the probability of a potassium channel subunit to be activated, the channel (that has four identical subunits) is open with probability n^4. The sodium channel has one subunit (the 'h-particle') that is different from the other three (the 'm-particles'), therefore this channel is open with probability m^3h where m and h again stand for the probability of the respective type of subunit to be activated.

Because n^4 gives the probability for each single potassium channel to be open, it also corresponds to the conducting portion of a whole population of potassium channels if we look at the level of a membrane patch that contains many channels of this kind. The potassium **conductance per unit membrane area** therefore is

$$g_K = \overline{g}_K n^4 \tag{46}$$

where $\overline{g}_K = 36\text{mS/cm}^2$ is the potassium conductance density when all channels are open, and with the same argument

$$g_{Na} = \overline{g}_{Na} m^3 h \tag{47}$$

where $\overline{g}_{Na} = 120\text{mS/cm}^2$ is the maximum sodium conductance per unit area. For the voltage-independent leak conductance, $g_L = \overline{g}_L = 0.3\text{mS/cm}^2$ by definition.

The schema shown above implies that n, m and h evolve according to the **rate equation**

$$\frac{di}{dt} = \alpha_i(1-i) - \beta_i i = \tau_i(i - i_\infty) \tag{48}$$

where $i \in \{n, m, h\}$ and the voltage-dependent relaxation **time constant** τ_i **and steady state value** i_∞ can be expressed in terms of the activation and deactivation rates α_i and β_i via

$$\tau_i = \frac{1}{\alpha_i + \beta_i} \qquad \text{and} \qquad i_\infty = \frac{\alpha_i}{\alpha_i + \beta_i} \tag{49}$$

The voltage dependence of the rates α_i and β_i is illustrated in fig. 4.4; the corresponding mathematical expressions (taken from [42]) are listed in appendix E.

Taken together, (45) and (48) describe the time evolution of the **four dynamic variables of the Hodgkin-Huxley model, namely** V**,** n**,** m **and** h. This set of differential equations can not be solved analytically, so to model the electrical behavior of a neuron according to Hodgkin and Huxley they have to be solved numerically. Two solutions for a cell with 50μm soma diameter are shown in fig. 4.4: The Hodgkin-Huxley model can produce action potentials when the membrane is depolarized and behaves **almost like a passive model for potentials more hyperpolarized than the resting potential**.

For section 5.1, we also need expressions for the steady state membrane current and conductance at a given V. In steady state, the activation variables n, m and h assume the values n_∞, m_∞ and h_∞ given by (49). With (45) through (47), the **steady state current density** then is

$$i_m = \overline{g}_{Na} m_\infty^3 h_\infty (V - E_{Na}) + \overline{g}_K n_\infty^4 (V - E_K) + \overline{g}_L (V - E_L) \tag{50}$$

The derivative of this expression with respect to membrane voltage is the **conductance of the membrane**:

$$\frac{di_m}{dV} = \overline{g}_{Na}\left[m_\infty^3 h_\infty + (V - E_{Na})\frac{d\,(m_\infty^3 h_\infty)}{dV}\right] + \overline{g}_K\left[n_\infty^4 + (V - E_K)\frac{d\,(n_\infty^4)}{dV}\right] + \overline{g}_L \tag{51}$$

Evaluated at the resting potential E, this results in a resting state conductance of 1.2mS/cm^2 for the Hodgkin-Huxley model[8].

[8] Note that this is *not* the same as $\overline{g}_{Na} m_\infty^3 h_\infty + \overline{g}_K n_\infty^4 + \overline{g}_L$, which is often used to compute the steady state membrane conductance of a Hodgkin-Huxley neuron and has a value of 0.68mS/cm^2 at resting potential.

5
Single cell experiments

This chapter describes how the neurons that make up a designed neural network were characterized and lists the results of these experiments, namely the electrical parameters of the cells. For reasons that will become obvious in section 5.1, the simpler of the two cell models introduced in the last chapter – the passive model – was chosen to describe the electrical behavior of the neurons. Given this model, a **complete characterization of the cells** consists of a set of five parameters, namely the somatic membrane conductance g_s and capacitance c_s, the respective values for the neuritic membrane, g and c, and the cytoplasmic resistivity r.

The capacitance of neuritic membranes is usually assumed to be $c = 1\mu$F/cm^2 in the literature (reviewed for example in [53] and [89]), but single values can be as low as 0.3μF/cm^2 for the giant axon of the earthworm or as high as 3μF/cm^2 for bullfrog sympathetic ganglion cells [78], where the high value is ascribed to membrane invaginations and foldings. To reduce the number of unknowns that have to be determined for cultured *Lymnaea* neurons, $c = 1\mu$F/cm^2 was assumed here, too, leaving g_s, c_s, g and r to be extracted from the measurements presented in this chapter. The validity of this assumption is discussed in section 5.2.

Initially, the plan was to further reduce the number of unknowns for cells *with* neurites by first measuring the somatic parameters g_s and c_s with independent experiments on *neuriteless* cell bodies. These **soma experiments** are discussed in section 5.1 and provide useful information about the properties of *Lymnaea* neurons. However, the results from section 5.2 – where the neuritic parameters g and r are determined from experiments with voltage sensitive dyes – indicate that the **somatic properties of neurons without neurites are different from those with neurites**, so the values of g_s and c_s in neurons with processes are determined in section 5.2 and compared to those of cell bodies without neurites.

As an additional result not directly related to the determination of membrane parameters, the optical measurements done for section 5.2 also provide **spatio-temporal maps of signal propagation** in *Lymnaea* neurites; these are briefly discussed in section 5.3.

5.1 Cells without neurites

To characterize the somatic membrane, healthy-looking but **neuriteless cell bodies** in one day old cultures of A-cluster neurons were selected. Each cell was impaled with a microelectrode and the voltage response of the cell to injected current steps was recorded as described in section 3.1. Fig. 5.1 shows a typical example of such a cell – measurements performed on this neuron will be used in the rest of this section to illustrate how the somatic membrane parameters were determined.

Equation (14) shows that, for such a step in the injection current, we expect to record mono-exponential voltage responses in a potential range were the passive model is a good description

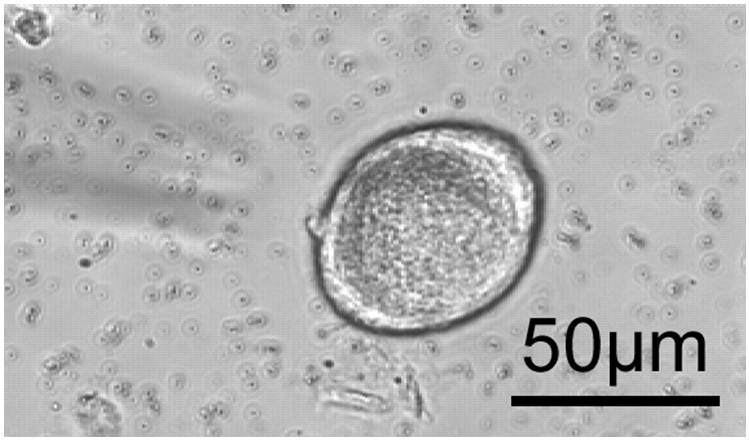

Figure 5.1: ***Example soma.*** *Micrograph of the cell body used to illustrate the determination of somatic membrane parameters. The shadow in the upper left corner shows the approaching microelectrode that is not yet in focus.*

of the membrane, whereas deviations from the mono-exponential form are expected in potential ranges where the membrane conductance *does* depend on trans-membrane voltage.

Why measure in two different potential ranges?

From the data presented below, it will become apparent that the somatic membrane of the cells used here is not perfectly passive in the range of the resting potential. Therefore, the voltage transients recorded in this potential range often deviated from the mono-exponential form and could lead to questionable results for the membrane parameters if fit to (14). To solve this problem, the somatic **membrane conductance G_s and capacitance C_s were measured in two different potential ranges**:

- **To determine** C_s, a strong hyperpolarizing current was injected into the cell, and current steps were then performed starting from this holding current. This ensured that the voltage transients were recorded in a potential range where the somatic conductance *is* independent of trans-membrane voltage and could well be fit to (14). This approach is possible for C_s because the somatic capacitance is voltage-independent and can thus be measured in any potential range.
- **To determine** G_s, current steps were applied when the cell was in or close to its resting state. The injected currents $I_{inj,\infty}$ were then plotted against the steady state potentials V_∞ they induced and the membrane conductance G_s was obtained from the slope of this steady-state current-voltage relation in the vicinity of the resting state. This method insured that the resulting value of G_s was a good characterization of the cell in the state it usually is in – namely, the resting state – while avoiding to (badly) fit non-mono-exponential voltage transients to (14).

Fig. 5.2 shows such measurements at two different potential levels and the corresponding fits for the cell from fig. 5.1. While the fits usually agree well with the data for small current steps, the voltage responses to larger current steps obviously are still only approximately mono-exponential, even though they were recorded at very hyperpolarized potentials.

First result: somatic membrane capacitance

Each of the red fits in fig. 5.2 resulted in a value for C_s. These values were independent of the steady state membrane potential and could therefore be averaged over all curves, leading to a

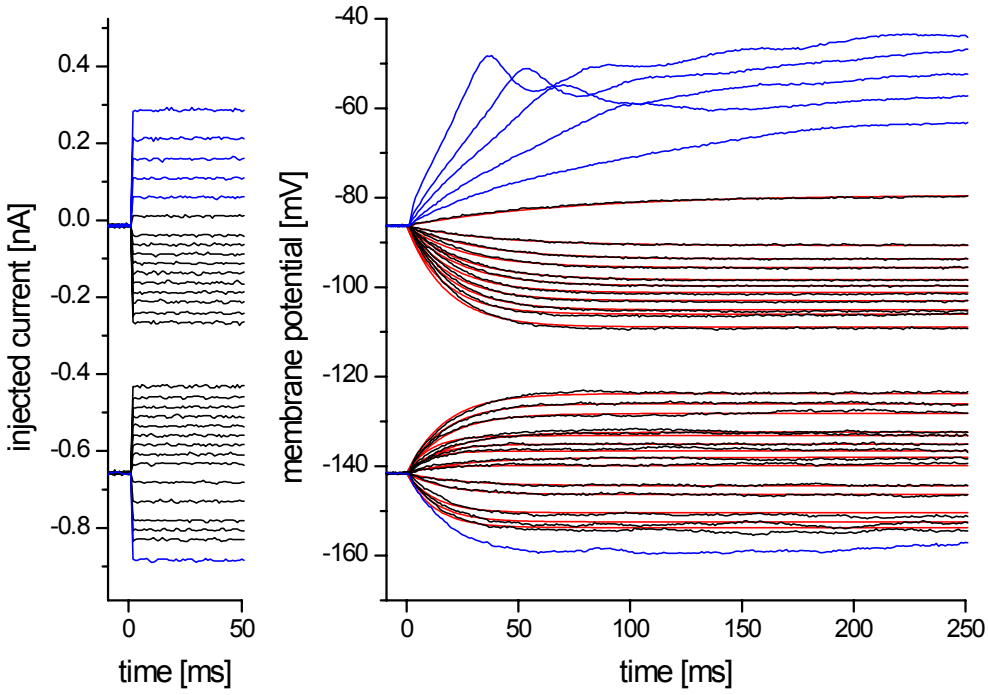

Figure 5.2: ***Data recorded from the example cell.*** *(**Left**) Current steps injected into the cell body. Only the first 50ms of the 1000ms current traces are shown. (**Right**) Voltage responses to these current steps (black and blue) and corresponding mono-exponential fits (red). Only the first 250ms are shown for clarity. (**Both**) In both graphs, the blue curves belong to measurements that did not reach a stable steady state because of a strong active component (top five traces) or - presumably - because of temporary membrane ruptures at very hyperpolarized potentials (bottom trace).*

value of $C_s = (0.21 \pm 0.06)$nF for the example soma. Assuming that the cell body is approximately spherical and using the average diameter of the cell obtained from fig. 5.1, this absolute capacitance was divided by the soma surface area, resulting in a **specific membrane capacitance** of $c_s = (2.4 \pm 0.7)\mu$F/cm^2 for the example neuron and an average of

$$c_s = (2.6 \pm 0.8)\mu\text{F/cm}^2$$

for all nine cell bodies used here, with single values ranging from 1.4μF/cm^2 to 4.5μF/cm^2.

These values are higher than the specific membrane capacitance of 1μF/cm^2 usually cited in the literature, but they are in a range similar to the high specific capacitances previously found for leech neurons [27] and bullfrog neurons [78], where they were ascribed to membrane invaginations that result in a membrane area higher than expected from the neuron's diameter.

Second result: somatic membrane conductance

As described above, the somatic membrane conductance in the resting state can be obtained from the slope of the steady-state current-voltage relation in the range of the resting potential. Fig. 5.3 shows this current-voltage relation for the example neuron – its slope is clearly not constant, revealing that the **neuron's conductance indeed does depend on the membrane potential even at or below resting potential**. To obtain an estimate of the membrane conductance around the resting potential (which is defined by zero membrane current), a line was fit to the approximately linear portion of the data in the range around zero current. The slope of this line gives a membrane conductance of about 3.0nS, its intersect with the zero current axis gives the cell's resting potential.

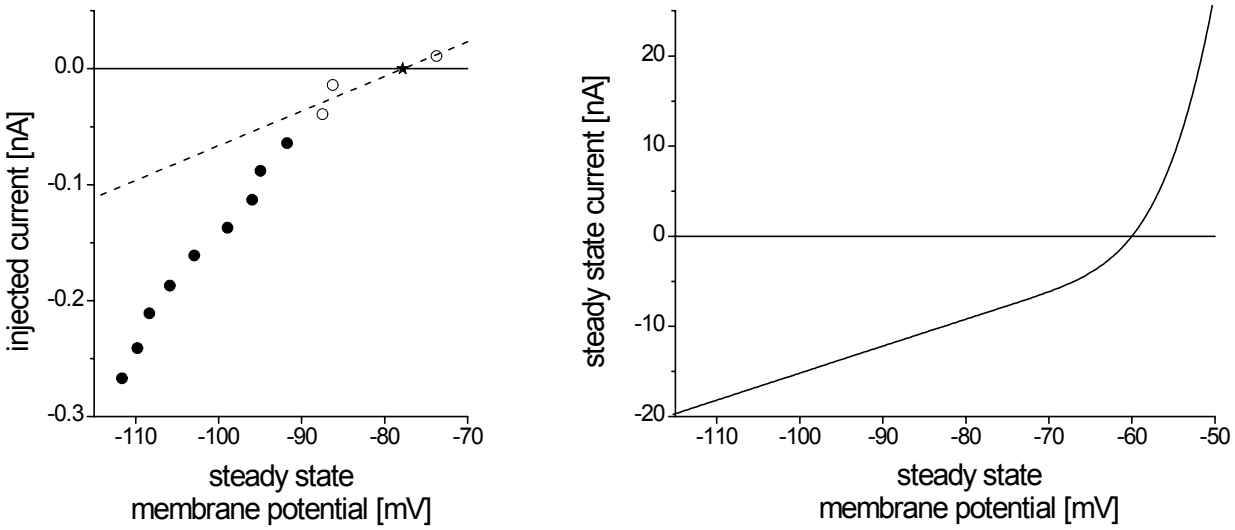

Figure 5.3: ***Steady-state current-voltage relations for the example soma and a Hodgkin-Huxley neuron.*** *(**Left**) Currents injected into the example cell (solid and open dots), plotted against the steady state membrane potential they induced. The data do not fall on a straight line, indicating that the membrane conductance is voltage-dependent. To obtain an estimate of the membrane conductance in or close to the resting state, a straight line was fit to through the approximately linear portion of the data around zero current (open dots). The slope of this (dashed) line gives the conductance around the resting state, while the intersect of the line with the zero current axis gives the resting potential of the neuron (indicated by an asterisk). (**Right**) For comparison, the steady-state current-voltage relation was computed for a cell with 50μm diameter, a resting potential of -60mV and Hodgkin-Huxley membrane parameters. The curve is completely different from the experimental data shown in the left plot.*

Plots of this kind for all nine cells in the sample were combined in fig. 5.4 (where the fifth data set from the top is the one of the example neuron). This figure contains a lot of information about the **electrical properties of pedal A-cluster neurons**:

- As can be seen from the different slopes of the dashed lines in the figure, the cells have a **wide variety of resting state conductances** G_s, with values ranging from 1.33nS to 7.42nS. Even if divided by the surface area of the corresponding cell, these values have a broad distribution, resulting in an average **membrane conductance per unit area** of
$$g_s = (0.063 \pm 0.051)\text{mS/cm}^2$$
with extreme values of 0.017mS/cm^2 and 0.142mS/cm^2. Compared to the resting state conductance of 1.2mS/cm^2 for a Hodgkin-Huxley neuron (see section 4.3), this is a very small value. However, it is well within the range of previously reported neural membrane conductances, which can be as low as 0.01mS/cm^2 [89].
- The dashed lines representing the resting state conductance usually agree well with the data in fig. 5.4 down to about -90mV, but several of the data sets show a change in conductance (that is, in slope) in the range of -110mV to -90mV, with *higher* conductances at more hyperpolarized potentials. As illustrated in fig. 5.3, this is very **different from the situation in the Hodgkin-Huxley model**, which has a constant and relatively *low* conductance up to about 10mV below resting potential and higher conductances at more depolarized potentials. Extrapolating the unusual high-conductance portion of the data in fig. 5.3 to zero current indicates that this current has its reversal potential in a very hyperpolarized range, suggesting that it may be due to a residual potassium conductance not present in the Hodgkin-Huxley model.
- The cells have a very **broad distribution of resting potentials** (indicated in fig. 5.3 by the

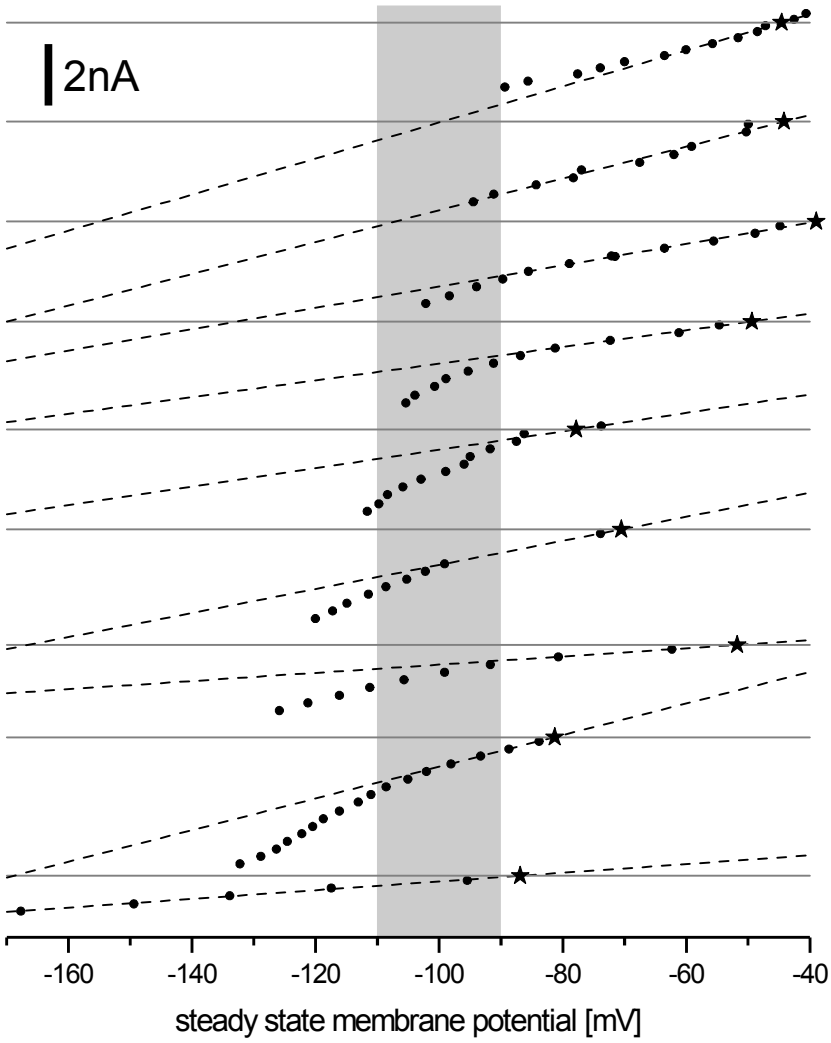

Figure 5.4: ***Steady-state current-voltage relations for nine cell bodies.*** *Currents injected into nine neurons (dots), plotted against the steady state membrane potential they induced in the cell. For each soma, the zero current axis is shown in dark grey. In the range between $-110mV$ and $-90mV$ (shaded area), some of the cells show a change in conductance. The dashed lines are fits to the approximately linear parts of the curves around $I_{inj} = 0$ – their slopes give estimates for the membrane conductances in the resting states and their intersects with the zero current axes determine the resting potentials (indicated by black asterisks).*

intersects of the dashed lines with the corresponding grey lines), with values ranging from -87mV to -39mV.

In summary, the membrane of *Lymnaea* pedal A-cluster neurons displays voltage-dependence even at very hyperpolarized potentials, and the Hodgkin-Huxley model does not agree well with the data from these cells, neither with respect to the magnitude nor with respect to the voltage-dependence of the conductance. In spite of its active properties, the membrane can be approximated in the vicinity of the resting potential with a passive model (using the capacitance and conductance values determined in this section) and the approximation is quite good in the range between -90mV and the resting potential. Because of these findings, **the entire rest of this work always describes the pedal A-cluster neurons with the passive model**.

5.2 Cells with neurites

As the neuritic parameters g and r can not be determined solely from electrophysiological measurements at the cell body (see section 4.2), **voltage data measured directly at different sites along the neurites** were needed. To obtain such data, voltage transients in the neurites of cultured pedal A-cluster neurons were recorded with voltage-sensitive dyes as described in section 3.2. Using the theoretical models for the electrical behavior of neurons introduced in chapter 4, we can now try to determine the neuritic parameters g and r by **fitting these imaging data to theoretical transients** from a model neuron, with g and r as the fit variables. To do this, the neurons are again modeled according to the *passive* cable theory rather than using Hodgkin-Huxley dynamics because this *active* parametrization of the membrane processes has – in the previous section – been demonstrated to be not well applicable to the snail neurons used here.

The present section first describes the imaging data that were used as the fit target, then discusses the fitting itself in two different versions – namely using the somatic parameters from section 5.1 or not using them – and finally gives the results: The neuritic parameters and a set of somatic parameters that differ from those obtained for neuriteless cell bodies in section 5.1.

The target data

For the imaging of voltage transients, cultured pedal A-cluster neurons with two straight and unbranched neurites were stained with the voltage-sensitive dye BNBIQ. The cell bodies were then impaled with a microelectrode, two current pulses were applied – first a depolarizing pulse that triggered an action potential and then a hyperpolarizing pulse – and the **propagation of action potential and hyperpolarization along the neurites was monitored** with the photodiode array as described in section 3.2. For each photodiode, the recorded fluorescence transient was corrected for bleaching as described in the same section. The choice of the passive model implies that only the hyperpolarizing pulses can be used to find g and r, because only they occur in a potential range where the membrane conductance is approximately voltage-independent (the depolarizing pulses will be used in section 5.3).

The fluorescence data $-\Delta F_n(t)$ recorded during the hyperpolarizations were reduced in their spatial and temporal extent:

- In the spatial direction, only transients from those diodes that actually recorded from the neurites were included in the target data for the fit, and only if they carried a signal above noise level.
- The time window of the data sets was restricted to a period of 90ms, starting 5ms before the onset of the hyperpolarizing current pulse. This window captures the entire fluorescence transients without including much time after the membrane potential has already returned to baseline.

If we want to fit the remaining sets of fluorescence data to voltage distributions computed for a model neuron, we run into the problem of different and unknown proportionality factors between voltage change and fluorescence change for the different diodes (see section 3.2). We solve this problem by using alternative I from section 3.2.3 (for reasons given there), which means that **we use only the *shapes* $S_n^{fluo}(t)$ of the fluorescence transients** (as defined by (2)) – and not their *amplitudes*. Naturally, this implies that we have to normalize the theoretical transients in the same manner before we can compare them to the target data during the fitting process. The resulting

target data for the three neurons for which imaging data are available (called 'A', 'B', and 'C') are shown in fig. 5.6.

The fit using the parameters of neuriteless cell bodies

Because the neurons used for imaging all had two neurites, analytical solutions for the theoretically expected voltage transients in the neurites after a brief hyperpolarizing current pulse at the soma were not available (see section 4.1.4). Instead, the theoretical transients had to be obtained by numerical simulation; the **determination of the neuritic parameters** therefore – for each of the three cells – involved the following steps:

1.) The construction of a model cell with the same soma diameter and neurite diameters and lengths as the cell in question (as illustrated in fig. 4.1) and with the somatic membrane parameters $g_s = 0.063\text{mS/cm}^2$ and $c_s = 2.6\mu\text{F/cm}^2$ from section 5.1.
2.) The choice of arbitrary starting values for the two parameters g and r of the model neuron.
3.) The numerical simulation of the theoretical transient shapes $S_n^{theo}(t)$ of the model neuron in response to the same current pulse as injected into the real neuron during the imaging experiment (for details of the simulation see appendix D).
4.) The computation of the theoretical shapes' deviation from the target data. As a measure for the deviation, the quantity χ^2/D – defined by (158) in appendix D – was used, which is just the 'chi-square' usually used for least square fitting, divided by the number D of data points in the target data set [69].
5.) The choice of a new pair of values for g and r in the model neuron.
6.) The repetition of steps 3, 4 and 5 until the minimum of χ^2/D is found. The g and r in the minimum are the neuritic parameters that best describe the experimental data.

When this fit procedure was performed for the three neurons for which imaging data were available, the **results in the minima** were

neuron	g [mS/cm^2]	$1/g$ [kΩcm^2]	r [Ωcm]	χ^2/D
A	0.054	19	447	1.15
B	−0.028	−36	385	1.70
C	0.036	28	236	0.85

where the column $1/g$ (corresponding to R_M in electrophysiologist nomenclature) was introduced for comparison. The values of $\chi^2/D \approx 1$ indicate that the shapes $S_n^{theo}(t)$ of the theoretical voltage transients corresponding to the minima of χ^2/D agree well with the target data for A and C [69]; for B, there is moderate agreement. In spite of this, however, the parameters obtained from the fits are **not very convincing for three reasons**:

- For cell B, the value obtained for the conductance g of the neuritic membrane is negative, which makes no sense at all.
- The input conductances of the model neurons that are obtained if the fit results g and r, the somatic conductance g_s from section 5.1 and the cell geometry are plugged into (28) do not agree with the steady state input conductances measured in the real neurons with current steps as in section 5.1. Specifically, the experimental and theoretical input conductances and the theoretical soma conductances of the three neurons are

neuron	experiment	fit	
	G [nS]	G_s [nS]	G [nS]
A	8.5	7.4	13.0
B	1.1	10.0	-
C	3.2	6.4	10.1

(for cell B, the theoretical input conductance G can not be computed because of the negative value of g). Note that for cells B and C, even the computed somatic conductance G_s alone – without the additional contributions from the input conductances of the two neurites – is larger than the experimentally obtained input conductance of the entire neuron.

- The theoretical somatic voltage transients for the best fits have much smaller amplitudes than the experimental voltage transients measured with the microelectrodes at the cell bodies of the three neurons. This is illustrated in the left part of fig. 5.5, where the experimental and theoretical transients at all three cell bodies are compared.

What is the reason for these considerable deviations between fit results and experimental data? If we assume that the cable model underlying the simulated transients gives a good description of the electrical behavior of neurons A through C, the only thing that can cause the discrepancies is a wrong value of one or several of the parameters that go into the model, namely the physical dimensions of the neurons and the values used for g_s, c_s and c. We now consider these **possible sources of error** to see which could have caused the deviations described above:

Possibility 1: The physical dimensions are wrong. The four physical dimensions of each neuron that are used in the fit are the soma diameter d_s, the two neurite lengths l_1 and l_2 and the neurite diameter d, and they are measured from a micrograph of the cell with an accuracy of (estimated) a few μm. Thus the relative error of l_1 and l_2 (which are on the order of several hundred μm) and of d_s (which is around 50μm) is at most a few % and is therefore too small to cause the deviations described above. In contrast, d is around 5μm, so its relative error could be rather large. To check if a wrong value of d could play a role in the observed deviations, artificial target

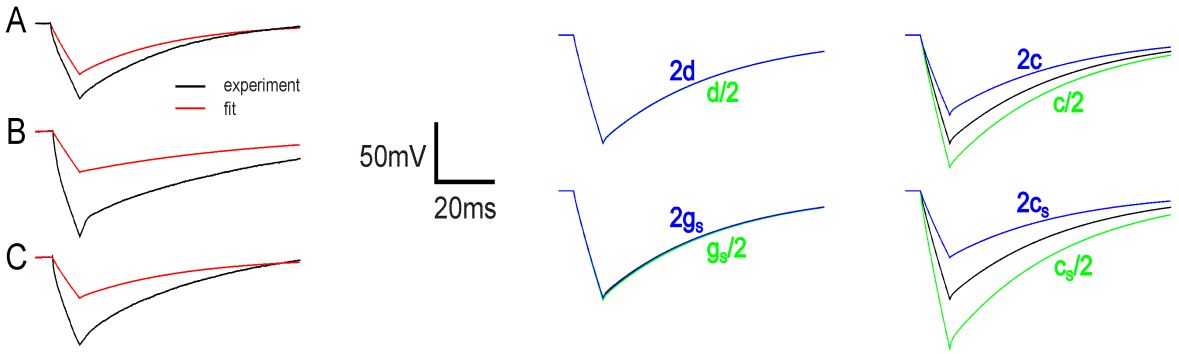

Figure 5.5: ***Somatic voltage transients from experiments and fits.*** *(**Left**) Somatic voltage responses (black) of cells A through C to brief current injections. If the optical target data from these experiments are fit as described in the text (using the parameters of neuriteless cell bodies), the somatic voltage transients corresponding to the best fits (red) have much too small amplitudes. (**Right**) Comparable transients from a model neuron. Artificial target data were simulated for the model cell and fit as with the real neurons. In each of the four panels, the black trace shows the somatic voltage transient of the model neuron and the blue and green traces show the transients corresponding to fit results obtained when one of the input parameters of the fit was half or twice its correct value: Wrong values of d or g_s have almost no effect, while a wrong value for either of the two capacitances c and c_s can cause deviations as they were observed for cells A, B and C.*

data were simulated for a model cell with the following physical dimensions (which are typical values for the cells used here) and electrical properties (which are the results from the fits done later on in this section): Soma diameter $d_s = 60\mu$m, neurite lengths $l_1 = 300\mu$m and $l_2 = 200\mu$m, neurite diameter $d = 5\mu$m, somatic membrane conductance $g_s = 0.020$mS/cm^2, somatic membrane capacitance $c_s = 1.1\mu$F/cm^2, neuritic membrane conductance $g = 0.035$mS/cm^2, neuritic membrane capacitance $c_s = 1.0\mu$F/cm^2, cytoplasmic resistivity $r = 394\Omega$cm. These artificial target data were then fit as described on page 45, using the correct values for all other parameters, but deliberately assuming wrong values for d. The resulting somatic voltage transients – shown in fig. 5.5 – are virtually identical to the original transient, indicating that a wrong value of d can not be responsible for the discrepancies observed for cells A through C.

Possibility 2: The value of c is wrong. The neuritic membrane capacitance was assumed to be $c = 1\mu$F/cm^2, which is the value most often cited for neuritic membranes [53][89]. To check if the observed discrepancies could be due to this value being different from the actual c in cultured *Lymnaea* neurites, the artificial target data from above were again fit, but this time assuming wrong values for c. These fit results are also shown in fig. 5.5; they indicate that discrepancies as they were observed for cell A through C could, in principle, be due to the real value of c in *Lymnaea* neurites being significantly smaller than the value of $c = 1\mu$F/cm^2 used in the fits.

Possibility 3: The value of g_s is wrong. For the fits, a value of $g_s = 0.063$mS/cm^2 was assumed – this is the average somatic membrane conductance of neuriteless cell bodies (see section 5.1). As mentioned above, however, the soma conductances obtained from this value and the soma diameters of neurons B and C with (3) are already larger than the experimentally obtained input conductances of these two cells, even without the additional input conductances of the two neurites. This means that the actual value of g_s in these two neurons must be considerably smaller than 0.063mS/cm^2. Thus, the discrepancies observed for these neurons are at least partly due to a wrong value of g_s. But such a wrong value can not explain all of the observed deviations: If the artificial target data from above are fit with wrong g_s, the resulting voltage traces at the cell body have the correct amplitude. This is illustrated in fig. 5.5; it implies that g_s is not the only parameter whose value was wrong in the fits.

Possibility 4: The value of c_s is wrong. The value of $c_s = 2.6\mu$F/cm^2 used in the fits is also derived from the experiments on neuriteless cell bodies in section 5.1. Fitting the artificial target data from above with a wrong value for this parameter leads to discrepancies between the correct somatic voltage transient and that obtained from the fit that are similar to the discrepancies observed for cell A, B and C, as is again illustrated in fig. 5.5. This suggests that c_s in the three cells may be smaller than 2.6μF/cm^2.

In summary, these considerations indicate that **cell bodies of Lymnaea neurons that have grown neurites in culture are different from those of neuriteless cell bodies** at least with respect to their membrane conductance g_s. Additionally, **either the somatic membrane capacitance c_s or the neuritic membrane capacitance c – or both – must be smaller than assumed up to now** on the basis of section 5.1 and of neurite capacitance values from the literature [53][89].

The fit with revised parameters

As we obviously can not use the value of g_s determined in section 5.1 and either c_s or c or both must also be smaller than previously thought, we are back to **five unknowns again**, namely g, r, g_s, c_s and c. With the additional information provided by the experimentally determined steady

state input conductances of the three neurons A, B and C (listed in the table on page 46), however, we can arrive at a rough estimate of the value of g_s for each cell and can thus reduce the number of fit parameters to four.

The **somatic membrane conductance g_s of a neuron of known geometry can be roughly estimated** from its total steady state input conductance as follows: According to (28), the input conductance of the neuron is

$$G = G_s + \sum_{j=1}^{J} \frac{\tanh L_j}{\lambda_j R_j} \tag{52}$$

where the sum runs over all neurites and $L_j = l_j/\lambda_j$ is the electrotonic length of neurite j. From the propagation maps for hyperpolarizing signals in all three neurons (that will be presented in the next section in figs. 5.7 and 5.8) one can derive that the cells are electrotonically compact, implying that $L_j < 1$. Thus we can safely make the approximation $\tanh L_j \approx L_j$. With this and the definitions of G_s and λ_j, (3) and (9), the input conductance of the neuron can be approximated by

$$G \approx g_s \pi d_s^2 + g \sum_{j=1}^{J} \pi d_j l_j \tag{53}$$

which, not surprisingly, is just the total membrane conductance of soma and neurites – this is what we expect for an electrotonically compact neuron because it is also approximately isopotential. If we additionally assume that $g \approx g_s$ (which is why the result of these considerations can only be a very rough estimate of g_s), we can solve for g_s and obtain

$$g_s \approx \frac{G}{\pi d_s^2 + \sum_{j=1}^{J} \pi d_j l_j} \tag{54}$$

Estimating g_s with this equation for each neuron individually **brings the number of unknown variables down to four**, namely g, r, c_s and c.

According to the simulations and fits in the right part of fig. 5.5, the deviations illustrated for neurons A, B and C in the left part of the figure could be due to the value of $c_s = 2.6\mu$F/cm^2 and/or $c = 1.0\mu$F/cm^2 used in the fits being larger than the real value in snail neurons. To **check whether using smaller values of c in the fit leads to better agreement** between the experimental and theoretical voltage transients at the soma, the fit procedure described on page 45 was repeated for each of the three neurons, but now with the estimated values of g_s according to (54) and for different values of c below 1.0μF/cm^2. While the amplitude of the theoretical transients at the soma that resulted from these fits slightly increased for decreasing c and thus approached the amplitude of the measured somatic transients, the improvement was only small: Even for a value of the neuritic membrane capacitance as small as $c = 0.2\mu$F/cm^2, the amplitude of the theoretical somatic transient was still only 83% (cell A), 46% (cell B) and 61% (cell C) of the experimental transient's amplitude. Thus even values of c that are well below the capacitance of a pure lipid bilayer [53] are not small enough to simultaneously fit the target data from the neurites *and* the somatic transient measured with the microelectrode – **a wrong value of c can therefore not explain the large deviations** in the left graphs in fig. 5.5. While this does not rule out the possibility that c actually *is* smaller than 1.0μF/cm^2, but is responsible for only a small part of the deviations, it shows that the predominant part of the deviations must be caused by $c_s = 2.6\mu$F/cm^2 being too large. In order to keep the number of fit parameters as small as possible, the neuritic

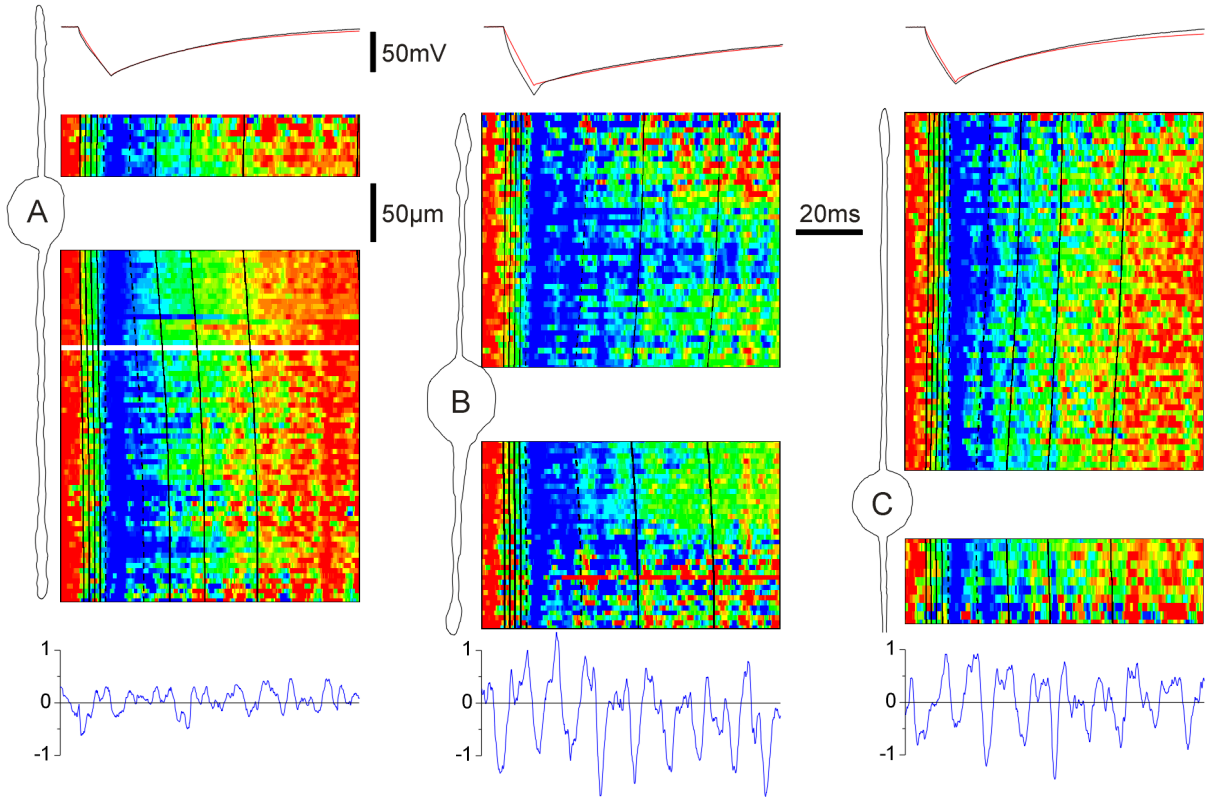

Figure 5.6: ***Target data and fits for all three neurons.*** *This figure shows fit results obtained with the revised soma parameters for neurons A, B and C. For each cell, the graphs show: (**Top**) Experimental voltage transient (black) at the soma in response to a hyperpolarizing current pulse and theoretical somatic transient for the best fit (red). (**Middle**) Outline drawing of the neuron, along with the superimposed graphs of target data and fit. The color code for the target shapes $S_n^{fluo}(t)$ runs from -1 (blue) to 0 (red) while the fits $S_n^{theo}(t)$ are represented as contour maps with lines for the values -0.1, -0.3, -0.5, -0.7 and -0.9 (the latter one dashed). (**Bottom**) Difference between target data and fit, for each diode divided by the standard deviation of the target data and averaged over all diodes.*

membrane capacitance was therefore left at $c = \mathbf{1.0\mu F/cm^2}$ **for the rest of this work**.

This leaves only **three unknown parameters**, namely g, r and c_s. These were now determined for each of the neurons A, B and C by fitting the target data basically as described on page 45, but with the following differences:

- For the somatic membrane conductance, the estimated value according to (54) was used instead of $g_s = 0.063\text{mS/cm}^2$.
- The fit was performed for different values of c_s smaller than $2.6\mu\text{F/cm}^2$.
- The fit result that best reproduced the experimentally obtained somatic voltage transient was selected as the final result.

These results are shown in fig. 5.6 for the three neurons, and the **parameter values for the best fits** are listed in the following table:

neuron	g_s [mS/cm^2]	c_s [μF/cm^2]	g [mS/cm^2]	r [Ωcm]	λ [μm]	τ [ms]	χ^2/D
A	0.038	1.5	0.043	469	899	23	1.15
B	0.005	0.9	0.030	476	1113	33	1.70
C	0.016	0.8	0.033	236	1237	30	0.84
mean	0.020	1.1	0.035	394	1083	29	
$\pm$s.d.	$\pm$0.017	$\pm$0.4	$\pm$0.007	$\pm$137	$\pm$171	$\pm$5	

For those more familiar with the values of R_M in electrophysiology literature: The mean values of $g_s = 0.020$mS/cm^2 at the soma and $g = 0.035$mS/cm^2 in the neurites correspond to $1/g_s = 50$kΩcm^2 and $1/g = 29$kΩcm^2.

Reliability of the fit results

As the values of $\chi^2/D \approx 1$ and the residues in fig. 5.6 indicate, the fits for cells A and C agree well with the target data [69], and for these two cells, the experimental somatic voltage transients and those for the fits also look rather similar. The fit for neuron B is not quite that good: The value of χ^2/D in the minimum is larger, the residue shows a slight curvature and the somatic transient corresponding to the fit lacks a fast component that is present in the experimental transient. But in general, **the new fits have solved two of the problems** that the fits using the somatic parameters from section 5.1 still had (see page 45): They do not lead to negative values of g and they result in somatic voltage transients that agree much better with the experimental transients than those from the previous fits.

The new fits do, however, not fully solve the third problem discussed on page 45, namely the discrepancies between the experimentally obtained total input conductances of the three cells and the input conductances as computed from g_s, g, r and the physical dimensions of the cells with (28): The experimental and computed values are

neuron	G from experiment [nS]	G from fit [nS]
A	8.5	8.9
B	1.1	3.4
C	3.2	4.9

In all three cases, **the input conductance G expected from the fit results is larger than the experimental value**, albeit the difference is rather small for cell A.

An attempt was made to solve this problem by repeating the fits with yet another strategy: Instead of using the somatic membrane conductance g_s estimated with (54), the value of g_s was computed from the momentary values of g and r during the fit by using (28). This forces the input conductance of the model cell to be equal to the experimentally obtained input conductance – however, it produces fit results that do not simultaneously agree with both the target data from the neurites and the somatic voltage transient.

What could be the reason for this failure to find a set of parameters that is consistent with the imaging data from the neurites, the voltage transient at the cell body *and* the input conductance value? One thing that comes to mind is the difference between the experimental conditions under which the neuritic and somatic data on the one hand and the total input conductance on the other hand were obtained: For the imaging experiments, it was crucial that the membrane voltage throughout the neuron had the same value at the beginning and at the end of the optical recording period to allow the separation of fluorescence intensity changes caused by voltage changes from those due to dye bleaching (see section 3.2.3). This calls for a brief stimulus and thus a *transient*

response, which, in addition, can yield more information about electrotonic architecture than a steady state response [63]. In contrast, determining the input conductance of a neuron requires, by definition, that the values of somatic membrane voltage and total current flowing into the soma be measured for two different *steady states* of the voltage distribution (usually the resting state and a more hyperpolarized state). If the neuron was perfectly passive, the membrane conductance obtained from transient responses and from steady states should be the same, but as the membrane of the cell is only approximately passive (see section 5.1), it is conceivable that **slow conductance changes may influence the value obtained for the input conductance with long-lasting current injections, but have less effect on the membrane conductance value obtained from a transient response**.

As the rough estimates of g_s that were computed with (54) and then used in the fits were based on the small experimentally obtained input conductances, they are presumably smaller than the real somatic membrane conductances of the three cells during a transient response. Because of this, and also because these values were rough estimates from the beginning, they are the least reliable inputs used for the fits. To see if the fit results would be considerably different if larger values were used for g_s, a series of test fits were performed that followed the same protocol as the new fits described above, but used values of g_s that were twice as large as the estimates from (54). The fits obtained in this manner show that the influence of g_s on most of the fit results is weak: The fits and the corresponding somatic voltage transients were virtually identical to those obtained with the estimated values of g_s, and the changes in the average values of c_s and r were only -1.9% and -1.5%, respectively. Only the average result obtained for g differed by -56% from that of the original fits.

In summary, **the fit results of $c_s = (1.1 \pm 0.4)\mu$F/cm^2 and $r = (394 \pm 137)\Omega$cm are quite reliable, but the values of $g_s = (0.020 \pm 0.017)$mS/cm^2 and $g = (0.035 \pm 0.007)$mS/cm^2, while being in the right range, may be too small (in the case of g_s) and too large (in the case of g)** to reflect the real conductances of cultured *Lymnaea* neurons. Note that a larger g_s and a smaller g would also be more consistent with the literature, were the somatic membrane usually is assumed to be more conductive than the neuritic membrane [14][15][45][49] – hence the name 'somatic *shunt* cable model'.

Rather dramatically, the residues for cells B and C (and to a lesser degree also that for cell A) shown at the bottom of fig. 5.6 reflect the 100Hz intensity oscillations of the excitation lamp (due to the 50Hz power supply frequency) that are also visible as vertical stripes in the target data. But as their period is considerably faster than the decay of the hyperpolarized voltage transient, they can not have severe influence on the fit result.

Discussion of the electrical parameters

Like the membrane conductances obtained for neuriteless cell bodies in section 5.1, the values of g_s estimated with the aid of (54) are highly variable, but their average $g_s = 0.020$mS/cm^2 is by about a factor of three smaller than that found for cells without neurites (which was $g_s = 0.063$mS/cm^2, see page 42). Interestingly, the average membrane capacitance of $c_s = 1.1\mu$F/cm^2 found here is also by about a factor of 2.4 smaller than the average of $c_s = 2.6\mu$F/cm^2 found for neuriteless cell bodies (see page 41). This means that the ratio of g_s and c_s – which is independent of errors in the measured membrane area due to sub-microscopic membrane invaginations – is similar in both cases. The number of channels per area of lipid bilayer therefore seems to be

about the same for cell bodies with or without neurites, but cells that have grown neurites seem to have a smaller somatic membrane area than neuriteless cells with the same diameter, suggesting that **their somatic membrane may display less extensive invaginations and foldings**.

The conductances g_s and g of the soma and neurites are both very small compared to the membrane conductance of a Hodgkin-Huxley neuron, which is on the order of 40 times larger (see section 4.3). However, the membrane conductance varies widely between different types of neurons, and the values found here are well within the range of previously reported conductances, which can be as low as 0.01mS/cm^2 (for the giant axon of the marine worm *Myxicola infundibulum* [89]). They are also similar to values reported for cultured leech neurites (g = 0.05mS/cm^2, [26]) and cultured hippocampal pyramidal neurons from rat (g = 0.07mS/cm^2, [65]).

The cytoplasmic resistivity of r = 394Ωcm found here is also rather high compared to the Hodgkin-Huxley value of 35Ωcm, but is again in the same range as values reported for other neuron types [53][89].

Most relevant for the following chapters is the **space constant** λ that results from these electrical parameters. Computing λ for cells A, B and C according to its definition (9) results in the values listed in the table above – they are all on the order of 1000μm. Given the typical lengths of cultured *Lymnaea* neurites of several hundred microns, this enormous space constant implies that the **cultured snail neurons are electrotonically compact**, meaning that their typical neurite lengths are smaller than their space constant – in such compact neurons, a voltage change induced at the cell body is hardly dampened along the neurites and spreads very quickly throughout the neuron, such that the cell is close to isopotential at any given time.

Because the cells are so compact, designed neural networks assembled from *Lymnaea* neurons may not be the ideal system for studying the influence of electrotonic cell architecture on the performance of the network. They hence are **more suitable for investigations concerning the *inter*cellular than the *intra*cellular signal processing** in small neural nets.

5.3 Maps of signal propagation

The imaging data obtained in the previous section – besides providing crucial information about the electrical properties of the cultured *Lymnaea* neurons – also allow us to construct **maps of signal propagation** for the three neurons. These maps are constructed and discussed in the present section.

The maps constructed here have a spatial resolution between 3.9μm at the edges and 5.3μm in the center of the photodiode array (see section 3.2.2) and cover about 500μm of neuron. Maps of similarly **high resolution and spatial extent** have previously been obtained for cultured leech neurons [26] and rat neurons [65], but due to the limited size of the recording devices used there, they had to be assembled from several 'shots', displacing the recording device with respect to the cell between recordings. Maps with a spatial resolution below 5μm and **obtained with a single shot**, like the maps shown here, existed only for leech neurites up to now [70].

Maps for neuron A

To obtain the maps, we start from the bleaching-corrected fluorescence transients $-\Delta F_n(t)$ recorded during action potential and hyperpolarization that were obtained in the previous section. But to

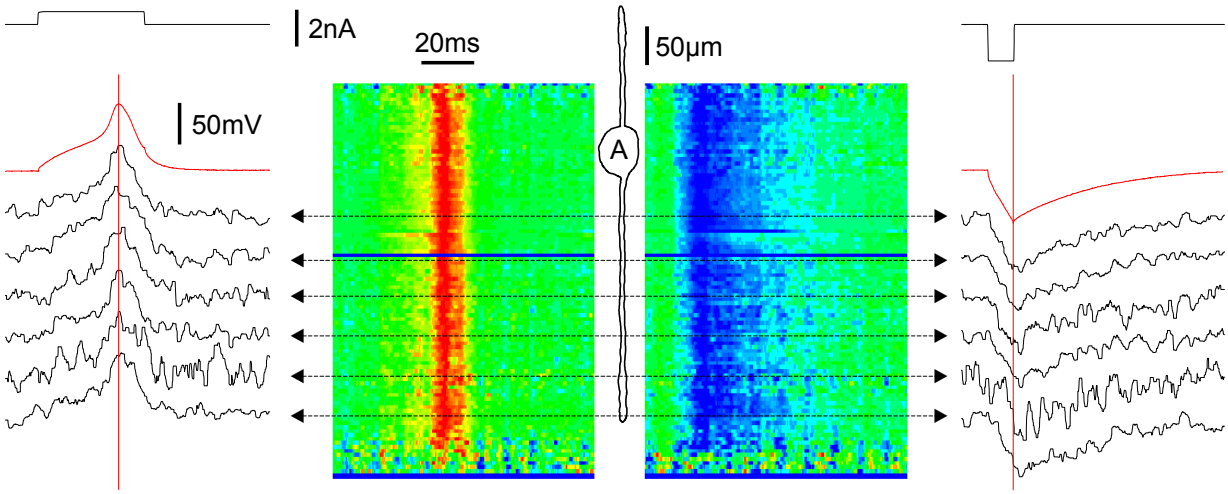

Figure 5.7: ***Spatio-temporal maps of signal propagation in neuron A.*** *(**Center**) Outline drawing of neuron A. (**Left**) Color-coded map of an action potential propagating through neuron A. The map was aligned with the drawing of the cell such that they share the same (vertical) spatial axis. (**Far left**) The current injected into the soma to trigger the action potential (top), the action potential as recorded with the electrode at the soma (red) and reconstructed voltage transients from the six different locations on the neurite that are indicated by the dashed, horizontal lines. The red, vertical line marks the time of the voltage peak at the soma. The action potential propagation along the neurite is almost instantaneous. (**Right**) Propagation map for the hyperpolarization. The color code is the same as for the left map – it ranges from red for the peak of the action potential at $+14$mV down to blue for the maximum hyperpolarization (-126mV). (**Far right**) The hyperpolarizing current injected into the soma (top), the somatic voltage transient it caused as recorded with the electrode (red) and reconstructed voltage transients for the six locations indicated by the dashed lines. The vertical, red line marks the time of maximum hyperpolarization at the soma. Over the approximately 300μm length of the neurite, the peak of the hyperpolarization is delayed by only about 2ms.*

solve the problem of unknown proportionality factors between the voltage changes at different sites on the neurite and the fluorescence intensity changes they cause, we now apply alternative II from section 3.2.3, that is, we make the additional assumptions of constant action potential amplitude and constant resting potential to reconstruct the voltage transient 'seen' by each diode.

Fig. 5.7 shows the results of this signal processing for neuron A. As this figure contains a lot of information about the properties of the neuron and the imaging method, it needs discussion: Concerning the **properties of the neuron**, fig. 5.7 shows that

- the time course of the action potential at any given location on the neurite is rather slow, displaying a half-width of about 15ms as compared to only 2ms for an action potential simulated with Hodgkin-Huxley dynamics (see fig. 4.4). This is another indication that the Hodgkin-Huxley model of neural membrane dynamics does not apply well to pedal A-cluster neurons from *Lymnaea stagnalis*. Such **slow action potentials** are normal in *Lymnaea* neurons [93], and the action potential also shows the 'type 2' shape typical for neurons from the pedal A-clusters [93], albeit not as strongly as the action potentials of cells B and C in fig. 5.8.
- the **spread of the action potential through the neurites is very fast** – so fast that hardly any delay can be detected between the action potential measured at the soma and at the tip of the 300μm-long neurite. Because the time it takes for the action potential to propagate throughout the neuron is so much shorter than the duration of the action potential, the cell is approximately isopotential at any given time.
- the amplitude and shape of the hyperpolarizing pulse are apparently constant along the neurite;

neither damping nor broadening of the signal are detectable. This also indicates that the neuron is **electrotonically compact** – consistent with the findings from the previous section.

- the hyperpolarization spreads very quickly, too. Presumably because the peak of this pulse is sharper than the peak of the action potential, it is easier to identify it in the noisy fluorescence transients. This allows us to estimate the time it takes for the hyperpolarization to propagate the 300μm from the soma to the tip of the neurite, resulting in a **propagation velocity of (very roughly) 150μm/ms**. Very similar velocities have previously been reported for cultured leech neurons [26][70] and hippocampal rat dendrites in cell culture [65].
- both action potential and hyperpolarization are clearly discernible even at the ultimate tip of the neurite. This proves that the killed end boundary condition briefly considered in section 4.1.1 is clearly not applicable here – it would force the membrane potential at the tip to be zero at all times.

And concerning the **imaging**, fig. 5.7 demonstrates that

- the signal processing as described in section 3.2.3 is suitable for reconstructing meaningful voltage transients for most of the diodes. A few exceptions can be seen as horizontal, blue lines in fig. 5.7: For two diodes at the bottom edge of the spatio-temporal maps and one diode close to the middle of the array, the baseline fluorescence intensity seemed to *increase* instead of bleaching according to the mono-exponential decay from (1) and could therefore not be fit to this equation[9]. Such exceptional diode signals were not used for determining the neuritic parameters in section 5.2.
- a stable excitation light source is important for successful imaging, because even the 100Hz-oscillations (caused by the 50Hz power supply frequency) of the lamp used here – that have a peak-to-peak amplitude of below 0.05% – are visible as vertical lines in the maps in fig. 5.7 – for example in the right half of the hyperpolarization map. This problem is more pronounced here than in other systems because the protein layer on which the cells grow (see chapter 2) causes a large background fluorescence that contributes to the oscillating signal, but not to the voltage-dependent signal.
- the image of the cell in the plane of the diode array – at least at its edges – seems to be a little blurred, because the voltage-dependent intensity changes are even detected by diodes that image an area a few μm *beyond* the tip of the neurite (see, for example, the bottom part of the maps in fig. 5.7). This blurring effectively smooths the map in the spatial dimension.

More maps for neurons B and C

Fig. 5.8 shows similar propagation maps for neurons B and C, constructed in the same way as in fig. 5.7. The results are the same: Again, the propagation of action potential as well as hyperpolarization is very fast and there is hardly any decrease in the amplitude of the hyperpolarizing pulse along the neurite. Especially for neuron B, there is again a rather strong modulation of the fluorescence intensity by the 100Hz-oscillations of the excitation light source, contaminating the actual voltage-dependent signal.

Taken together, the maps presented here show that **imaging of neuritic voltage transients** with fluorescent dyes is not only **crucial for determining the electrical parameters of a neuron** (as done in the previous section), but can also **provide a lot of additional information about the**

[9] Such an apparent increase could arise from very small overall intensity combined with large noise (for the two diodes at the only weakly illuminated edge of the photo-diode array) or from a fluoresceing object such as a stained glia cell drifting through the 'receptive field' of the diode during the recording (in the case of the third diode).

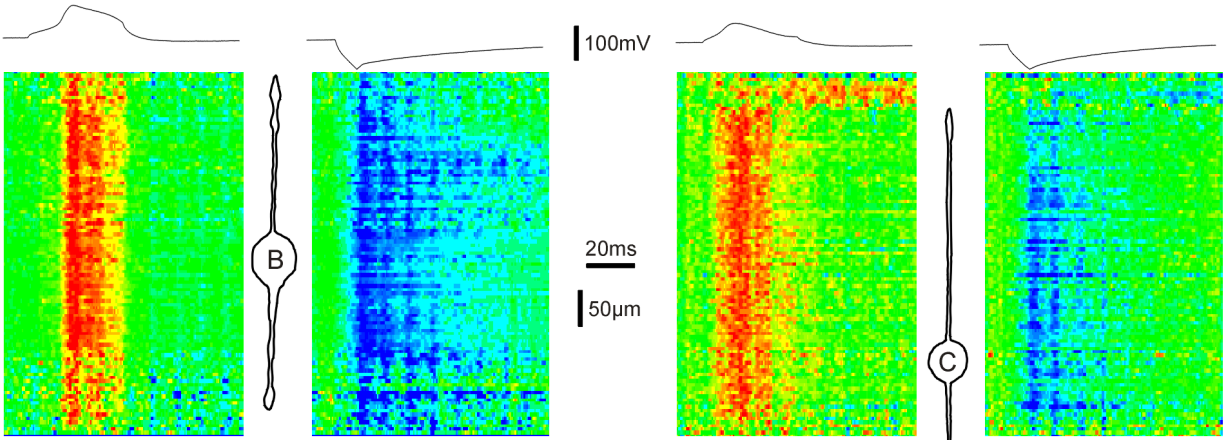

Figure 5.8: ***Propagation maps for neurons B and C.*** *For each neuron, this figure shows an outline drawing of the cell (note that the bottom neurite of cell B extends beyond the figure) and a propagation map for an action potential (to the left of the drawing) and a hyperpolarization (to the right). The color code was chosen individually for each cell such that it ranged from red for the peak of the action potential (+32mV for cell B and +10mV for cell C) to blue for the hyperpolarizing peak (−158mV and −128mV, respectively). The trace above each map shows the potential recorded at the soma with a microelectrode. Injected currents were the same as in fig. 5.5.*

voltage dynamics in neurons that is not available from standard electrophysiology alone.

6
Theory, part 2: Models of electrical synapses

As discussed in section 1.2, the A-clusters in the pedal ganglia of *Lymnaea stagnalis* provide a source of many similar neurons that can be expected to re-establish their electrical synapses in cell culture – which is the reason why they are used in this study. The present chapter, before introducing and discussing two models of electrical synapses in sections 6.2 through 6.5, summarizes what is presently known about the molecular structure of electrical synapses because this structural information is needed for constructing the equivalent circuits in the two models.

6.1 Structure of electrical synapses

Electrical synapses are a sub-class of a type of cell-cell contact called 'gap junction' – they are **gap junctions between nerve cells**. Some typical features of gap junctions are illustrated in fig. 6.1: The plasma membranes of the two cells that form the junction come close together, leaving a gap of only a few nanometers. If sectioned perpendicular to the membrane plane, the junction exhibits a seven layer structure, and electron micrographs of freeze-fractured junctions reveal hexagonal channels that are sometimes tightly packed in a 2D-lattice. The size of the junction plaque can vary considerably, ranging from several microns across in liver gap junctions down to only a few channels in some electrical synapses [97]. Each channel consists of two hemichannels – one from each cell – and each hemichannel has six monomeric subunits that are proteins with four trans-membrane helices. The **pore size of the channels is large** compared to other ion channels, usually 1-3nm in diameter, and allows the passage of ions and molecules whose molecular weight is below about 1000 Daltons.

At the molecular level, a lot is known about *vertebrate* gap junctions (for a series of minireviews on many aspects see [6][57][58][60][64][80][87][91][92]): Their monomers are members of a family of proteins called 'connexins'; fittingly, a hemichannel consisting of six connexins (that can be of different types) is called a 'connexon'. Each connexin has four membrane-spanning helices that form the channel, two extracellular loops that are important in cell-cell recognition and docking between the hemichannels, and cytoplasmic domains that influence physiological properties of the channel such as selectivity and voltage dependence.

Invertebrates have no connexins!

Unfortunately, no connexin homologues have been found in *in*vertebrates despite extensive search [19] and despite the fact that invertebrates do have functional gap junctions that show a structure very similar to that of vertebrate gap junctions if examined with electron microscopy or atomic force microscopy [46]. **Two protein families** have now been suggested as the molecular basis of invertebrate gap junctions: In the lobster *Nephrops norvegicus*, ductin has been identified as

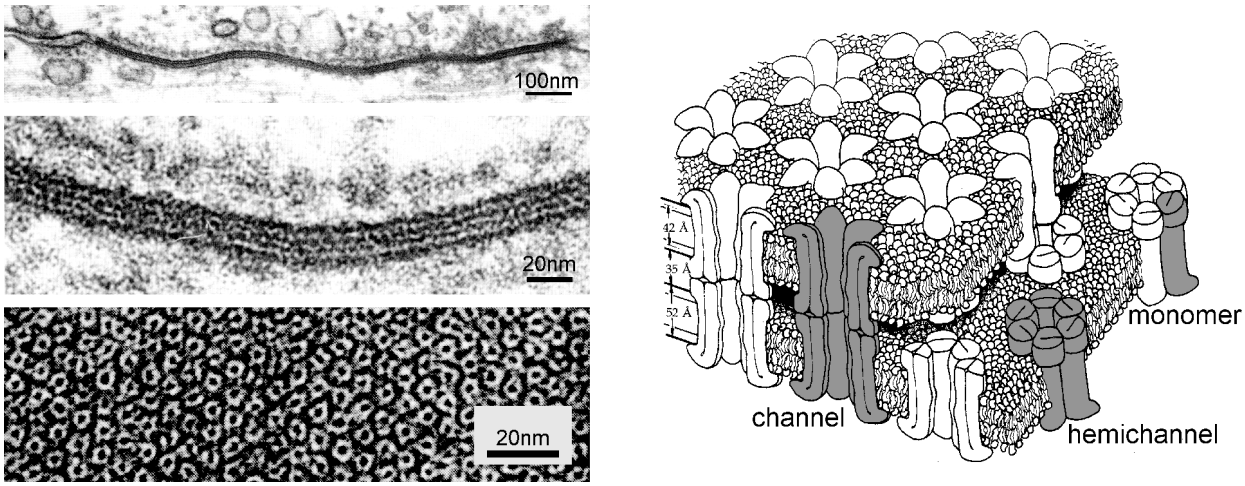

Figure 6.1: ***Gap junction structure.*** *(**Left, top**) A long gap junction from a salamander brain in thin section. At the far left and right edges, the membranes of an axon (top) and a dendrite (bottom) are several tens of nm apart; at the synapse, their form a thin gap. From* [3]. *(**Left, middle**) Enlarged view of the same synapse. The gap junction exhibits the typical seven layer structure. (**Left, bottom**) Micrograph of a gap junction from rat liver. The junction is viewed perpendicular to the membrane. Single channels are resolved; they form a hexagonal lattice. From* [47]. *(**Right**) Diagram of a gap junction showing the molecular components of the channels. From* [41].

the major protein component of gap junction plaques [20]. Just as the connexins, ductin has four trans-membrane helices and forms hexamers of very similar dimensions as the connexons, but it shares no sequence homology with the connexins and its intracellular C-terminus is significantly shorter than the corresponding terminus in connexins that is implicated in selectivity and gating [46]. Proteins of yet another family – called 'OPUS' proteins (after the drosophila mutants l(1)**o**gre, **p**as, **u**nc-7 and **s**hakB) or, more recently, 'innexins' (for invertebrate connexins) – have been identified as the likely molecular basis of gap junctions in the nematode *Caenorhabditis elegans*, the fruitfly *Drosophila melanogaster* and the grasshopper *Schistocerca americana* [33]. These innexins, too, have a tertiary structure similar to the connexins but share no sequence similarities with them.

Whether the ductins or innexins also form the gap junctions in the pond snail is not known, so all we can say about the structure of the electrical synapses studied here is that they are likely to be **large-diameter pores connecting the cytoplasms of the two cells and allowing the passage of small ions and molecules**.

6.2 Simple model based on isopotential cells

According to the previous section, electrical synapses are just molecular tubes connecting the cytoplasms of two neurons. This suggests that the equivalent circuit element that best describes the electrical behavior of an electrical synapse is a conductance – in the simplest case, when the electrical synapse shows no voltage-dependence, an **ohmic conductance**. In the oldest equivalent circuit for an electrical synapse, a junction capacitance in parallel to the conductance was briefly considered, but immediately demonstrated to be negligible because the time constant of the junction is so much smaller than the time constant of the neural membrane that the junction effectively behaves like a conductance alone [2].

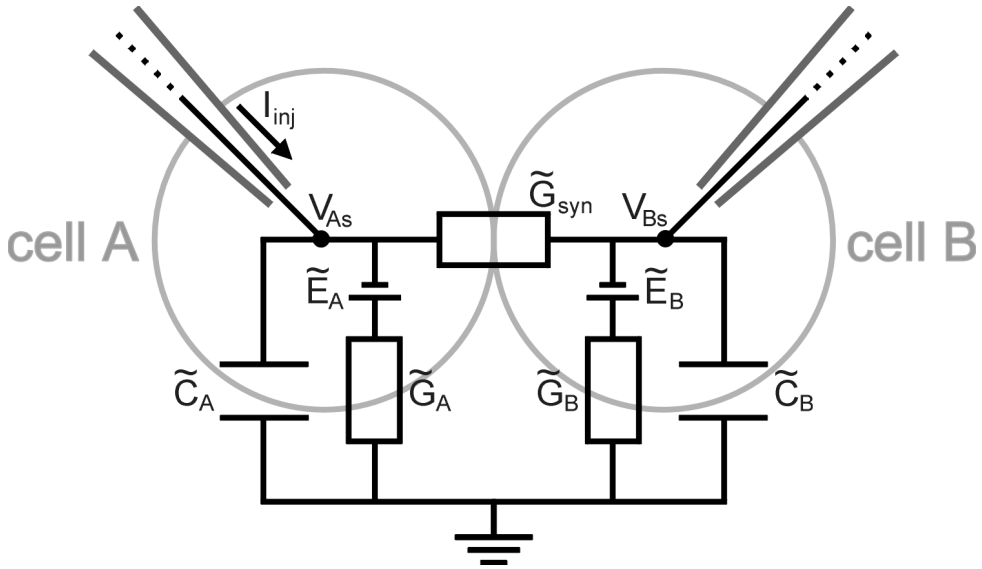

Figure 6.2: ***Simple model for an electrically coupled pair of neurons.*** *This figure shows the equivalent circuit for a cell pair connected via an electrical synapse if each cell is represented by a single isopotential compartment. The cell and synapse parameters in this simplified model all carry a tilde to distinguish them from the corresponding parameters in the detailed model in the next section. Cell A is always presynaptic; no current is injected into cell B.*

Given the models of single cells introduced in chapter 4, the straightforward way to model a pair of neurons connected by an electrical synapse therefore is to represent both cells with equivalent circuits as in fig. 4.1 and to connect the two circuits via a conductance that stands for the synapse. But before this detailed model is discussed in the next section, it is instructive to consider a simplified version. What distinguishes this **simple model** from the detailed model is that it describes each cell as a single isopotential compartment, **neglecting any voltage gradients within the cell**; the equivalent circuit for this model is shown in fig. 6.2. This model is similar to the model of two electrically coupled cells first introduced by Bennett [2], but it includes two additional batteries $\widetilde{E}_A$ and $\widetilde{E}_B$ that stand for the resting potentials of the two cells. Note that, to distinguish them from the parameters of the detailed model introduced in the next section, all parameters in the simplified model feature a tilde.

Differential equations for the membrane voltages

For the derivation of the synaptic conductance $\widetilde{G}_{syn}$ from experimental data in chapter 7, we need expressions for the voltage responses of the coupled cell pair to current injections into the presynaptic cell. These voltage responses[10] $V_{As}(t)$ and $V_{Bs}(t)$ are governed by **two differential equations** that are readily obtained by summing all the currents entering and leaving the cells. For the presynaptic cell A, this gives

$$I_{inj} = \widetilde{C}_A \frac{dV_{As}}{dt} + \widetilde{G}_A(V_{As} - \widetilde{E}_A) + \widetilde{G}_{syn}(V_{As} - V_{Bs}) \tag{55}$$

where all variables are defined by fig. 6.2. And for the postsynaptic cell B, the corresponding equation is

$$\widetilde{G}_{syn}(V_{As} - V_{Bs}) = \widetilde{C}_B \frac{dV_{Bs}}{dt} + \widetilde{G}_B(V_{Bs} - \widetilde{E}_B) \tag{56}$$

[10] Note that the index 's' for 'soma' could be omitted, because for the isopotential model the voltage is the same throughout the neuron. But to avoid confusion in the next section, we keep it.

For any experimental cell pair, seven variables in these equations are unknown, namely the cell's conductances $\widetilde{G}_A$ and $\widetilde{G}_B$, capacitances $\widetilde{C}_A$ and $\widetilde{C}_B$ and resting potentials[11] $\widetilde{E}_A$ and $\widetilde{E}_B$ and the synaptic conductance $\widetilde{G}_{syn}$ (that we're most interested in). In the rest of this section, we derive **equations that link these unknown variables to measured currents and voltages** and thus allow us to determine them from experimental data in chapter 7. As a first step, we obtain expressions for the resting potentials and conductances from steady state experiments:

Steady state

In steady state, $dV_{As}/dt = dV_{Bs}/dt = 0$. If we put this into (55) and (56) and solve for the somatic voltages V_{As} and V_{Bs} of the two neurons, we obtain

$$V_{As} = \widetilde{E}_A - \frac{\widetilde{G}_B\widetilde{G}_{syn}\left(\widetilde{E}_A - \widetilde{E}_B\right)}{\widetilde{G}_A\widetilde{G}_B + \widetilde{G}_{syn}\left(\widetilde{G}_A + \widetilde{G}_B\right)} + \frac{\widetilde{G}_B + \widetilde{G}_{syn}}{\widetilde{G}_A\widetilde{G}_B + \widetilde{G}_{syn}\left(\widetilde{G}_A + \widetilde{G}_B\right)} I_{inj} \tag{57}$$

$$= \widetilde{E}_A - \frac{\widetilde{R}_A\left(\widetilde{E}_A - \widetilde{E}_B\right)}{\widetilde{R}_A + \widetilde{R}_B + \widetilde{R}_{syn}} + \frac{\widetilde{R}_A\left(\widetilde{R}_B + \widetilde{R}_{syn}\right)}{\widetilde{R}_A + \widetilde{R}_B + \widetilde{R}_{syn}} I_{inj} \tag{58}$$

$$V_{Bs} = \widetilde{E}_B + \frac{\widetilde{G}_A\widetilde{G}_{syn}\left(\widetilde{E}_A - \widetilde{E}_B\right)}{\widetilde{G}_A\widetilde{G}_B + \widetilde{G}_{syn}\left(\widetilde{G}_A + \widetilde{G}_B\right)} + \frac{\widetilde{G}_{syn}}{\widetilde{G}_A\widetilde{G}_B + \widetilde{G}_{syn}\left(\widetilde{G}_A + \widetilde{G}_B\right)} I_{inj} \tag{59}$$

$$= \widetilde{E}_B + \frac{\widetilde{R}_B\left(\widetilde{E}_A - \widetilde{E}_B\right)}{\widetilde{R}_A + \widetilde{R}_B + \widetilde{R}_{syn}} + \frac{\widetilde{R}_A\widetilde{R}_B}{\widetilde{R}_A + \widetilde{R}_B + \widetilde{R}_{syn}} I_{inj} \tag{60}$$

where, for (58) and (60), the conductances $\widetilde{G}_A$, $\widetilde{G}_B$ and $\widetilde{G}_{syn}$ were replaced by their inverses, namely $\widetilde{R}_A = 1/\widetilde{G}_A$, $\widetilde{R}_B = 1/\widetilde{G}_B$ and $\widetilde{R}_{syn} = 1/\widetilde{G}_{syn}$. While the equations in terms of resistances are simpler than in terms of conductances, the impact that the coupling and the injection current have on the steady-state voltage in the two neurons is better illustrated by (57) and (59). To see the **effect of synapse and current injection**, we consider several special cases:

- **No synapse, no current injection:** In this case, $\widetilde{G}_{syn} = 0$ and $I_{inj} = 0$. The second and third term on the right sides of the equations vanish and we find – not surprisingly – that the steady-state potential in each neuron is equal to its resting potential.
- **Current injection, but no synapse:** If we set $\widetilde{G}_{syn} = 0$ and $I_{inj} \neq 0$, there can be no effect of the injected current on neuron B; its potential is again equal to its resting potential. For cell A, we find that $V_{As} = \widetilde{E}_A + \widetilde{R}_A I_{inj}$, which is the steady-state version of (13) and shows that cell A, again just as expected, behaves like an isolated cell body.
- **Synapse, but no current injection:** With $\widetilde{G}_{syn} \neq 0$ and $I_{inj} = 0$, we see the effects of the coupling alone: The last terms on the right sides of both equations vanish, but the middle terms don't. They change the potential in each neuron in the direction of the other cell's resting potential, so even without current injection, the somatic potentials measured in the neurons are *not* the resting potentials. If we subtract (57) and (59) for this special case, we find that

$$V_{As} - V_{Bs} = \frac{\widetilde{R}_{syn}}{\widetilde{R}_A + \widetilde{R}_B + \widetilde{R}_{syn}}\left(\widetilde{E}_A - \widetilde{E}_B\right) \tag{61}$$

[11] The potentials measured in the two cell bodies when no current is injected into the cells are *not* the resting potentials. This is because for $E_A \neq E_B$ (which is usually the case), there is always a small amount of current flowing across the synapse that will pull the potentials in the cell bodies towards each other and away from their resting values.

This equation shows that, in all cases, the potential difference measured between the two cell bodies is smaller than the difference between the two resting potentials, so an electrical synapse between two neurons always pulls their steady-state potentials towards each other, but it also shows that for a synapse resistance $\widetilde{R}_{syn}$ that is much larger than the resistances $\widetilde{R}_A$ and $\widetilde{R}_B$ of the two neurons, the measured difference between the two somatic potentials is very close to the actual difference between the two resting potentials, so the effect of weak coupling on the somatic potentials is very small.

- **Synapse and current injection:** The third terms in both equations describe the additional voltage changes in the two neurons if not only $\widetilde{G}_{syn} \neq 0$, but also $I_{inj} \neq 0$. Both expressions are proportional to and have the same sign as the injection current, so a current step starting from zero injection current will always change the voltages in the two cells in the same direction. The postsynaptic term divided by the presynaptic term is $\widetilde{G}_{syn}/(\widetilde{G}_B + \widetilde{G}_{syn})$ and is called the 'coupling coefficient' k_{AB} ([2], also see (66) below); if the synaptic conductance $\widetilde{G}_{syn}$ is small compared to the conductance $\widetilde{G}_B$ of the postsynaptic neuron, k_{AB} is also very small and the impact of the injection current on the presynaptic neuron is much bigger than on the postsynaptic neuron. If, on the other hand, $\widetilde{G}_{syn}$ is much larger than $\widetilde{G}_B$, a current step injected into the presynaptic neuron changes the two somatic voltages by almost the same amount.

Resting potentials and conductances in terms of experimental data

We now seek to express the resting potentials and conductances in the equivalent circuit from fig. 6.2 in terms of currents and steady-state voltages that can be obtained with current step experiments:

If the current injected into the presynaptic cell is stepped from $I_{inj,0} = 0$ to $I_{inj,\infty}$, (55) and (56) yield four **steady state current balances** – one for each cell's steady state before the step (index 0) and after the step (index ∞):

$$\begin{aligned} 0 &= \widetilde{G}_A(V_{As,0} - \widetilde{E}_A) + \widetilde{G}_{syn}(V_{As,0} - V_{Bs,0}) && (62)\\ I_{inj,\infty} &= \widetilde{G}_A(V_{As,\infty} - \widetilde{E}_A) + \widetilde{G}_{syn}(V_{As,\infty} - V_{Bs,\infty}) && (63)\\ \widetilde{G}_{syn}(V_{As,0} - V_{Bs,0}) &= \widetilde{G}_B(V_{Bs,0} - \widetilde{E}_B) && (64)\\ \widetilde{G}_{syn}(V_{As,\infty} - V_{Bs,\infty}) &= \widetilde{G}_B(V_{Bs,\infty} - \widetilde{E}_B) && (65) \end{aligned}$$

A result that can immediately be obtained from these current balances is the expression for the coupling coefficient k_{AB} already mentioned above: The **coupling coefficient** is defined as the ratio of the post- and presynaptic voltage change [2]; by subtracting (64) and (65), we find that

$$k_{AB} = \frac{\Delta V_{Bs}}{\Delta V_{As}} = \frac{\widetilde{G}_{syn}}{\widetilde{G}_B + \widetilde{G}_{syn}} \qquad (66)$$

where $\Delta V_{As} = V_{As,\infty} - V_{As,0}$ and $\Delta V_{Bs} = V_{Bs,\infty} - V_{Bs,0}$. From its definition, it is obvious that the coupling coefficient k_{AB} is a good way to characterize the electrical synapse from a functional point of view because it quantifies the impact that presynaptic voltage changes can have on the somatic potential of the postsynaptic neuron. But (66) also shows that the coupling coefficient does not provide information about the synaptic conductance itself. Instead, it depends on the conductance $\widetilde{G}_B$ of the postsynaptic neuron and can therefore have different values for the two possible directions of signal transfer across the same synapse.

If (instead of subtracting them as above) we solve (64) and (65) for $\widetilde{G}_{syn}/\widetilde{G}_B$ and equate the two terms, we get an expression for the **resting potential of the postsynaptic cell**, cell B:

$$\widetilde{E}_B = \frac{V_{As,\infty}V_{Bs,0} - V_{As,0}V_{Bs,\infty}}{\Delta V_A - \Delta V_B} \tag{67}$$

Therefore, the resting potentials of both neurons in a pair can be found by doing two current step experiments, ascribing the role of presynaptic cell A first to one neuron and then to the other.

With both resting potentials known, an expression for the presynaptic neuron's conductance $\widetilde{G}_A$ can be obtained by eliminating $\widetilde{G}_{syn}$ from (62) and (63) and with the use of (67). This yields

$$\widetilde{G}_A = \frac{V_{As,0} - V_{Bs,0}}{\left(\widetilde{E}_A - \widetilde{E}_B\right)(\Delta V_{As} - \Delta V_{Bs})} I_{inj,\infty} \tag{68}$$

Plugging this into (62) gives

$$\widetilde{G}_{syn} = \frac{\widetilde{E}_A - V_{As,0}}{\left(\widetilde{E}_A - \widetilde{E}_B\right)(\Delta V_{As} - \Delta V_{Bs})} I_{inj,\infty} \tag{69}$$

and substituting this into (64) results in

$$\widetilde{G}_B = -\frac{V_{As,0} - \widetilde{E}_A}{V_{Bs,0} - \widetilde{E}_B} \frac{V_{As,0} - V_{Bs,0}}{\left(\widetilde{E}_A - \widetilde{E}_B\right)(\Delta V_{As} - \Delta V_{Bs})} I_{inj,\infty} \tag{70}$$

With (67) through (70), the **resting potentials and conductances of the two neurons and the synaptic conductance can be calculated from the steady-state voltages** measured at the two cell bodies before and after a current step injected into one of the cells.

This leaves only the capacitances to be determined – naturally, they can only be obtained by analyzing the dynamics of the cell pair's voltage response.

Dynamic solutions

To derive the time course of the two voltages $V_{As}(t)$ and $V_{Bs}(t)$ in response to a step in the presynaptic injection current from $I_{inj,0} = 0$ to $I_{inj,\infty}$ at time $t = 0$, we need to **solve the coupled differential equations** (55) and (56). Translated into the standard form of two coupled inhomogeneous differential equations, they look like

$$\frac{dV_{As}}{dt} = -\frac{\widetilde{G}_A + \widetilde{G}_{syn}}{\widetilde{C}_A} V_{As} + \frac{\widetilde{G}_{syn}}{\widetilde{C}_A} V_{Bs} + \frac{I_{inj} + \widetilde{G}_A \widetilde{E}_A}{\widetilde{C}_A} \tag{71}$$

$$\frac{dV_{Bs}}{dt} = \frac{\widetilde{G}_{syn}}{\widetilde{C}_B} V_{As} - \frac{\widetilde{G}_B + \widetilde{G}_{syn}}{\widetilde{C}_B} V_{Bs} + \frac{\widetilde{G}_B \widetilde{E}_B}{\widetilde{C}_B} \tag{72}$$

The transients solving this differential equation system are derived in appendix F; they are

$$\begin{aligned} V_{As} = V_{As,\infty} &- \left(\frac{\widetilde{G}_A + \widetilde{G}_{syn} - \widetilde{C}_A \nu_+}{\widetilde{C}_A (\nu_- - \nu_+)} \Delta V_{As} - \frac{\widetilde{G}_{syn}}{\widetilde{C}_A (\nu_- - \nu_+)} \Delta V_{Bs} \right) e^{-t/\tau_-} \\ &+ \left(\frac{\widetilde{G}_A + \widetilde{G}_{syn} - \widetilde{C}_A \nu_-}{\widetilde{C}_A (\nu_- - \nu_+)} \Delta V_{As} - \frac{\widetilde{G}_{syn}}{\widetilde{C}_A (\nu_- - \nu_+)} \Delta V_{Bs} \right) e^{-t/\tau_+} \end{aligned} \tag{73}$$

$$\begin{aligned} V_{Bs} = V_{Bs,\infty} &+ \left(\frac{\widetilde{G}_{syn}}{\widetilde{C}_B (\nu_- - \nu_+)} \Delta V_{As} + \frac{\widetilde{G}_A + \widetilde{G}_{syn} - \widetilde{C}_A \nu_-}{\widetilde{C}_A (\nu_- - \nu_+)} \Delta V_{Bs} \right) e^{-t/\tau_-} \\ &- \left(\frac{\widetilde{G}_{syn}}{\widetilde{C}_B (\nu_- - \nu_+)} \Delta V_{As} + \frac{\widetilde{G}_A + \widetilde{G}_{syn} - \widetilde{C}_A \nu_+}{\widetilde{C}_A (\nu_- - \nu_+)} \Delta V_{Bs} \right) e^{-t/\tau_+} \end{aligned} \tag{74}$$

with the two time constants τ_+ and τ_- and their inverses ν_+ and ν_- defined by

$$\nu_{+/-} = \frac{1}{\tau_{+/-}} \tag{75}$$

$$= \frac{1}{2}\left[\frac{\widetilde{G}_A+\widetilde{G}_{syn}}{\widetilde{C}_A} + \frac{\widetilde{G}_B+\widetilde{G}_{syn}}{\widetilde{C}_B} \pm \sqrt{\left(\frac{\widetilde{G}_A+\widetilde{G}_{syn}}{\widetilde{C}_A} - \frac{\widetilde{G}_B+\widetilde{G}_{syn}}{\widetilde{C}_B}\right)^2 + 4\frac{\widetilde{G}_{syn}}{\widetilde{C}_A}\frac{\widetilde{G}_{syn}}{\widetilde{C}_B}}\right] \tag{76}$$

Equations (73) and (74) show that the response of the model system from fig. 6.2 to a current step in cell A for both neurons is a **sum of only two exponential transients** and a constant. Note, however, that the dependence of the two time constants on the conductances and capacitances of the model is rather complicated; even for such a simple model, the form of the response is not exactly obvious.

For a given pair of neurons, the two capacitances $\widetilde{C}_A$ and $\widetilde{C}_B$ can be determined by fitting an experimentally obtained set of transients $V_{As}(t)$ and $V_{Bs}(t)$ to (73) and (74) with only $\widetilde{C}_A$ and $\widetilde{C}_B$ as fit variables – all other parameters can be derived from the two steady states before and after the current step as described above.

6.3 Detailed model

Compared to the isopotential model introduced above, the present section discusses a **more realistic model** that does not neglect the voltage gradients in the neuritic cables. Instead, it represents both neurons by equivalent circuits as in fig. 4.1 and connects them via an electrical synapse represented by a conductance – the complete model is shown in fig. 6.3. Again, all membranes are considered passive; for the membrane and cytoplasmic parameters g_s, c_s, g, c and r, the values from chapter 5 are used.

With the simpler model from the previous section, one can obtain the synaptic conductance $\widetilde{G}_{syn}$ from experimental data without any prior knowledge about the exact geometry or electrical properties of the two neurons involved. But due to the fact that this model neglects all cable effects in the neurites, the value of $\widetilde{G}_{syn}$ obtained in this manner can only be an approximation of the actual conductance of the synapse. **The detailed model discussed here will allow us to estimate how good this approxinmation is.**

Synaptic conductance in terms of experimental data

As for the simpler model, we first derive an **expression for the synaptic conductance** G_{syn} in

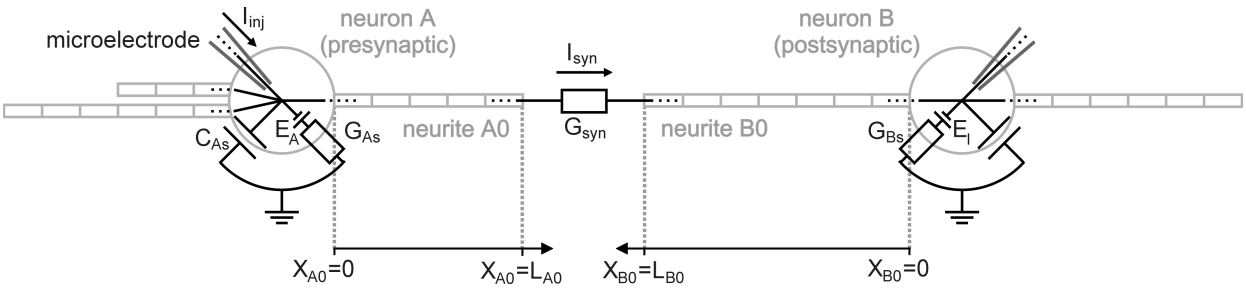

Figure 6.3: ***Detailed model of an electrically coupled cell pair.*** *This schema shows the equivalent circuit for two neurons that are coupled via an electrical synapse located at the distal tip of one of their neurites. All neurites are assembled from compartments as shown in fig. 4.1; for analytical computations, these compartments are infinitesimally small. The presynaptic neuron is always called 'neuron A'.*

terms of currents injected into and voltages measured at the cell bodies in steady state. According to Ohm's law, G_{syn} is related to the current I_{syn} flowing through the synapse and the membrane voltages $V(L_{A0})$ and $V(L_{B0})$ at the tips of the two neurites A0 and B0 via

$$G_{syn} = \frac{I_{syn}}{V(L_{A0}) - V(L_{B0})} = \frac{I_{syn}}{[V^e(L_{A0}) + E_A] - [V^e(L_{B0}) + E_B]} \tag{77}$$

where (8) was used to replace the membrane potential V by the electrotonic potential V^e. If a current step is injected into the presynaptic cell A (while no current is applied to cell B) and the two steady states before and after the current step are compared, one can easily show that (77) also applies to the *changes* in synaptic current and electrotonic potentials, while the unknown resting potentials E_A and E_B cancel:

$$G_{syn} = \frac{\Delta I_{syn}}{\Delta V^e(L_{A0}) - \Delta V^e(L_{B0})} \tag{78}$$

Here again, Δ means 'after' minus 'before'.

In the experimental situation, the current and potential changes on the right side of (78) can not be directly measured with electrodes, so we need to **express all three of them in terms of injection currents and somatic potentials**:

- **The synaptic current** I_{syn} is equal to the axial current entering neurite B0 at its tip, so $I_{syn} = -I_{B0}(L_{B0})$ – the minus sign arises from the definition of the axial current according to (12). Because no current is injected into the postsynaptic neuron B, the current balance of cell B requires that the current $-I_{B0}(L_{B0})$ entering neurite B0 is equal to all currents leaving the neuron, so

$$-I_{B0}(L_{B0}) = I^m_{B0} + \left(G_{Bs} + \sum_{j=1}^{J_B} G_{Bj} \right) V^e_{Bs} \tag{79}$$

  where I^m_{B0} is the current leaving neurite B0 through its membrane, G_{Bs} is the somatic membrane conductance of neuron B, the G_{Bj} are the input conductances of all other (sealed end) neurites of cell B defined by (126) and V^e_{Bs} is the electrotonic potential at the soma of neuron B. If I^m_{B0} in this current balance is replaced with the aid of (122) and the resulting relation is solved for $-I_{B0}(L_{B0})$, we obtain

$$\begin{aligned} I_{syn} &= -I_{B0}(L_{B0}) && (80)\\ &= \left(G_{Bs} + \frac{\tanh L_{B0}}{\lambda_{B0} R_{B0}} + \sum_{j=1}^{J_B} G_{Bj} \right) V^e_{Bs} \cosh L_{B0} && (81)\\ &= G_B V^e_{Bs} \cosh L_{B0} && (82) \end{aligned}$$

  Note that with the aid of (126), the term in brackets can be identified as the input conductance G_B that neuron B would have if *all* its neurites, including neurite B0, had a sealed end – or, in other words, if there was no synapse.

- **The electrotonic potential at the tip of neurite A0**, $V^e(L_{A0})$, is

$$V^e(L_{A0}) = \frac{V^e_{As}}{\cosh L_{A0}} - \lambda_{A0} R_{A0} I_{A0}(L_{A0}) \tanh L_{A0} \tag{83}$$

  according to (120). As above, we can eliminate the current change $\Delta I_{A0}(L_{A0})$ at the tip of neurite A0 (which is equal to the change in synaptic current, ΔI_{syn}) with the aid of the cell's current balance. In the case of the presynaptic neuron A, the balance is

$$I_{inj} = G_{As} V^e_{As} + \sum_{j=1}^{J_A} G_{Aj} V^e_{As} + I^m_{A0} + I_{A0}(L_{A0}) \tag{84}$$

  where I_{inj} is the current injected into soma A via an electrode and all other terms are just as in

(79). Replacing the membrane current I^m_{A0} of neurite A0 with the aid of (122) yields a relation that can be solved for $I_{A0}(L_{A0})$; the result is

$$I_{syn} = I_{A0}(L_{A0}) = I_{inj}\cosh L_{A0} - G_A V^e_{As}\cosh L_{A0} \tag{85}$$

where the definition of G_A is completely analogous to the one of G_B in (80). With this and (83), the electrotonic potential on the presynaptic side of the synapse is

$$V^e(L_{A0}) = \left(\frac{1}{\cosh L_{A0}} + \lambda_{A0}R_{A0}G_A\sinh L_{A0}\right)V^e_{As} - \lambda_{A0}R_{A0}I_{inj}\sinh L_{A0} \tag{86}$$

- By the same argument, the **electrotonic potential at the tip of neurite B0**, $V^e(L_{B0})$, is

$$V^e(L_{B0}) = \frac{V^e_{Bs}}{\cosh L_{B0}} - \lambda_{B0}R_{B0}I_{B0}(L_{B0})\tanh L_{B0} \tag{87}$$

according to (120) and $I_{B0}(L_{B0})$ can be replaced via (80), resulting in

$$V^e(L_{B0}) = \left(\frac{1}{\cosh L_{B0}} + \lambda_{B0}R_{B0}G_B\sinh L_{B0}\right)V^e_{Bs} \tag{88}$$

With (80), (83) and (88), we can now express the right side of (78) solely in terms of experimentally accessible voltages and currents and of parameters known from chapter 5 or from the cell pair's geometry:

$$G_{syn} = \frac{G_B\Delta V_{Bs}\cosh L_{B0}}{\left(\frac{1}{\cosh L_{A0}}+\lambda_{A0}R_{A0}G_A\sinh L_{A0}\right)\Delta V_{As} - \lambda_{A0}R_{A0}\Delta I_{inj}\sinh L_{A0} - \left(\frac{1}{\cosh L_{B0}}+\lambda_{B0}R_{B0}G_B\sinh L_{B0}\right)\Delta V_{Bs}} \tag{89}$$

where we made use of $\Delta V^e = \Delta V$ in all cases.

Other useful relations

The major aim of this section, namely to find an expression that allows us to extract the synaptic conductance between two neurons from experimental data, is achieved with (89). But the equations derived so far also allow us, just as for the simple model in the previous section, to understand the influence that coupling and current injection have on the voltage distribution in the two cells. For this purpose, we again (as with (62) and (63) in the simpler model) seek to **express the two steady state somatic potentials V_{As} and V_{Bs} solely in terms of cell parameters and I_{inj}.**

This can be done with the aid of the overall current balance of the cell pair (obtained by equating the two alternative expressions (80) and (85) for the synaptic current I_{syn})

$$I_{inj} = G_A V^e_{As} + G_B V^e_{Bs}\frac{\cosh L_{B0}}{\cosh L_{A0}} \tag{90}$$

and a modified version of (77) from which $V^e(L_{A0})$ and $V^e(L_{B0})$ were eliminated with (88) and (83). These two equations, if solved for V^e_{As} and V^e_{Bs}, result in

$$V_{As} = E_A - \frac{G_B\cosh L_{B0}(E_A-E_B)}{G_AG_B\gamma + G_A\frac{\cosh L_{A0}}{\cosh L_{B0}} + G_B\frac{\cosh L_{B0}}{\cosh L_{A0}}} + \frac{\left(G_B\gamma + \frac{\cosh L_{A0}}{\cosh L_{B0}}\right)I_{inj}}{G_AG_B\gamma + G_A\frac{\cosh L_{A0}}{\cosh L_{B0}} + G_B\frac{\cosh L_{B0}}{\cosh L_{A0}}} \tag{91}$$

$$V_{Bs} = E_B + \frac{G_A\cosh L_{A0}(E_A-E_B)}{G_AG_B\gamma + G_A\frac{\cosh L_{A0}}{\cosh L_{B0}} + G_B\frac{\cosh L_{B0}}{\cosh L_{A0}}} + \frac{I_{inj}}{G_AG_B\gamma + G_A\frac{\cosh L_{A0}}{\cosh L_{B0}} + G_B\frac{\cosh L_{B0}}{\cosh L_{A0}}} \tag{92}$$

where the abbreviation

$$\gamma = (R_{syn} + \lambda_{A0}R_{A0}\tanh L_{A0} + \lambda_{B0}R_{B0}\tanh L_{B0})\cosh L_{A0}\cosh L_{B0} \tag{93}$$

(with $R_{syn} = 1/G_{syn}$) was introduced[12].

Equations (91) and (92) have **the same form as the corresponding expressions for the simpli-**

[12] γ will later turn out to be equal to $\widetilde{R}_{syn}$ (see (102)).

fied model, namely (57) and (59): They have a term that describes the displacement of the two somatic potentials V_{As} and V_{Bs} from the resting potentials due to the coupling and a term that stands for the additional change in potential when current is injected into cell A.

Dynamics

Even for a single, uncoupled neuron, we have no analytical description of the voltage transients caused by a current step at the soma (see section 4.1.4). Therefore, the voltage dynamics in an electrically coupled pair of neurons have to be obtained by numerical simulation for the equivalent circuit introduced in fig. 6.3.

6.4 Comparing the two models

The previous two sections introduced two different models for a pair of neurons coupled by an electrical synapse: A simplified model that assumes that each cell is isopotential and a detailed model that does not make this approximation, but for which additional information about the geometries and electrical properties of the two cells is needed. Both models, if applied to experimental voltage transients, provide values for the conductances of the two cells and of the synapse. In the present section, we derive equations that **express the resting potentials and conductance values obtained with the simpler model in terms of those obtained with the detailed model**. Using the electrical cell parameters derived in chapter 5, these relations then allow us to estimate how well the approximation made in the simpler model is applicable to A-cluster neurons from the pedal ganglia of *Lymnaea stagnalis*.

Relations between the resting potentials from the two models

The postsynaptic resting potential $\widetilde{E}_B$ of the simple model can be expressed in terms of parameters from the detailed model by using (91) and (92) to replace the somatic potentials V_{As} and V_{Bs} in (67). This results in

$$\widetilde{E}_B = E_B + \frac{\cosh L_{A0} - 1}{G_B\gamma + \frac{\cosh L_{A0}}{\cosh L_{B0}} - 1}\,(E_A - E_B) \tag{94}$$

with γ defined by (93). Similarly, the resting potential of the presynaptic cell obtained with the simplified model is

$$\widetilde{E}_A = E_A + \frac{\cosh L_{B0} - 1}{G_A\gamma + \frac{\cosh L_{B0}}{\cosh L_{A0}} - 1}\,(E_B - E_A) \tag{95}$$

and the difference between the two is

$$\widetilde{E}_A - \widetilde{E}_B = \left(1 - \frac{\cosh L_{B0} - 1}{G_A\gamma + \frac{\cosh L_{B0}}{\cosh L_{A0}} - 1} - \frac{\cosh L_{A0} - 1}{G_B\gamma + \frac{\cosh L_{A0}}{\cosh L_{B0}} - 1}\right)(E_A - E_B) \tag{96}$$

As will be shown in chapter 7, $G_A\gamma$ and $G_B\gamma$ for neurons in designed networks are on the order of 10. As $\cosh L_{A0}/\cosh L_{B0}$ and $\cosh L_{B0}/\cosh L_{A0}$ are always > 0, the two denominators in this equation are > 0, and the numerators are also > 0 because the $\cosh$ are ≥ 1. Taken together, this means that both fractions in the last equation are ≥ 0, so **the difference between the two resting potentials obtained with the isopotential model will always be smaller than the one obtained with the detailed model**.

Under which circumstances is the deviation of $\widetilde{E}_A$ from E_A and $\widetilde{E}_B$ from E_B smallest? Generally, we expect the parameters obtained with the isopotential model to be similar to those obtained with

the more detailed model in cases where both neurons actually *are* close to being isopotential. As far as the resting potentials are concerned, the above equations show that good agreement between the two models can occur for two different reasons:

Obviously, the resting potentials obtained with the two models are *identical* if $E_A = E_B$. This makes sense if we consider the voltage distribution according to the detailed model in a cell pair with equal resting potentials when no current is injected (for example by looking at (91) and (92)): In this case, there will be no current flowing across the electrical synapse because the membrane potential is constant over the entire cell pair. So, for the special situation when $E_A = E_B$, the two cells really *are* isopotential when no current is injected, and it is not surprising that the isopotential model will give the same resting potentials as the detailed model.

But usually, $E_A \neq E_B$. In this case, the cells can only come close to being isopotential if the major part of the voltage drop between the cell bodies occurs at the synapse, not along the neuritic cables that connect it to the cell bodies. For a small voltage drop along the neurites, the neuritic membrane conductance g and the cytoplasmic resistivity r need to be so small that the neuritic space constants λ_{A0} and λ_{B0} are large compared to the neurite lengths (see (9)). Under these conditions, the electrotonic lengths L_{A0} and L_{B0} are small – such neurons are called 'electrotonically compact'. When L_{A0} and L_{B0} are small, $\cosh L_{A0} \approx 1$ and $\cosh L_{B0} \approx 1$ and $\gamma \approx R_{syn} + l_{A0}R_{A0} + l_{B0}R_{B0}$, which is just the combined axial resistance of the synapse and the two cables connecting it to the cell bodies. In addition, the condition that the voltage drop must almost exclusively occur at the synapse itself requires that $l_{A0}R_{A0}$ and $l_{B0}R_{B0}$ be much smaller than R_{syn}, such that even $\gamma \approx R_{syn}$.

In summary, the **deviation of $\widetilde{E}_A$ from E_A and $\widetilde{E}_B$ from E_B is smallest if either the two cells have the same resting potential** (which hardly ever occurs) **or if both neurons are electrotonically compact**.

Relations between the conductances from the two models

Additional relations between the parameters of the simplified model and the detailed model can be found by comparing the expressions for the somatic potentials V_{As} and V_{Bs} in the two models, namely (57) and (59) for the simpler model and (91) and (92) for the detailed model. By equating the expressions for V_{As} and V_{Bs} from the two models, one finds that

$$\widetilde{E}_A - \frac{\widetilde{G}_B\widetilde{G}_{syn}\left(\widetilde{E}_A - \widetilde{E}_B\right)}{\widetilde{G}_A\widetilde{G}_B + \widetilde{G}_{syn}\left(\widetilde{G}_A + \widetilde{G}_B\right)} = E_A - \frac{G_B \cosh L_{B0}\,(E_A - E_B)}{G_A G_B \gamma + G_A \frac{\cosh L_{A0}}{\cosh L_{B0}} + G_B \frac{\cosh L_{B0}}{\cosh L_{A0}}} \quad (97)$$

$$\widetilde{E}_B + \frac{\widetilde{G}_A\widetilde{G}_{syn}\left(\widetilde{E}_A - \widetilde{E}_B\right)}{\widetilde{G}_A\widetilde{G}_B + \widetilde{G}_{syn}\left(\widetilde{G}_A + \widetilde{G}_B\right)} = E_B + \frac{G_A \cosh L_{A0}\,(E_A - E_B)}{G_A G_B \gamma + G_A \frac{\cosh L_{A0}}{\cosh L_{B0}} + G_B \frac{\cosh L_{B0}}{\cosh L_{A0}}} \quad (98)$$

$$\frac{\widetilde{G}_B + \widetilde{G}_{syn}}{\widetilde{G}_A\widetilde{G}_B + \widetilde{G}_{syn}\left(\widetilde{G}_A + \widetilde{G}_B\right)} = \frac{G_B\gamma + \frac{\cosh L_{A0}}{\cosh L_{B0}}}{G_A G_B \gamma + G_A \frac{\cosh L_{A0}}{\cosh L_{B0}} + G_B \frac{\cosh L_{B0}}{\cosh L_{A0}}} \quad (99)$$

$$\frac{\widetilde{G}_{syn}}{\widetilde{G}_A\widetilde{G}_B + \widetilde{G}_{syn}\left(\widetilde{G}_A + \widetilde{G}_B\right)} = \frac{1}{G_A G_B \gamma + G_A \frac{\cosh L_{A0}}{\cosh L_{B0}} + G_B \frac{\cosh L_{B0}}{\cosh L_{A0}}} \quad (100)$$

If (97) and (98) are subtracted and the result is solved for $\widetilde{E}_A - \widetilde{E}_B$ and equated with (96), the resulting relation – together with (99) and (100) – defines the parameters $\widetilde{G}_A$, $\widetilde{G}_B$ and $\widetilde{G}_{syn}$ from

the isopotential model in terms of parameters from the detailed model. If solved for these three variables, this system of equations implies that

$$\widetilde{G}_A = G_A + \frac{\frac{\cosh L_{B0}}{\cosh L_{A0}} - 1}{\gamma} \tag{101}$$

$$= G_A + \frac{\frac{\cosh L_{B0}}{\cosh L_{A0}} - 1}{(R_{syn} + \lambda_{A0} R_{A0} \tanh L_{A0} + \lambda_{B0} R_{B0} \tanh L_{B0}) \cosh L_{A0} \cosh L_{B0}} \tag{102}$$

$$\widetilde{G}_B = G_B + \frac{\frac{\cosh L_{A0}}{\cosh L_{B0}} - 1}{\gamma} \tag{103}$$

$$= G_B + \frac{\frac{\cosh L_{A0}}{\cosh L_{B0}} - 1}{(R_{syn} + \lambda_{A0} R_{A0} \tanh L_{A0} + \lambda_{B0} R_{B0} \tanh L_{B0}) \cosh L_{A0} \cosh L_{B0}} \tag{104}$$

and

$$\widetilde{R}_{syn} = \gamma = (R_{syn} + \lambda_{A0} R_{A0} \tanh L_{A0} + \lambda_{B0} R_{B0} \tanh L_{B0}) \cosh L_{A0} \cosh L_{B0} \tag{105}$$

where $\widetilde{G}_{syn}$ was replaced by its inverse, $\widetilde{R}_{syn}$, because the result for $\widetilde{R}_{syn}$ looks simpler.

We again expect **good agreement between the two models if both cells are electrotonically compact**, because then the approximation of constant membrane potential within each neuron will be well applicable. This is indeed the case: As discussed above, electrotonic compactness implies that $\cosh L_{A0} \approx 1$ and $\cosh L_{B0} \approx 1$, such that the two fractions in (101) and (103) are close to 0 and therefore $\widetilde{G}_A \approx G_A$ and $\widetilde{G}_B \approx G_B$. And compactness also implies that (as shown above) $\gamma \approx R_{syn}$, thus also $\widetilde{R}_{syn} \approx R_{syn}$.

In current step experiments, signals can be transferred across an electrical synapse between two neurons in either of two directions. Setting cell 1 = cell A and cell 2 = cell B or cell 1 = cell B and cell 2 = cell A in (101) through (105), we expect the following results from the isopotential model in the two cases (note that γ is symmetric in A and B and will therefore be the same in both directions):

	cell 1 presynaptic	cell 2 presynaptic
$\widetilde{G}_1 =$	$G_1 + \frac{\frac{\cosh L_{20}}{\cosh L_{10}} - 1}{\gamma}$	$G_1 + \frac{\frac{\cosh L_{20}}{\cosh L_{10}} - 1}{\gamma}$
$\widetilde{G}_2 =$	$G_2 + \frac{\frac{\cosh L_{10}}{\cosh L_{20}} - 1}{\gamma}$	$G_2 + \frac{\frac{\cosh L_{10}}{\cosh L_{20}} - 1}{\gamma}$
$\widetilde{G}_{syn} =$	γ	γ

(106)

Thus, the **results obtained with the isopotential model for the cell and synapse conductance should not depend on the direction of signal transfer** if the detailed model is a good description of a pair of coupled neurons.

What about the capacitances?

The expressions derived in the present section relate the resting potentials, cell conductances and synaptic conductance found with the isopotential model to the corresponding parameters from the detailed model. For the cell capacitances $\widetilde{C}_A$ and $\widetilde{C}_B$, no such relations can be derived because in the detailed model there is no single parameter corresponding to the capacitance of the whole cell.

So how well will the two models agree for *Lymnaea* neurons?

For all of the parameters discussed above, we expect the results obtained with the two different models to be similar if the neurons are electrotonically compact. As shown in section 5.2, *Lym-*

naea neurons in cell culture *are* rather compact, so how well will the results from the two models agree for these neurons?

The average length of the proximal neurites A0 and B0 in all pairs studied in section 7.1 is 178μm, and the maximum proximal neurite length is 526μm. With a typical space constant of $\lambda \approx 1000\mu$m (see section 5.2), this means that the electrotonic lengths of the proximal neurites in these pairs are usually around $L \approx 0.2$, and at most $L \approx 0.5$. The hyperbolic cosine and tangent of L – that determine how well the two models agree – therefore are

L	0.2	0.5
$\cosh L$	1.102	1.128
$\tanh L$	0.197	0.462

and the requirement of $\cosh L \approx 1$ and $\tanh L \approx L$ is fulfilled for the average cell in such a network. In short, **we expect to obtain similar values if we apply the isopotential or the detailed synapse model to pairs of *Lymnaea* neurons in culture**.

6.5 Cell pairs with multiple contacts

So far, our models have treated cell pairs of simple geometry that are coupled via a single, localized electrical contact. Naturally, the situation *in vivo* or in a conventional cell culture is different; there, the highly branched neurites of each cell usually touch several other cells at many different locations. While the designed neural networks introduced and studied in the present thesis were clearly *not* developed to reproduce any specific *in vivo* network, it is still interesting to compare the strength of the synapses formed under controlled conditions to those of synapses in more natural networks.

To **determine the coupling strength in random networks**, one can perform the same current step experiments that were used to characterize synapses in

- isolated, randomly growing cell pairs
- randomly growing cell pairs embedded in a network of many cells

The present section demonstrates that, **in both cases, the equivalent circuit can be reduced to the circuit of a one-contact synapse** and that therefore **the equations derived in section** 6.2 **are applicable here**, as well.

Cell pairs in randomly growing cultures usually make physical contact at several locations, and there is evidence that neuron pairs from the snail *Helisoma* (if they are both in a state of active growth at the time the neurites get in touch) establish an electrical synapse at every point of contact [35]. Unfortunately, all attempts to localize the site of electrical coupling in randomly growing *Lymnaea* neurons failed (see section 7.2.1), so we lack the complete geometrical information needed to model such cell pairs and their contacts with detailed circuits as in section 6.3. Instead, we again **assume that each individual cell is isopotential** and model the pairs with a simplified circuit similar to the one introduced in section 6.2. Figs. 6.4 and 6.5 illustrate the simplified circuits for isolated and embedded cell pairs – as we consider only the steady state in this section, all capacitances were omitted from the circuits. The reduction to the steady state circuit of a one-contact synapse (which is just fig. 6.2 without capacitances) can be done as follows:

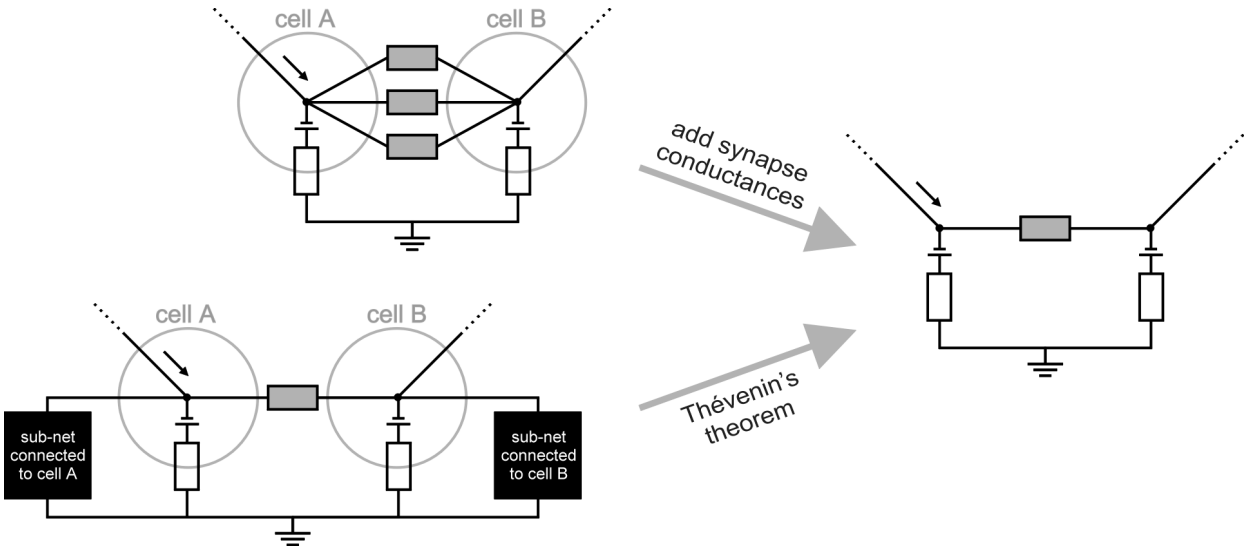

Figure 6.4: ***Isolated pairs and a subclass of embedded pairs can be described with the simplified model.*** *(**Left, top**) Equivalent circuit for an isolated pair of neurons with multiple contacts if each cell is described by a single compartment. The multiple electrical synapses between the cells are represented by parallel conductances. (**Left, bottom**) Equivalent circuit for a cell pair embedded in a network that can be split into two sub-nets (represented by black boxes) whose only connection is the synapse between the embedded pair. (**Right**) Both networks can be reduced to the circuit of the isopotential model by adding the parallel conductances or by applying Thévenin's theorem. Synapse conductances are grey and cell conductances are white; the black arrows indicate where current is injected.*

Isolated cell pair

If an isolated cell pair with multiple contact points is modelled as two isopotential compartments connected by several ohmic conductances that stand for the individual synapses, it is immediately obvious how this circuit can be reduced to the circuit for an equivalent one-contact synapse: The **equivalent synapse conductance is just the sum of the parallel conductances** and all equations derived in section 6.2 are applicable. Current step experiments performed on such a pair therefore yield a value of $\widetilde{G}_{syn}$ that corresponds to the total conductance of the individual synapses. All other parameters of the equivalent circuit, such as the cell conductances and resting potentials, are not affected by this summation; if the isopotential model is applied to an isolated cell pair, the results obtained for these parameters therefore do not depend on the number of synaptic contacts between the two neurons.

Note that, in the rest of this section, we always make the reduction discussed above for all cell contacts, so $\widetilde{G}_{syn}$ **from now on always means the total conductance of all the individual synapses between a given pair of neighboring cells**.

Embedded cell pair: A special case

The reduction to an equivalent one-contact circuit is less straightforward in the case of two neurons that are connected not only to each other, but also to additional cells in their vicinity. To demonstrate that this reduction is still possible and that we can apply the equations from section 6.2 to such pairs, too, we first consider a very **special case** of such a network, namely a **net that can be split into two sub-networks whose only connection is the synapse we want to characterize** (see fig. 6.4).

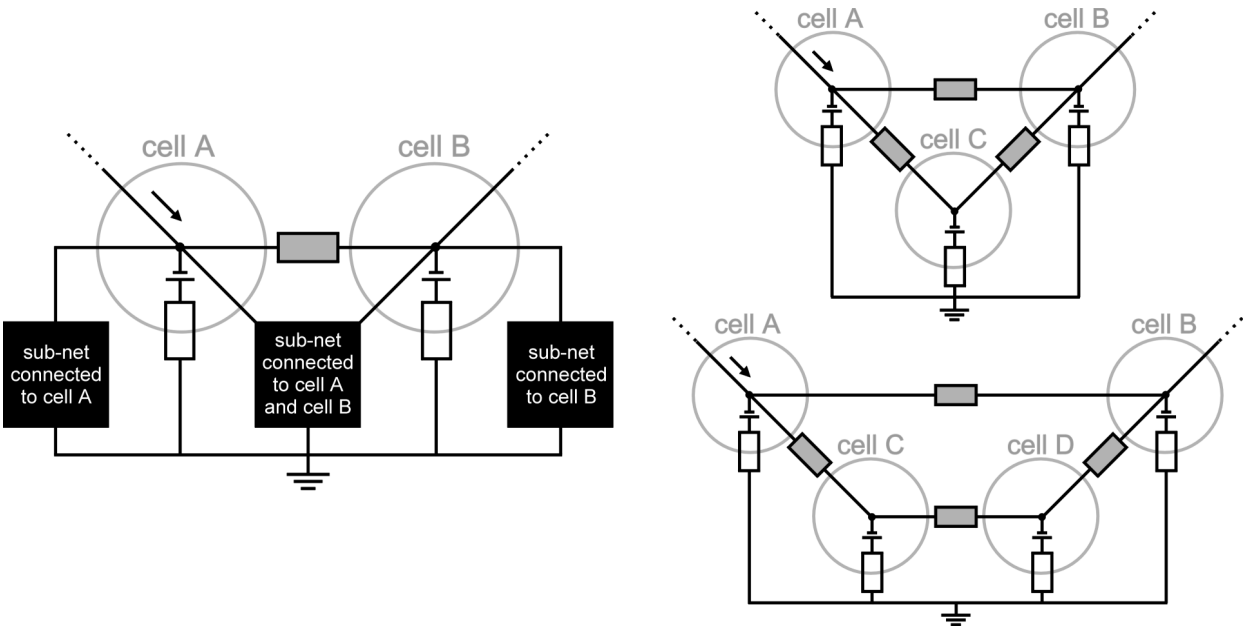

Figure 6.5: ***General case of an embedded cell pair.*** *(**Left**) Circuit describing all possible embedded cell pairs. The network surrounding the pair is divided into three subnets (black boxes): One connected only to cell A, one connected only to cell B, and one connected to both A and B. (**Right**) These circuits illustrate two possible pathways through which current can flow from A to B in parallel to the synapse between A and B. Synapse conductances are grey and cell conductances are white. The arrows indicate where current is injected.*

In this case, the sub-network connected to cell A, together with the conductance and battery of A, forms a two-terminal network, the two terminals being the soma of neuron A and ground. Similarly, the sub-net attached to B, together with B, forms another two-terminal network of voltage sources and conductances, this time between soma B and ground. According to Thévenin's theorem [44], any two-terminal network of voltage sources and conductances is equivalent to a single conductance in series with a single voltage source. This means that **this special case of a network behaves just like an isolated cell pair** and the synaptic conductance $\widetilde{G}_{syn}$ obtained from current step experiments with the aid of (69) is exactly the synaptic conductance between A and B. In contrast, the conductances $\widetilde{G}_A$ and $\widetilde{G}_B$ and the resting potentials $\widetilde{E}_A$ and $\widetilde{E}_B$ obtained as described in section 6.2 in this case are combinations of the conductances and resting potentials of the many cells in the network and are not easy to interpret as long as we do not know the exact connectivity of the network – but this is no problem, because the sole purpose of our measurements on embedded cell pairs is to determine the conductance of the synapse between them.

In summary, **a network that can be divided into two sub-nets only connected via the synapse between A and B still allows us to determine the conductance of this synapse** with the aid of the equations from section 6.2.

Embedded cell pair: General case

But in general, the network surrounding a cell pair will consist not only of two sub-nets attached to cells A and B, but also of a third group of cells that provide **additional pathways for current flow between A and B**. The following considerations will show that in this general case (depicted in fig. 6.5), the **synaptic conductance that is obtained from current step experiments is only**

an upper limit for the actual synaptic conductance between A and B:

We first consider the case shown in fig. 6.5, middle. There, a third cell C has synapses with both A and B, so current can flow from A to B not only via the synapse we are interested in, but also via cell C. In this configuration, the current balances for cell A and cell B no longer look like (62) through (65); instead, they are

$$I_{inj} = \widetilde{G}_A(V_{As} - \widetilde{E}_A) + \widetilde{G}_{syn}(V_{As} - V_{Bs}) + \widetilde{G}_{AC}(V_{As} - V_{Cs}) \tag{107}$$

$$\widetilde{G}_{syn}(V_{As} - V_{Bs}) + \widetilde{G}_{BC}(V_{Cs} - V_{Bs}) = \widetilde{G}_B(V_{Bs} - \widetilde{E}_B) \tag{108}$$

where $\widetilde{G}_A$, $\widetilde{G}_B$, $\widetilde{E}_A$ and $\widetilde{E}_B$ are the equivalent conductances and resting potentials of A and B together with the two sub-nets connected to them (see the special case above), $\widetilde{G}_{AC}$ and $\widetilde{G}_{BC}$ are the synaptic conductances from A to C and from B to C, and everything else is defined as in section 6.2. A third equation is provided by the current balance for cell C, namely

$$\widetilde{G}_{AC}(V_{As} - V_{Cs}) + \widetilde{G}_{BC}(V_{Bs} - V_{Cs}) = \widetilde{G}_C(V_{Cs} - \widetilde{E}_C) \tag{109}$$

and this equation, if solved for V_{Cs}, allows us to eliminate V_{Cs} from the balances for A and B. The resulting equations can be brought into the same form as the current balances for an isolated cell pair (compare to (62) through (65)); they then are

$$I_{inj} = \widetilde{G}'_A(V_{As} - \widetilde{E}'_A) + \widetilde{G}'_{syn}(V_{As} - V_{Bs}) \tag{110}$$

$$\widetilde{G}'_{syn}(V_{As} - V_{Bs}) = \widetilde{G}'_B(V_{Bs} - \widetilde{E}'_B) \tag{111}$$

where the ***apparent*** **synaptic conductance** $\widetilde{G}'_{syn}$ between A and B is

$$\widetilde{G}'_{syn} = \widetilde{G}_{syn} + \frac{\widetilde{G}_{AC}\widetilde{G}_{BC}}{\widetilde{G}_{AC} + \widetilde{G}_{BC} + \widetilde{G}_C} \tag{112}$$

and where $\widetilde{G}'_A$, $\widetilde{G}'_B$, $\widetilde{E}'_A$ and $\widetilde{E}'_B$ are functions of $\widetilde{G}_A$, $\widetilde{G}_B$, $\widetilde{G}_C$, $\widetilde{G}_{AC}$, $\widetilde{G}_{BC}$, $\widetilde{E}_A$, $\widetilde{E}_B$ and $\widetilde{E}_C$ (whose exact form can easily be derived but is not relevant for our considerations).

The fact that – even in the presence of cell C – the current balances for A and B are formally the same as in the case of an isolated cell pair (compare to (62) through (65)) means that this network will again behave like an isolated pair if probed with current steps. The only difference relevant for us is that now the ***apparent*** **synaptic conductance** $\widetilde{G}'_{syn}$ **we obtain with (69) is no longer equal to the** ***actual*** **synaptic conductance** $\widetilde{G}_{syn}$ we are interested in. But before we estimate how large the difference between $\widetilde{G}'_{syn}$ and $\widetilde{G}_{syn}$ really is, we consider yet another constellation, namely the one shown in fig. 6.5 at the right:

There, the additional current pathway from A to B passes *two* cells (neurons C and D) instead of just one cell as in the circuit shown in the middle. In complete analogy to the argument given above, we can again use the current balances for cells C and D to replace the variables V_{Cs} and V_{Ds} that will show up in the current balances for A and B and we can again bring the resulting equations into the form of current balances for an isolated pair, but this time with an apparent synaptic conductance given by

$$\widetilde{G}''_{syn} = \widetilde{G}_{syn} + \frac{\widetilde{G}_{AC}\widetilde{G}_{BD}\widetilde{G}_{CD}}{\left(\widetilde{G}_{AC} + \widetilde{G}_{CD} + \widetilde{G}_C\right)\left(\widetilde{G}_{BD} + \widetilde{G}_{CD} + \widetilde{G}_D\right) - \widetilde{G}_{CD}^2} \tag{113}$$

How accurately can the synaptic conductance be measured in embedded pairs?

To **estimate how far the apparent synaptic conductances** $\widetilde{G}'_{syn}$ **and** $\widetilde{G}''_{syn}$ in the two exemplary

cases **deviate from the actual value**, we jump ahead and make use of results from sections 7.1 and 7.2. There, the ratio κ between the average synaptic conductance and the average single cell input conductance is found to be on the order of $\kappa \approx 1/10$ for neurons in designed networks (that is, on patterned substrates and with synapses restricted to a single point of contact) and on the order of $\kappa \approx 1/3$ for neurons in conventional cell culture (that is, with randomly growing neurites that make contact with other cells at several locations).

If we inspect the expressions for $\widetilde{G}'_{syn}$ and $\widetilde{G}''_{syn}$ ((112) and (113) from above), we find that the difference between the apparent and the real synaptic conductance – namely, the second terms on the right sides of the equations – is

- of order $\kappa\widetilde{G}_{syn}$ if the alternative current pathway between A and B passes through one additional cell and
- of order $\kappa^2\widetilde{G}_{syn}$ if it passes through two additional cells
- and so on for higher numbers of intermediate cells (as can be derived in the same fashion as above).

For neurons in designed networks, this implies that every cell that has direct synaptic contact to both A and B increases the apparent synaptic conductance we measure in experiments by about 10%, and every current pathway from A to B that includes two or more additional neurons increases it by negligible amounts. **For small, designed neural networks, in which a given neuron is in touch with very few other cells, the strength of a synapse between a pair can therefore be measured with current step experiments to within a few tens of percents.**

The situation is different for pairs embedded in a network in conventional cell culture. There, every neuron that both cells in the pair have synapses with will increase the value obtained for the synapse conductance by about one third of its real value, and even current pathways that pass two or three other neurons can still contribute on the order of 11% and 4%, respectively. For the rather sparse networks used in section 7.2, we therefore expect that the measured synapse conductance – while having the right order of magnitude – may be considerably larger than the true conductance. Or, in other words, the **equations from section** 6.2**, applied to pairs of neurons embedded in a random neural network in vitro, will give only an upper limit for the true synapse conductance.**

Can the method be applied *in vivo*?

Note that current step experiments have, in the past, even been used to measure the electrotonic coupling strength between two cells embedded in a neural network *in vivo* [1][50]. But two possible complications have to be considered in this case: First, neurons in the ganglion may have smaller neurite diameters than neurons in cell culture and may therefore be less electrotonically compact than cultured nerve cells, with the result that the isopotential model from section 6.2 may be not well applicable to these neurons. And second, the neurons in a ganglion are much more densely packed than in a sparse cell culture, so there could be massive numbers of cells that form electrical synapses with both neurons of the pair one wants to study. In this case, with each of those cells increasing the apparent synaptic conductance by about one third of the actual value, the **experimental result for the synaptic conductance may deviate considerably from the real synaptic conductance**.

7
Experiments with synapses

This chapter describes current step experiments with single-point synapses (in section 7.1) and multi-point synapses (section 7.2) and discusses and compares their results. For the single-point synapses, which can be described either with the isopotential model from section 6.2 or with the detailed model from section 6.3, the results obtained with both models are compared – as expected for electrotonically cells, the two model turn out to be almost equivalent. Finally, section 7.3 analyzes the requirements for the transmission of action potentials from the pre- to the postsynaptic neuron and discusses the implications for neural network design.

7.1 The simplest synapse: One contact point

For the design of neural networks with simple and defined geometry and connectivity, it is desirable to have control over as many properties of the synapses in the net as possible, the most important ones being

- which neurons form synapses with which other neurons
- the locations of the synapses
- the type of synapse
- the synaptic strength

As explained in section 1.2, the type of synapse formed in *Lymnaea stagnalis* cell cultures is largely determined by the type of neurons selected as raw material for the designed network; the A-cluster neurons from the pedal ganglia that were used here re-establish their *in vivo* electrical synapses when placed in cell culture, as was expected (see below). On the synaptic strength, we have no control so far, but section 7.2.2 briefly discusses how it could be influenced in the future.

Concerning the other two points, the present section demonstrates that **it is – to a certain extent – possible to control which cells form synapses at which locations with the aid of guided growth**. Using the synapse models from the previous chapter, the present section also determines the strength of the synapses formed under such conditions of controlled neurite encounter.

Inducing synapses by guided neurite encounter

Given the method for guiding the outgrowth of snail neurons introduced in section 2.3, the straightforward way to control the connectivity of a designed network is to position neurons on a patterned substrate which guides the newly growing neurites in a way that lets them make physical contact only at the locations where synapses are desired.

To demonstrate that this approach works, pairs of A-cluster neurons were planted on the same lanes of linearly patterned substrates or on brickwall-patterned substrates in order to establish the simplest synapse geometry possible, namely a synapse restricted to a single point of contact

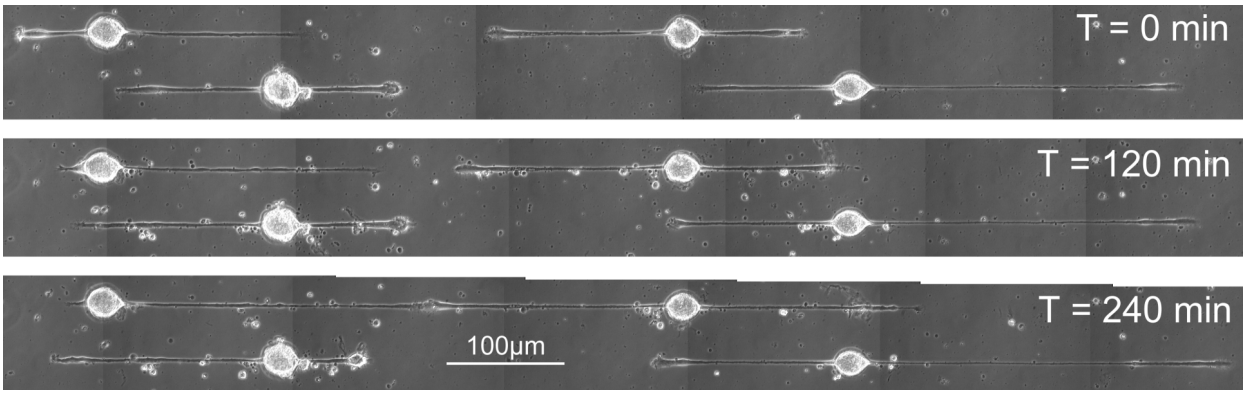

Figure 7.1: ***Guidance-controlled formation of a simple synapse on a linear pattern.*** *This figure shows two pairs of colinearly growing neurons at the beginning of a monitoring period (**top**), two hours later (**middle**) and four hours later (**bottom**). The distance between the two neurons in the upper pair continually decreases as the two neurites grow along the invisible lane of intact substrate. In the bottom panel, the growth cones have met and formed an electrical synapse. In contrast, the lower pair fails to form a contact in spite of identical culture conditions and a similar soma-soma distance. Also note that both of the neurons on the left side have one growing neurite and one retracting neurite at the same time.*

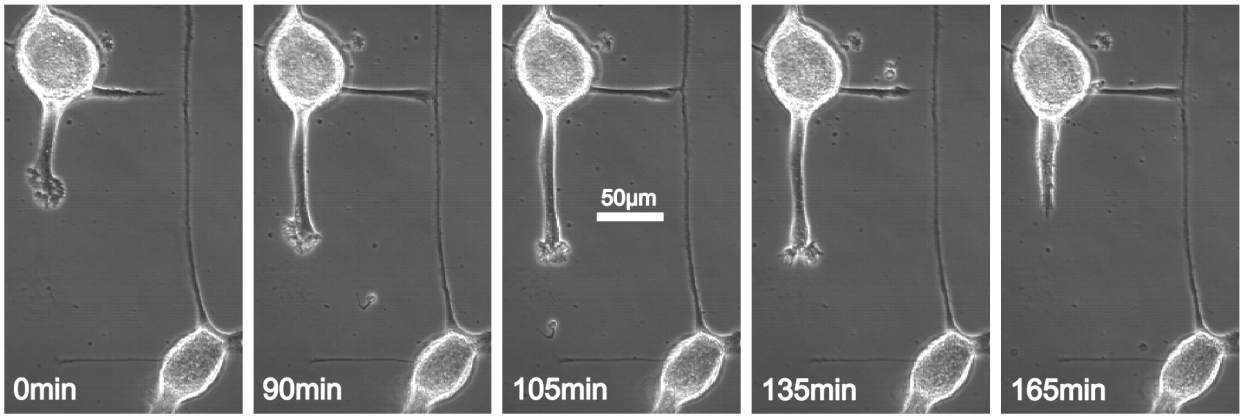

Figure 7.2: ***Guidance-controlled formation of a simple synapse on a brickwall pattern.*** *The five panels show two neurons growing on a brickwall pattern at different times after the onset of a monitoring period. After 90min, the horizontal neurite of the upper cell makes physical contact with the vertical neurite of the lower cell. Then, the neurite retracts and looses contact again, and finally, it shows renewed growth and establishes a stable contact in the last panel. Perpendicular contacts like this - with a growth cone meeting an extant neurite - can lead to functioning electrical synapses, too. Also note that between the second and third panel, one neurite of the upper cell grew while the other retracted, and vice versa between the fourth and the last panel.*

between two cells. As described in section 2.3, around 80% of the stably adhering neurons grew new neurites, most of which faithfully followed the linear lanes. Some of the neuron pairs whose neurites approached each other to within a few hundred μm were monitored before and during their growth cones made contact; figs. 7.1 and 7.2 show examples of such encounters.

The figures illustrate several **results from such pairing experiments**:

- The most important result is that the approach does indeed work: **Growth cone guidance can be used to establish a physical contact between two selected neurons** – and, as will be shown later in this section, such a contact point usually features a functioning electrical

synapse.

- For an electrical synapse to form, it is not necessary that two growth cones collide; a synapse can also be formed if a growth cone meets an extant neurite of another cell (as in fig. 7.2) or if a growth cone meets the cell body of another neuron (see fig. 7.4) – this means that there is **a large number of possible contact geometries** in designed networks.
- But the figures also demonstrate that synapse formation induced in this manner is not completely predictable: In spite of identical culture conditions and very similar soma-soma distance, a second neuron pair in fig. 7.1 did not establish a synapse because the two neurites failed to make physical contact, and the synapse formed in fig. 7.2 became stable only after physical contact was established for the second time. So, obviously, **positioning neurons on a pattern that allows their neurites to make contact only enables synapse formation but can not enforce it** due to the highly variable growth rates of the neurites and due to occasionally occurring neurite retractions. Out of the 13 pairs that were monitored, only ten finally established a stable contact, but three failed to make contact within the next several hours and were not monitored any longer.
- The **large variability in growth rates also makes the exact location of the synapse hard to predict** (or control); depending on the growth rates of the two neurites involved, the synapse in fig. 7.1 could have been established anywhere along the guiding lane between the two cell bodies.

Nine of the monitored pairs and 14 additional pairs (that had not previously been monitored) were used for electrophysiological studies to determine their synapse conductance; for altogether 15 of these pairs, both neurons could successfully be impaled with microelectrodes as described in section 3.1 and remained physiologically normal long enough for current step experiments as suggested by chapter 6. All of these pairs had exactly one contact point whose location was either known because its formation had been monitored, because it was obvious from the morphology of the pair or because it was determined after the electrophysiological experiments by injection of Lucifer yellow into one of the cells (see section 7.2.1).

Pairs without synapses

With four of the 15 pairs, injection of currents into either of the cells caused no detectable voltage change in the other cell, even if very large current amplitudes were applied. Before we proceed to the other eleven pairs (which had functioning electrical synapses), we discuss **two possible reasons why these four pairs failed to establish a detectable synapse**:

First of all, **a small percentage of the neurons isolated from the pedal ganglia may have originated from neighboring cell clusters** instead of the A-clusters due to the similarities in cell size and color that often made it difficult to unequivocally localize the borders between adjacent clusters during cell preparation. A cell pair containing such a cell can not necessarily be expected to form a synapse in culture because it may not have been connected *in vivo*.

And second, findings from two studies on *Helisoma* neurons suggest that **even cells that do form connections in vivo may fail to do so in vitro if one of the two neurons is not actively growing** at the time the cells make physical contact [36][37]. For one of the four pairs, we do not know if both neurons were still growing because the pair had not been monitored before the experiments. For a second pair, it is obvious that only *one* cell was growing at the time of first contact, because the other cell had no neurites at all (the contact in this case was formed by a growth cone getting in touch with a neuriteless soma). And for the remaining two pairs, indeed,

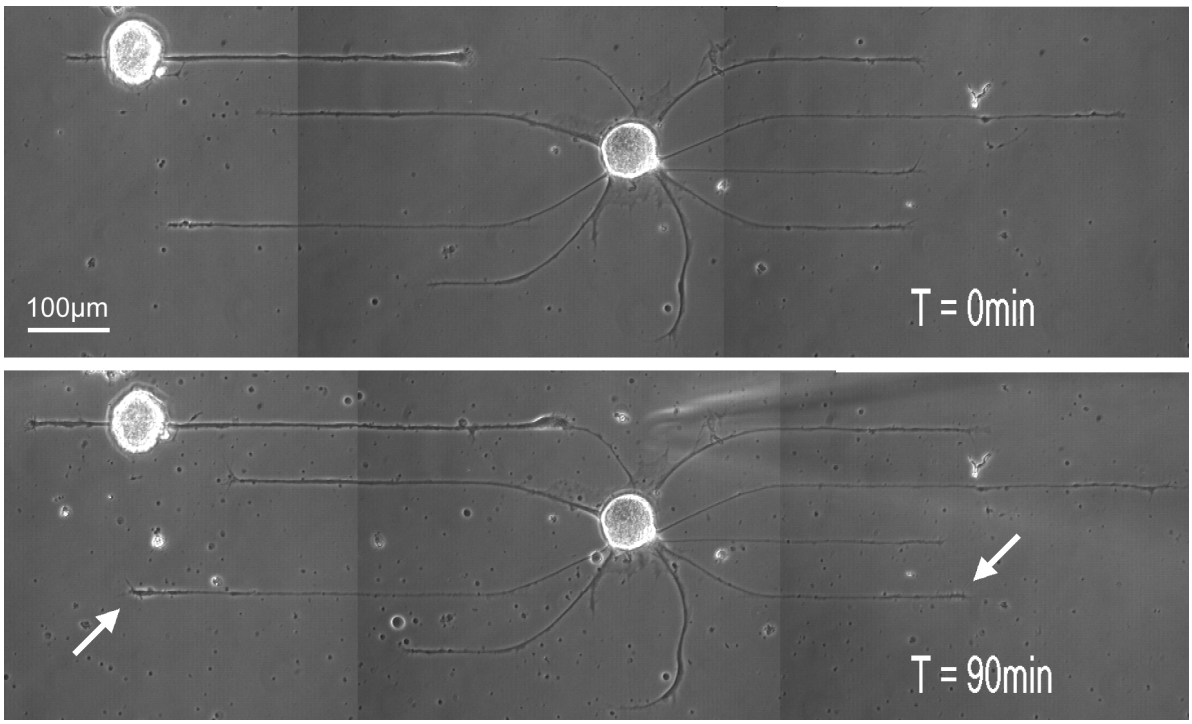

Figure 7.3: ***A cell pair that failed to establish a synapse.*** *This figure shows an example of a pair that made physical contact, but established no functioning synapse. The two panels show the pair at the beginning of the monitoring period (**top**) and 90min later, just after the neurites got in touch (**bottom**). During this period, the proximal neurite of the right cell showed no growth, which may be the reason why no synapse was formed. Note, however, that other neurites of the same cell (indicated by arrows) still were in an active state of growth.*

one of the two neurites involved in the contact had ceased to grow at the time of encounter – one of these pairs is shown in fig. 7.3. Note, however, that in this case *other* neurites of the same neuron were still growing. This suggests that even an active state of growth of the *neuron* may not be sufficient for synapse formation; **maybe the very *neurite* in contact with the other cell has to be growing** for a synapse to form.

Pairs with synapses: Evaluation using the isopotential model

For the remaining eleven pairs, current injection into one cell changed the membrane potential in the other cell, too. Fig. 7.4 shows four examples of such single-point synapses establish in different constellations, namely with a growth cone meeting an existing neurite, a soma or (most common) another growth cone. Exemplary voltage recordings from the same four pairs are shown in fig. 7.5 and illustrate the full **range of coupling strengths** found with electrical single-point synapses between *Lymnaea* neurons in culture: Some pairs are so weakly coupled that even large presynaptic voltage changes change the potential in the other neuron only slightly (such as pair i). In an intermediate range of coupling efficiency (like in pairs vii and ix), the small postsynaptic potentials due to presynaptic spikes can add up and, for strong presynaptic activity, occasionally bring the postsynaptic neuron above firing threshold. And some pairs are so strongly coupled that a few presynaptic spikes are enough to trigger a postsynaptic action potential (as in pair ii). In all cases, however, not only presynaptic depolarization, but also presynaptic hyperpolarization can spread to the postsynaptic neuron. This is a clear indication that **we are, indeed, dealing with electrical synapses**.

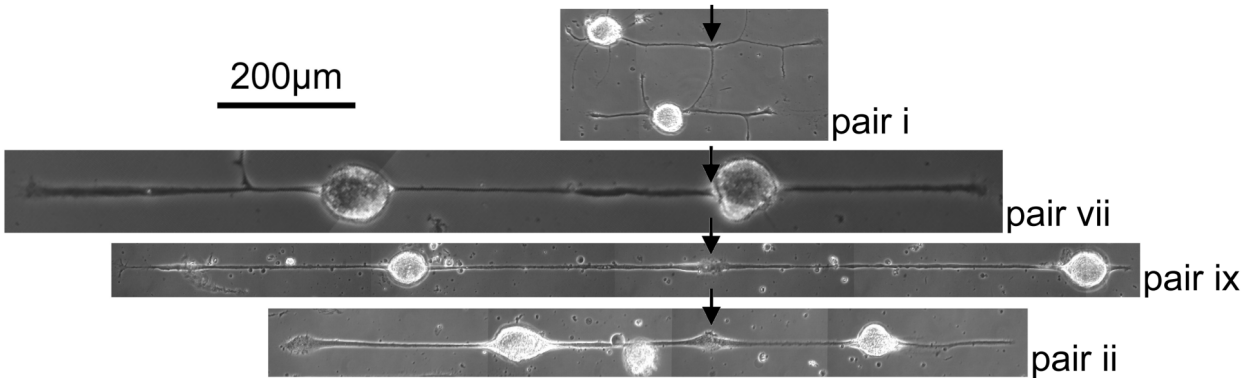

Figure 7.4: ***Four example pairs with single-point synapses.*** *Micrographs of four neuron pairs with functioning single-point synapses after one day in culture; cell 1 is always at the left and cell 2 at the right. Pair i was cultured on a brick wall pattern and formed a synapse when a growth cone met an existing neurite. Pairs vii, ix and ii were cultured on a linearly pattern substrate. In pair vii, the synapse was formed when a growth cone met a cell body, and the synapses in pairs ix and ii were established when two growth cones met. In all micrographs, the black arrow indicates the location of the synapse. Voltage recordings from these four pairs are shown in figure 7.5. Note that figure 7.1 shows how pair ix made contact.*

Fig. 7.5 also gives the coupling coefficients k_{12} and k_{21} and the synapse conductance $\widetilde{G}_{syn}$ for the example cell pairs – these values are determined later on in this section. The numbers illustrate that **neither the coupling coefficient alone nor the synapse conductance alone is sufficient for predicting whether postsynaptic action potentials can occur** in a pair. This is discussed in more detail in section 7.3.

We now use pair ix (which is also the upper cell pair in fig. 7.1) as an example to demonstrate how the parameters from the isopotential model, especially the synaptic conductance $\widetilde{G}_{syn}$, were determined for each of the eleven pairs with the aid of the equations from section 6.2. The **procedure** was as follows:

1.) Both cells were impaled with microelectrodes and hyperpolarizing current steps of different amplitude were alternately injected into one of the two cells while no current was injected into the respective other cell. Fig. 7.6 shows injection currents and somatic voltage responses for the example pair. For clarity, some of the transients were omitted from the figure and only the first 800ms of the responses are shown. For each of the injected current steps, the corresponding pre- and postsynaptic voltage signals in the following are referred to as a 'pair of transients'.
2.) For each pair of transients, the steady state values $V_{As,0}$, $V_{Bs,0}$, $V_{As,\infty}$ and $V_{Bs,\infty}$ before and after the step were used to calculate the postsynaptic resting potential $\widetilde{E}_B$ according to (67). By applying this equation for both directions of signal transfer, the resting potentials of both cells were determined[13].
3.) With both resting potentials known, (68) through (70) were used to compute the synaptic conductance $\widetilde{G}_{syn}$ and the conductances $\widetilde{G}_A$ and $\widetilde{G}_B$ of the pre- and postsynaptic neuron for each pair of transients (again using only the steady state values).
4.) Using $\widetilde{G}_{syn}$, $\widetilde{G}_A$ and $\widetilde{G}_B$, the pair of transients was simultaneously fit to the theoretical transients given by (73) and (74), with only the capacitances $\widetilde{C}_A$ and $\widetilde{C}_B$ as fit variables.

[13] Note that 'cell 1' and 'cell 2' are always used to distinguish between the two neurons themselves, while the terms 'cell A' and 'cell B' refer to the momentary pre- or postsynaptic role of the neuron. So during the experiment, cell 1 has the role of cell A at some times and acts as cell B at other times.

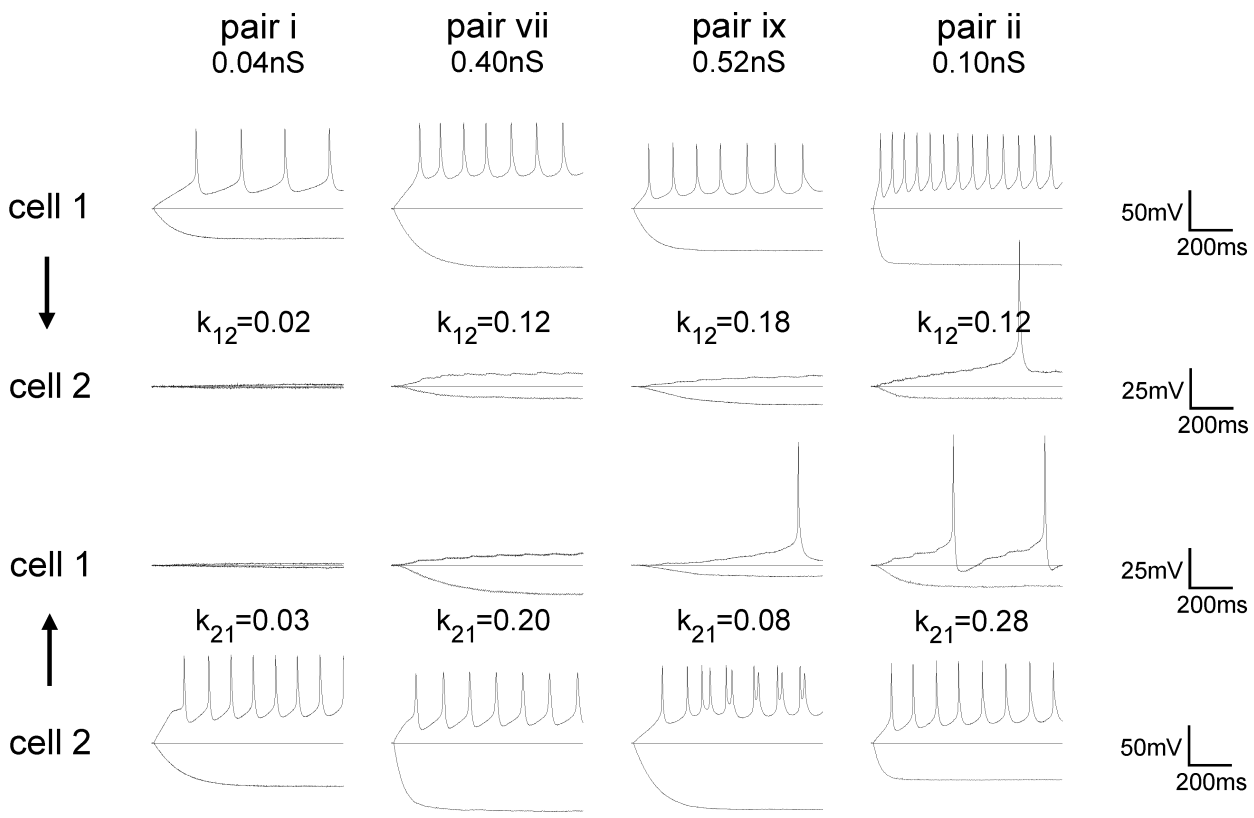

Figure 7.5: ***Electrical coupling in the four example cell pairs.*** *For the four pairs from fig. 7.4, this figure shows some exemplary voltage recordings in response to presynaptic current steps. Each column shows data from one pair. The* ***first and second row*** *show transients recorded from the two cells when cell 1 was presynaptic; for the* ***third and fourth row****, cell 2 was presynaptic. In each diagram, the top trace is the response when depolarizing current was injected into the presynaptic neuron and the bottom trace is the response to hyperpolarizing current. Note that the scale for the postsynaptic signals is two times larger than for the presynaptic signals. The coupling coefficients k_{12} and k_{21} found for the two directions of signal transfer are given for each pair, and the number at the top of each column indicates the synapse conductance $\widetilde{G}_{syn}$ as determined later in this section.*

Fig. 7.6 shows the fit curve for each voltage transient in red.

Before we proceed to a discussion of the results of this evaluation for the example pair and the rest of the pairs, we discuss several **typical features of the current step experiments and fits** that are illustrated by fig. 7.6:

- Comparing the voltage changes marked in blue in the left and right column confirms that – as expected from (66) – the **coupling coefficient can indeed be different for the two directions of signal transfer** across the synapse: Even though the largest presynaptic voltage change ΔV_{As} in the left column (that is, for signal transfer from cell 1 to cell 2) is bigger than the largest ΔV_{As} in the right column, the postsynaptic voltage change ΔV_{Bs} it causes is only about half as big as in the right column, resulting in a much smaller coupling coefficient from cell 1 to cell 2 than from cell 2 to cell 1. With (66), this indicates that cell 2 has a larger input conductance than cell 1, which is also supported by the finding that a given current, if injected into cell 2, causes a smaller presynaptic voltage change than if injected into cell 1.

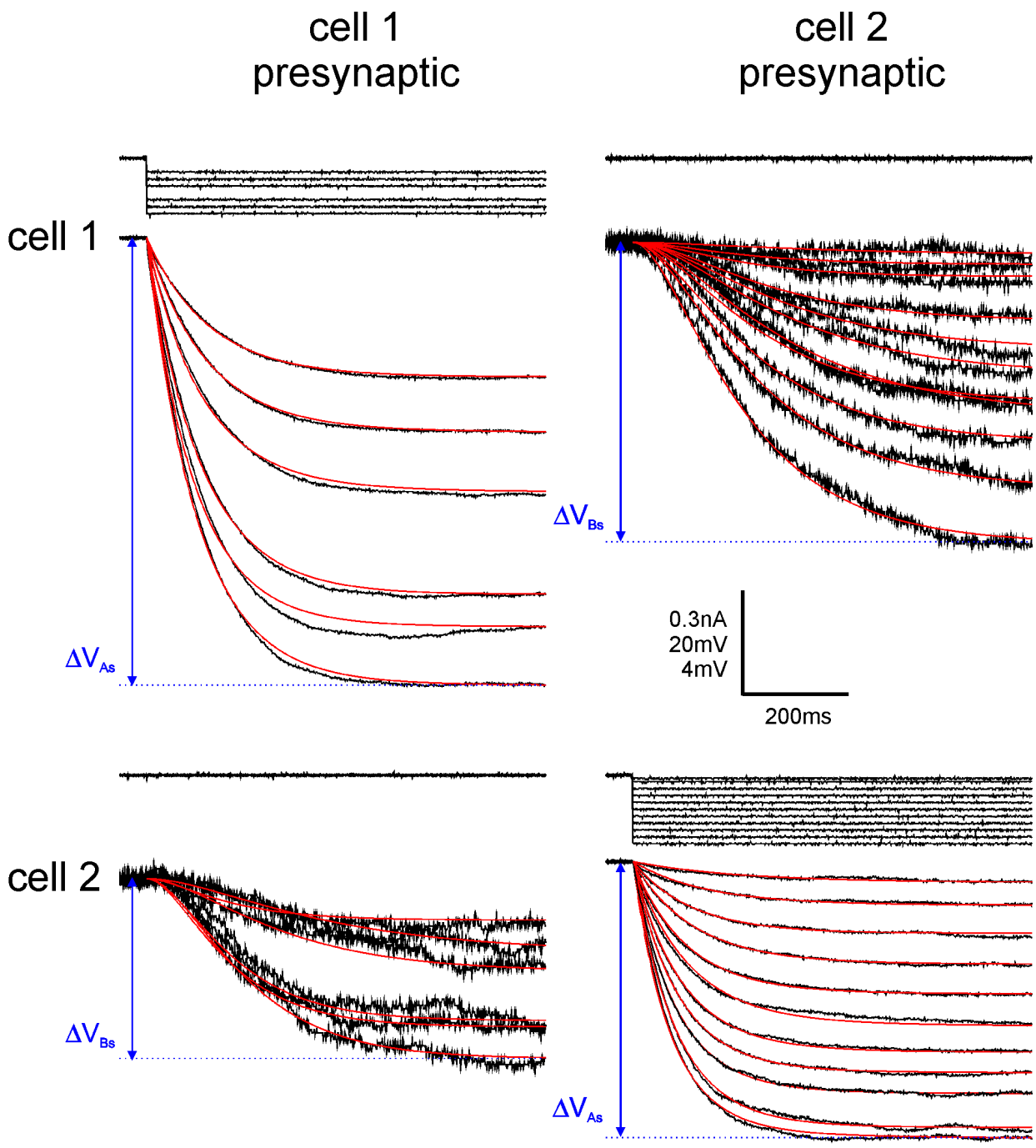

Figure 7.6: ***Current step responses and fits for a cell pair coupled by a one-point synapse.*** *This figure shows the voltage responses to hyperpolarizing current steps recorded from pair ix. In the* ***left column****, cell 1 is presynaptic; the four graphs show (top to bottom) the current traces injected into cell 1, the voltage responses of cell 1 (black) and fits (red), the current injected into cell 2 (which is zero because cell 2 is postsynaptic) and the voltage responses of cell 2 (black) and fits (red). In the* ***right column****, cell 2 is presynaptic and the sequence of graphs from top to bottom is the same as in the left column. Note that the postsynaptic voltage responses are blown up by a factor of five with respect to the presynaptic voltage signals: The scale bar is 20mV for presynaptic voltages, 4mV for postsynaptic voltages and 0.3nA for currents. The fits were obtained as described in the text. Comparing the pre- and postsynaptic voltage changes (marked in blue) for selected traces in the left and right column demonstrates that the coupling coefficient* $k = \Delta V_{Bs}/\Delta V_{As}$ *is different for the two directions of signal transfer (as expected from (63)).*

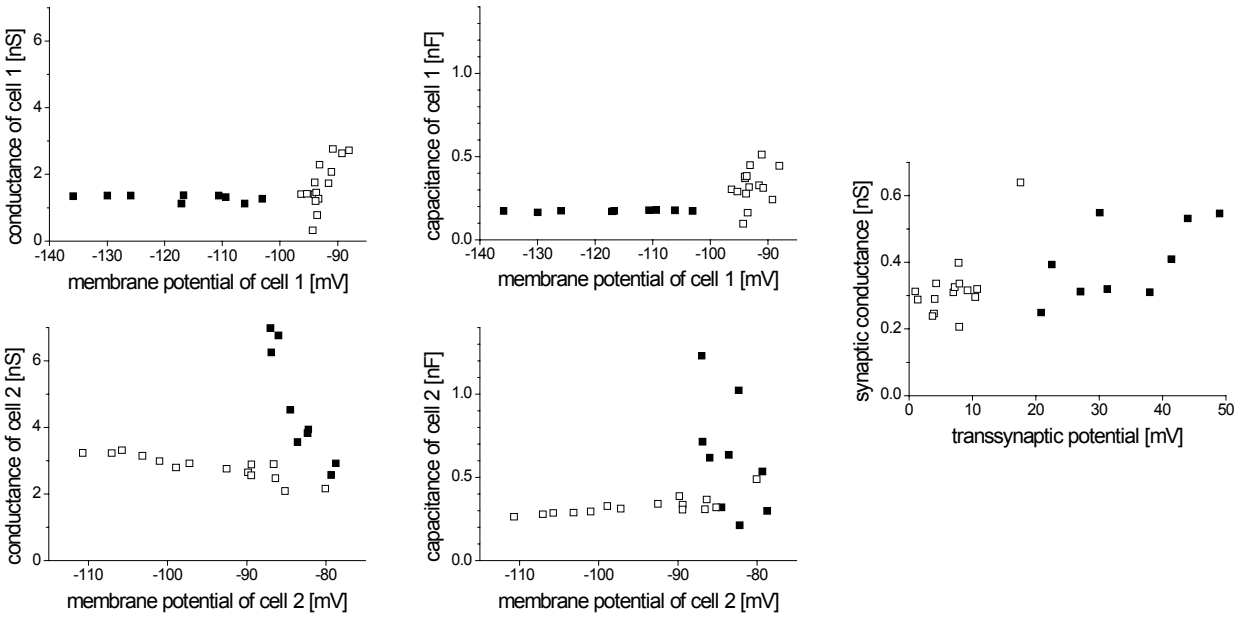

Figure 7.7: ***Results obtained for the example cell pair with the aid of the isopotential model.*** *These five plots summarize the values obtained from the measurements shown in fig. 7.6 (and from some additional transient pairs that have been omitted from fig. 7.6 for clarity) when the isopotential model is applied. Specifically, the plots show $\widetilde{G}$ for cell 1 (**left, top**) and for cell 2 (**left, bottom**), $\widetilde{C}$ for cell 1 (**middle, top**) and for cell 2 (**middle, bottom**) and the synaptic conductance $\widetilde{G}_{syn}$ (**right**). The cell conductances and capacitances are plotted against the respective cell's membrane potential, whereas the synaptic conductance is plotted against the voltage drop across the synapse. The solid symbols in each case denote values obtained with cell 1 acting as presynaptic cell, the open symbols belong to transient pairs measured with cell 2 presynaptic.*

- Because the membrane potential of the neurons was often not perfectly stable, the voltage traces sometimes show fluctuations that make the determination of steady state values as well as the fitting with theoretical curves rather difficult, especially if the fluctuations are not much smaller than the voltage changes caused by the current steps, themselves. This is most apparent in the lower left panel in fig. 7.6. Correspondingly, the values of $\widetilde{G}_{syn}$, $\widetilde{G}_A$, $\widetilde{G}_B$, $\widetilde{C}_A$ and $\widetilde{C}_B$ obtained from such transients sometimes vary a lot between different pairs of transients.
- Apart from these very noisy potential traces, the fits (shown in red) usually agreed moderately well with the experimental transients. The most obvious systematic exceptions are very strongly hyperpolarized traces such as the bottom three transients recorded from cell 1 in the left column, were the experimental curve does not reach a stable steady state value and can therefore not be well fit to the theoretical curve. Note that such unstable membrane potentials in the very hyperpolarized range were already observed for the neuriteless cell bodies in section 5.1 (compare to fig. 5.2).

Results obtained with the isopotential model for an example pair

Fig. 7.7 shows the raw results of the procedure described above for the example neuron pair; it contains values obtained from the measurements shown in fig. 7.6 and from some additional measurements that have been omitted from fig. 7.6 for clarity. Each of the five plots in the figure combines results from both directions of signal transfer: The solid symbols show the results when cell 1 was presynaptic and the open symbols stand for transients when cell 2 was presynaptic.

As each data point in the figure was obtained from a pair of transients rather than from a single

steady state of the cell pair, the data point can not be ascribed to a single membrane potential. In the figure, the cell parameters are therefore plotted against the average of the two steady state potentials at the beginning and end of the transients. Similarly, the synaptic conductances are plotted against the absolute value of the average of the two trans-synaptic potential differences before and after the current step.

The figure illustrates **several findings that were similar in all of the cell pairs** used here:

For the cell conductances and cell capacitances (left and middle column in the figure), the data obtained when the respective cell was postsynaptic (open symbols in the top graphs and solid symbols in the bottom graphs) show much higher variability than those measured when the cell was presynaptic. This higher variability is due to the low signal-to-noise ratios of the postsynaptic voltage transients (see fig. 7.6). The **results obtained when a cell is presynaptic are thus more reliable than those measured when the cell is postsynaptic**.

While the conductance values obtained for cell 1 when it is presynaptic do not depend on membrane potential, the values obtained for cell 2 when it is presynaptic show an interesting dependence: They are slightly larger for membrane potentials below -100mV than at less hyperpolarized potentials. Such a conductance change in the potential range of about -90mV to -110mV was observed for several of the cell pairs used here; it reflects the change in conductance previously found for cell bodies without neurites (see fig. 5.4) and is thus due to the fact that the neural membrane is not perfectly passive in this potential range.

Apart from this weak dependence of the cell conductance on the membrane potential -100mV, the values of the cell conductances and capacitances obtained from different pairs of transients for a given direction of signal transfer in a pair were usually similar and showed no systematic dependence on membrane potential. For the following discussion of the results from all eleven neuron pairs, they were therefore averaged, resulting in **two values for each cell's conductance and capacitance – one for each direction of signal transfer**.

Results for all pairs

In the case of the synapse itself, it is particularly interesting to check if its conductance shows any signs of voltage dependence, because the conductance of several types of gap junctions in vertebrates and invertebrates has been found to depend on the trans-synaptic voltage [4] – fig. 7.8 shows examples of such voltage-dependent conductances for two types of rodent connexins, Cx32 and Cx50. For an electrical synapse between a pair of identified neurons in the visceral ganglion of *Lymnaea stagnalis*, the coupling coefficient has also been found to depend on the amount of stimulation current injected into the presynaptic neuron [50], but for electrical synapses between neurons in the pedal ganglia, all that is known is that they are non-rectifying [56].

To examine whether the synapses between the eleven neuron pairs studied here show any signs of voltage-dependence, the values obtained for $\widetilde{G}_{syn}$ for a given direction of signal transfer in each pair were divided by their average and plotted against the absolute value of the trans-synaptic potential difference in fig. 7.8. If the conductance of the synapses was voltage-dependent in the range of up to 100mV, the slopes of the clouds of data points in this figure should systematically deviate from the horizontal lines that indicate a value of one for each of the cell pairs. But they do not, meaning that the **electrical synapses between cultured neurons from the A-clusters in the pedal ganglia of *Lymnaea* are not voltage-dependent**. Just as the cell conductances and capacitances above, the values of $\widetilde{G}_{syn}$ obtained for a given direction of signal transfer in each

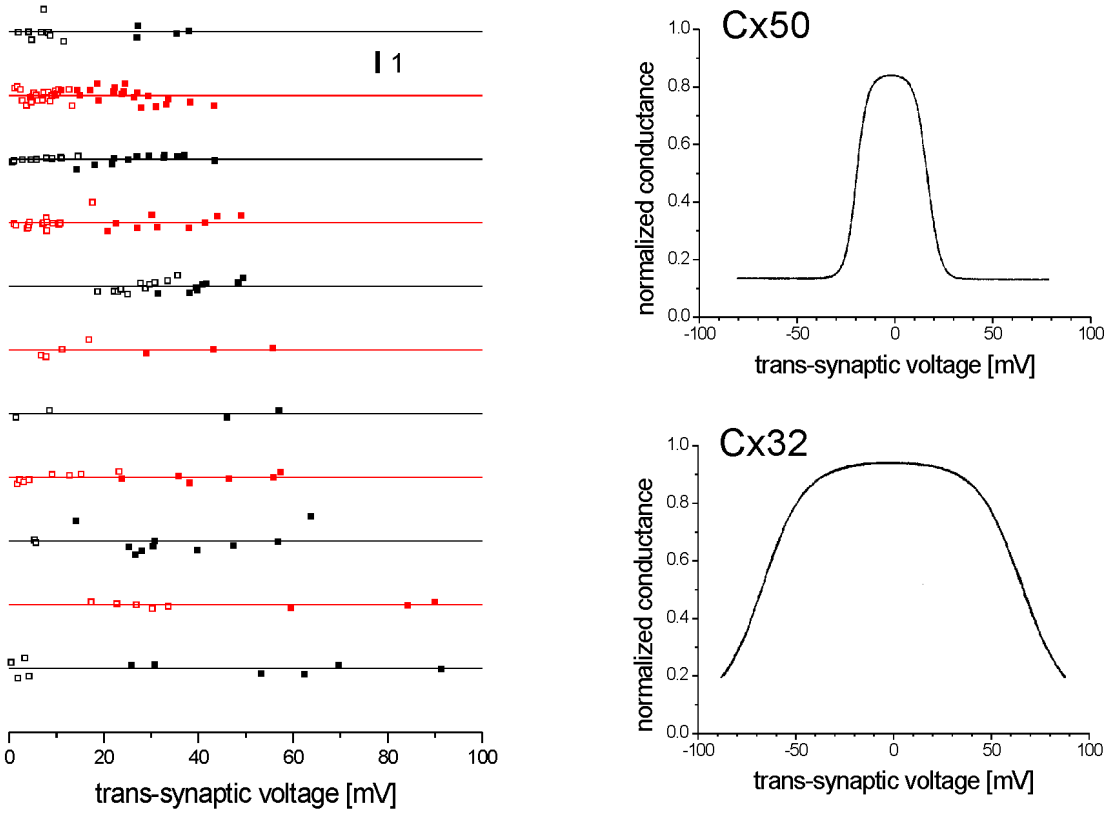

Figure 7.8: ***Electrical synapses between Lymnaea neurons are not voltage-dependent.*** *(**Left**) Synaptic conductances $\widetilde{G}_{syn}$ of all eleven cell pairs for the two directions of signal transfer, divided by the respective average conductance and plotted against the transsynaptic potential. For the solid symbols, cell 1 was presynaptic; for the open symbols, cell 2 was presynaptic. For each data set, the horizontal line corresponds to the average conductance. There are no signs of voltage dependence. (**Right**) For comparison, these two graphs show the voltage dependence of the normalized conductance for two kinds of connexins. These data were obtained by pairing Xenopus oocytes that expressed the respective gap junction proteins. From* [91].

pair were therefore averaged over all pairs of transients, again resulting in two mean values of $\widetilde{G}_{syn}$ for every pair, namely one with cell 1 presynaptic and one with cell 2 presynaptic.

The averaged results for all eleven cell pairs are shown in figs. 7.9 through 7.12; for completeness, all averages and standard deviations are also listed in a table in appendix G.

Before we proceed to the synaptic conductances – whose determination is the main purpose of the present section – we inspect the results for the cell conductances $\widetilde{G}_1$ and $\widetilde{G}_2$. The fact that there are two values for each of these conductances (one for each direction of signal transfer) allows us to check if the results obtained for the eleven cell pairs are consistent with the assumption that a pair of electrically coupled neurons is well described by the detailed model from section 6.3. This is because, according to (106), the conductance values $\widetilde{G}_1$ and $\widetilde{G}_2$ obtained from the isopotential model should not depend on the direction of signal transfer if the detailed model is valid. A straightforward way to see if they do is to plot the results obtained for one direction against those obtained for the other direction, which is done in fig. 7.9 for both cells. If the results did not depend on the direction of signal transfer, all data points should fall on the diagonals in the two graphs. It turns out, however, that the majority of data points in both graphs lie above the diagonals, indicating that the value obtained for the conductance of a neuron tends to be slightly

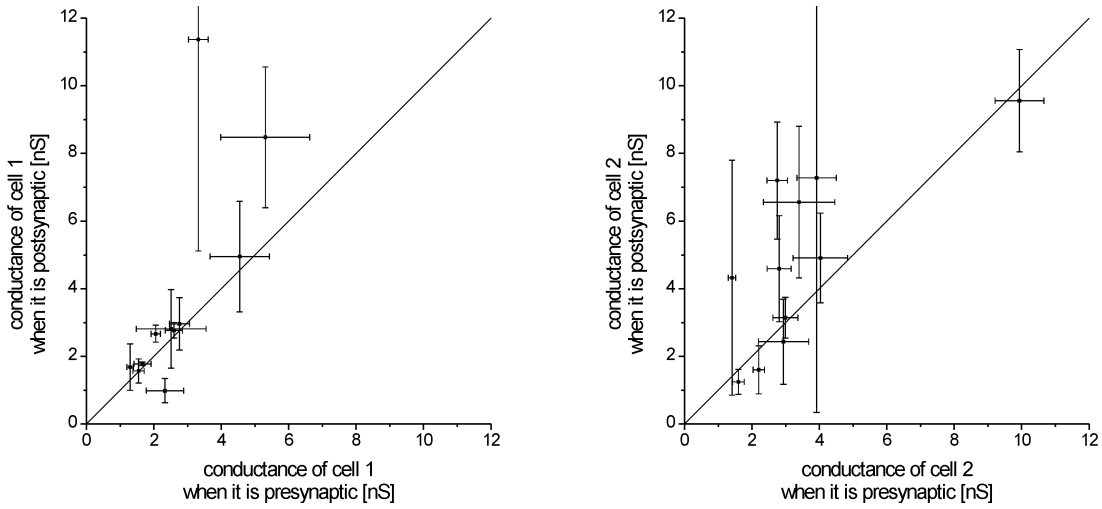

Figure 7.9: ***Results for the cell conductances of all neuron pairs with a single point of contact.*** *For cell 1 (**left**) and cell 2 (**right**) of each cell pair, these graphs plot the cell conductance value obtained when the cell is postsynaptic against the value obtained when it is presynaptic. The error bars correspond to the standard deviations of the two values. If the detailed model is a good description of the coupled cell pair, the data points should fall on the diagonal.*

larger when the neuron is postsynaptic than when it is presynaptic. This finding suggests that **a pair of nerve cells coupled by an electrical synapse has properties that are not perfectly described by the detailed model**, but it is not clear what exactly causes the deviations observed in fig. 7.9.

A second result apparent in the figure is that the vertical error bars are usually larger than the horizontal ones. This confirms that – just as for the example neuron – the results obtained when a cell is postsynaptic are much more variable than when it is presynaptic.

To get an impression of the **distribution of cell conductances**, the mean value of the two results for each cell's conductance was computed and plotted as a cumulative distribution function in the left part of fig. 7.12 (open black symbols). Most of the conductances are in the range of 2-5nS (corresponding to input resistances of several hundred MΩ), with extreme values of 1.4nS and 9.7nS.

As can be seen in fig. 7.10, where the same kind of plot as in fig. 7.9 is now done for $\widetilde{C}_1$ and $\widetilde{C}_2$, the value obtained for a cell's capacitance also is larger when the cell is postsynaptic than when it is presynaptic. However, in the case of the capacitances there is no conclusion as to the validity of the detailed model that can be derived from this finding (see section 6.4). Again, the mean value of the two capacitance results for each cell was computed and included in a cumulative distribution function in the right part of fig. 7.12 (open black symbols). Typical values are between 300pF and 500pF, with maximum and minimum values of 143pF and 1261pF.

From (106), we also expect that the synaptic conductance values obtained for the two directions of signal transfer should be the same. To see if they are, fig. 7.11 shows the same kind of graph as in figs. 7.9 and 7.10 now for the synaptic conductances, plotting the synaptic conductance value obtained for one direction against that obtained for the other. Surprisingly, even though the values obtained for the cell conductances and capacitances do depend on the direction of signal transfer (see above) and the values of the synaptic conductances are derived from the same

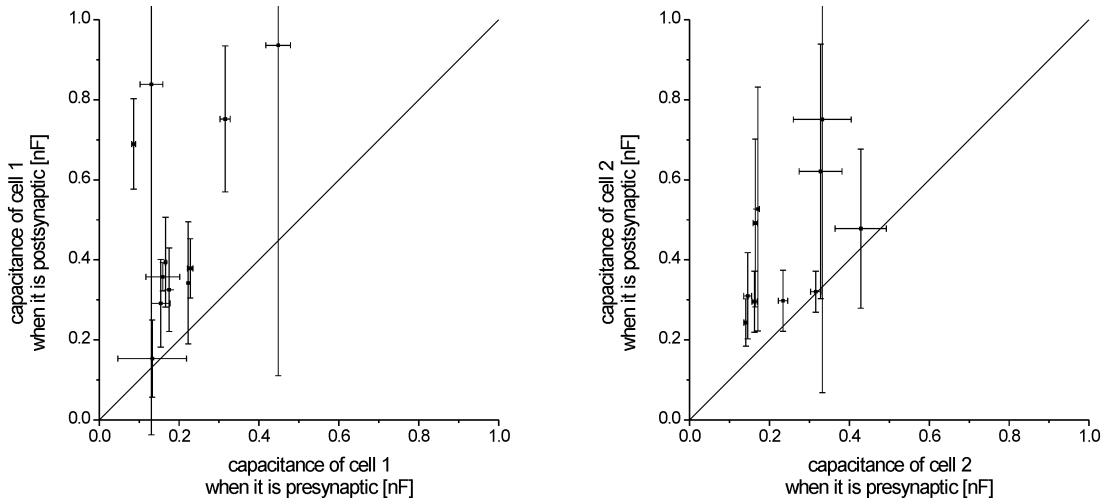

Figure 7.10: ***Results for the cell capacitances of all neuron pairs with a single point of contact.*** *For cell 1 (**left**) and cell 2 (**right**) of each cell pair, these graphs plot the cell capacitance value obtained when the cell is postsynaptic against the value obtained when it is presynaptic. The error bars correspond to the standard deviations of the two values. The capacitance obtained from the isopotential model is always higher when a cell is postsynaptic than when it is presynaptic.*

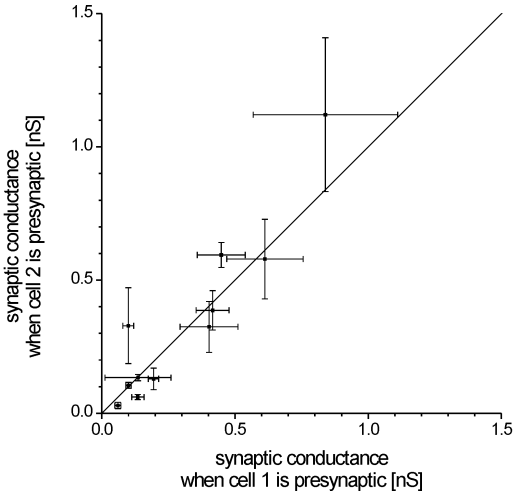

Figure 7.11: ***Results for the synapse conductances of all neuron pairs with a single point of contact.*** *This graph plots the synapse conductance value obtained when the cell 2 is presynaptic against the value obtained when cell 1 is presynaptic. The error bars correspond to the standard deviations of the two values. If the detailed model is a good description of the coupled cell pair, the data points should fall on the diagonal.*

pairs of transients, they do not depend on which cell is presynaptic, because the data points do not systematically deviate from the diagonal in fig. 7.11. **Whatever effect causes the cell conductance and capacitance values to depend on the direction of signal transfer therefore seems to cancel out in the case of the synaptic conductances.**

For each cell pair, the two values of $\widetilde{G}_{syn}$ are thus rather similar and we can compute their mean to obtain a single value for the synaptic conductance in each pair. The distribution function of these mean values is again displayed in the left part of fig. 7.12 (open blue symbols and inset); the values range from 0.04nS to 0.98nS. For vertebrate gap junctions, single channel conductances

between 0.03nS and 0.3nS have been reported [87], so if the gap junction channels between *Lymnaea* neurons had similar conductances, the values of $\widetilde{G}_{syn}$ found here would mean that there are **very few open channels in a single-point synapse**. However, the limited permeability of *Lymnaea* electrical synapses for dye molecules (see section 7.2.1) and the small outer diameter of the gap junction channels in *Helisoma* [35] suggest that the pore diameter of invertebrate gap junction channels may be considerable smaller than that of connexons. In this case, the synaptic conductances found here would correspond to more than just a few channels, but would presumably still be small compared to the number of channels per gap junction plaque found in freeze fractures of *Helisoma* electrical synapses, namely ≈170 [35].

The distribution of the $\widetilde{G}_{syn}$ shown in fig. 7.12 also implies that in pairs of neurons with guided neurites and a single site of physical contact, the synaptic conductance typically is about an order of magnitude smaller than the input conductances of the two neurons, corresponding to a ratio of $\kappa \approx 1/10$ as defined on page 72. According to section 6.5, this demonstrates that **even in designed networks with many neurons, current step experiments can be used to estimate the conductance of an electrical synapse** between a given pair; with $\kappa \approx 1/10$ the error in $\widetilde{G}_{syn}$ due to alternative current pathways through adjacent neurons will be tolerable.

As many studies on electrical synapses characterize the synaptic strength with the coupling coefficient rather than with the synaptic conductance, we also compute the **coupling coefficients** for all eleven pairs and both directions of signal transfer. To do this, the coupling coefficients for all pairs of transients were obtained from the steady states before and after the current step according to (66), and were averaged over all pairs of transients for a given pair and direction of signal transfer. The resulting values of k_{12} and k_{21} are shown in the left part of fig. 7.13 in the form of a cumulative distribution function (open symbols): Most of the coupling coefficients are around 0.10, with extreme values of 0.01 and 0.27. This is **at the lower limit of the range of coupling coefficients reported for different molluscan species** both *in vitro* and *in vivo* [1][5][36][62][61] – as will be shown and discussed in section 7.2, this is presumably due to there being only a single point of contact between the neurons.

The right part of the same figure plots the same data against the synaptic conductance $\widetilde{G}_{syn}$ (again as open symbols). The graph confirms that the coupling coefficient, while being a good measure for the impact of presynaptic voltage changes on the postsynaptic potential, is only weakly correlated to the synaptic conductance – this is because it depends not only on $\widetilde{G}_{syn}$, but also on the conductance $\widetilde{G}_B$ of the postsynaptic neuron (see (66)). **For characterizing the electrical synapse itself, the coupling coefficient is thus not a good measure.**

Isopotential model versus detailed model

So far, we have always used the isopotential model from section 6.2 to describe the electrically coupled cell pairs. But due to the simple geometry of the linearly growing cells in the pairs, they can also be described with the detailed model from section 6.3, which does not neglect voltage drops along the neuritic cables. According to section 6.4, we expect the results obtained from the two models to be similar, because cultured *Lymnaea* neurons are electrotonically compact and therefore actually *are* close to isopotential. We now check how similar they really are.

To do this, we use equations (101) through (105) to compute the cell input conductances G and the synapse conductances G_{syn} from the $\widetilde{G}$ and $\widetilde{G}_{syn}$ found with the isopotential model, the cell's physical dimensions and the electrical parameters from section 5.2 – note that G_{syn} can also be

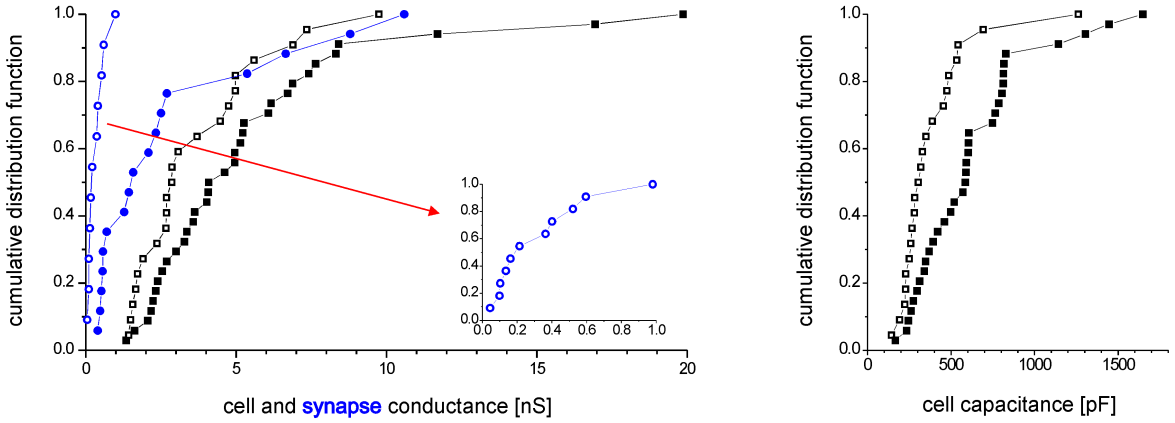

Figure 7.12: ***Cumulative distribution functions for the results from all cell pairs.*** *(**Left**) Distribution functions of the cell conductances (black) and synaptic conductances (blue) of all cell pairs studied - those with a single point of contact (open symbols) and those with multiple points of contact (solid symbols). The inset shows an enlarged version of the synaptic conductance distribution function for pairs with a single contact. (**Right**) Distribution functions of the cell capacitances of cells from pairs with a single contact (open symbols) or multiple contacts (solid symbols).*

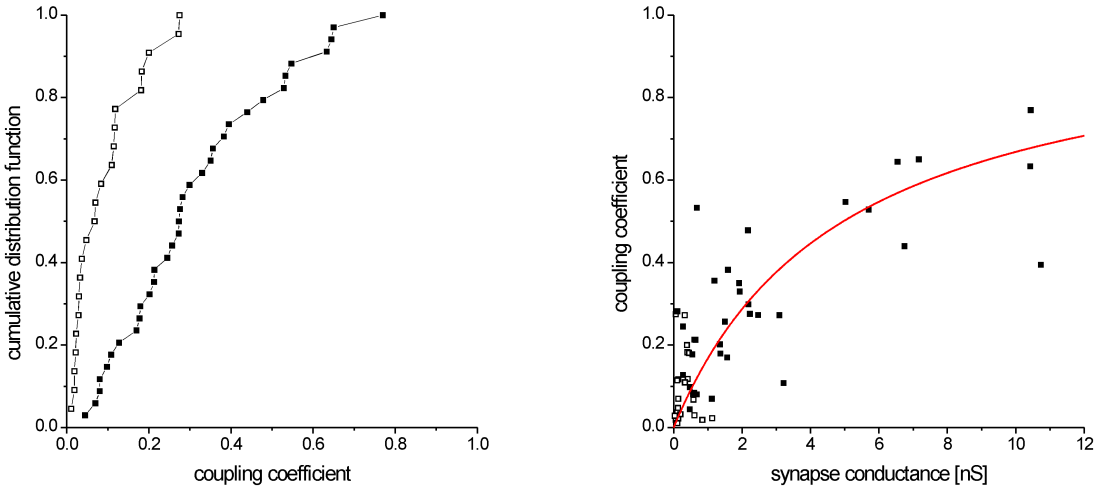

Figure 7.13: ***Coupling coefficients for all cell pairs.*** *In both graphs in this figure, open symbols denote coupling coefficients from pairs with a single point of contact and solid symbols are coupling coefficients from pairs with multiple contacts. (**Left**) Cumulative distribution functions of the coupling coefficients. (**Right**) Coupling coefficients plotted against synapse conductance. The two are only weakly correlated because k_{AB} depends not only on $\widetilde{G}_{syn}$, but also on $\widetilde{G}_B$. The red curve shows the coupling coefficient according to (63) for a postsynaptic conductance of $\widetilde{G}_B = 5$nS and was obtained by fitting the data from multiple-contact synapses to (63).*

derived directly from experimental data, cell dimensions and electrical parameters with the aid of (89), which (by definition) gives the same result.

The resulting G and G_{syn} are compared to the results from the isopotential model by plotting them against $\widetilde{G}$ and $\widetilde{G}_{syn}$ in the left and middle part of fig. 7.14. **For the cell input conductances, the agreement between the two models is very good**: The black data points in the left part all are very close to the diagonal corresponding to $G = \widetilde{G}$. The input conductances of electrically coupled snail neurons in designed networks can hence be accurately measured with current step experiments.

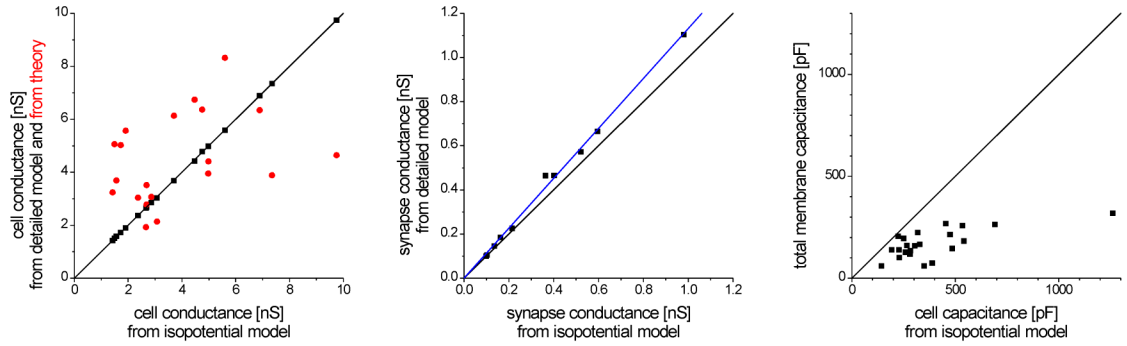

Figure 7.14: ***Comparing results obtained with the isopotential model and the detailed model and from theory.*** *(**Left**) Values of G obtained with the detailed model (black) and calculated from the physical dimensions of the cell with the electrical parameters from chapter 5 (red), plotted against the $\widetilde{G}$ obtained for the same cells with the isopotential model. The black line is the diagonal. The two models agree well, but the difference between the calculated G and the experimental results is large for some of the cells. (**Middle**) Values of G_{syn} obtained with the detailed model, plotted against $\widetilde{G}_{syn}$ obtained for the same pairs with the isopotential model. The black line is the diagonal and the blue line is a linear fit with slope 1.13, thus the G_{syn} are around 13% larger than the G. (**Right**) Total membrane capacitances calculated from the geometry of the cell and c and c_s from chapter 5, plotted against the capacitances obtained for the same cells with the isopotential model. The black line is the diagonal. The $\widetilde{C}$ obtained with the isopotential model are larger than the total membrane capacitances.*

The agreement is not that perfect for the synapse conductances, however, as the data points in the middle part of the figure all lie above the diagonal. A linear fit to the data and through the origin (shown in blue in the figure) gives a slope of 1.13, showing that the synaptic conductances obtained with the detailed model – which are the true synapse conductances if the detailed model is good – are about 13% larger than the values found with the isopotential model. **Applying the isopotential model to pairs of electrically coupled neurons will therefore result in slightly too small synaptic conductance estimates.**

For the cell capacitance $\widetilde{C}$, there is no corresponding parameter in the detailed model that we could compare to it.

In summary, **voltage drops along the neuritic cables of cultured Lymnaea neurons can obviously be neglected without introducing large errors into the values obtained for cell and synapse conductances from current step experiments.**

The results are consistent with the electrical cell parameters from optical recording

The fact that the results from detailed and isopotential model are similar confirms our finding from section 5.2, namely that the cells used here are electrotonically very compact. But there is a further test we can make to see whether the results of the present section are consistent with the electrical parameters from chapter 5: We can use these parameters and the physical dimensions of the neurons in the pairs to compute the **theoretically expected input conductances** of the neurons according to (28) and then compare this value to the one found with the current step experiments.

This is done in the left part of fig. 7.14 by plotting the value from this calculation against the $\widetilde{G}$ derived from the experimental results with the isopotential model (see red dots). Two things are apparent from this plot:

- While there is clearly a correlation between the calculated conductance and the $\widetilde{G}$ obtained from current step experiments, some of the red dots are high above or far below the diagonal, indicating that the computed conductance is more than three times larger than $\widetilde{G}$ for some cells and smaller than half of it for others. This is immediately **explained by the high variability of the electrical parameters g_s, g and r** between neurons: In section 5.2, we found $g_s = (0.020 \pm 0.017)$mS/cm^2, $g = (0.035 \pm 0.007)$mS/cm^2 and $r = (394 \pm 137)\Omega$cm. Therefore, using the mean values of these parameters – as was done when the input conductances of the cells were computed – *must* for some cells produce too large results and for others too small ones.
- But the fact that the red dots do not systematically deviate from the diagonal in either of the two directions confirms that the mean values of g_s, g and r – which were derived from optical recordings of signal propagation in the neurites of single cells – are consistent with the mean input conductances measured with very different experiments, namely by probing electrically coupled cell pairs with current steps. **Especially for the values of g_s and g, which were the least reliable results of section** 5.2**, this confirms that they are in the correct range.**

As stated above, there is no cell parameter directly comparable to the $\widetilde{C}$ from the isopotential model. We can, however, argue that $\widetilde{C}$ would be equivalent to the total membrane capacitance of soma and neurites if the cell would really behave like a single, perfectly isopotential compartment. Therefore, total membrane conductance of each neuron was computed via

$$C_{total} = c_s \pi d_s^2 + \sum_{j=1}^{J} c \pi d_j l_j \tag{114}$$

where the first part is the somatic membrane conductance (see (3)) and the second part is the sum of all neuritic membrane conductances (compare to (4)), and C_{total} was plotted against $\widetilde{C}$ in the right part of fig. 7.14. It is smaller than $\widetilde{C}$ (and therefore below the diagonal) for all cells, but the dots are closer to the diagonal for small $\widetilde{C}$ than for large $\widetilde{C}$. This makes sense, because cells with small $\widetilde{C}$ – as the cell bodies are all very similar in size – will tend to have fewer and/or shorter neurites and will thus behave more like a single compartment than a cell with large $\widetilde{C}$.

7.2 The strong synapse: Multiple contact points

The synapses discussed in the previous section were localized to a single point of contact between two neurons, which is the simplest synapse geometry possible and therefore the most desirable for simple, designed neural networks. To see how the conductance of such a synapse relates to that of a more biological configuration with several points of contact between the coupled cells, the **synapse conductances for pairs of neurons in conventional cell culture** are determined in the present section.

Cultured neurons from the snail *Helisoma* have been reported to form electrical synapses at *all* points of contact between two neurites [35]. If this was also true for *Lymnaea* neurons, this behavior could be exploited to manipulate the coupling strength between two neurons in a designed network simply by controlling the number of contacts between their neurites with the aid of guided outgrowth. To see if two neurons establish electrical synapses at all points of contact, it is necessary to localize the synapses, and the first part of the present section describes some attempts to do so by staining with intracellular dyes.

In the second part of the section, the conductances of synapses with multiple contact points are determined with the isopotential model and compared to those of synapses with only a single

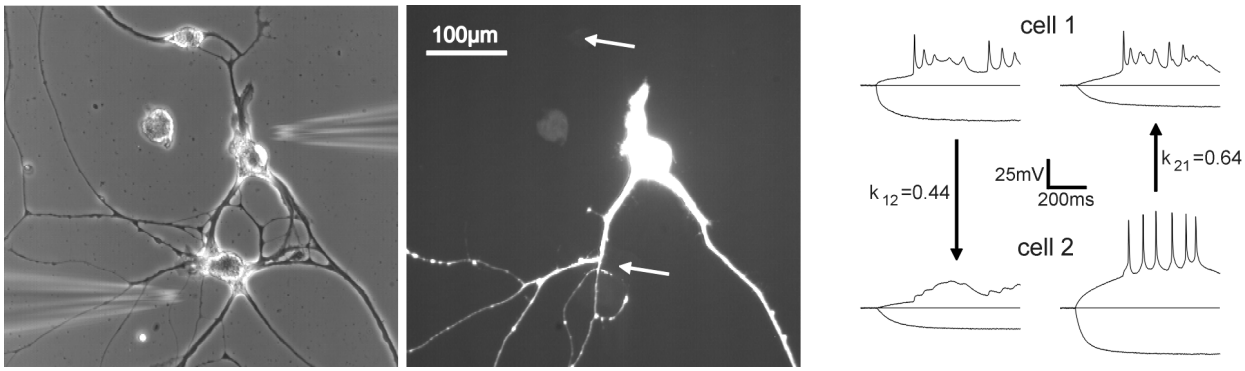

Figure 7.15: ***No dye coupling despite strong electrical coupling.*** *(**Left**) Micrograph of an pair of snail neurons embedded in a sparse network in conventional cell culture. The neuron close to the upper micro-electrode is cell 1, that one close to the lower electrode is cell 2. (**Right**) Voltage transients recorded from the cell pair in response to presynaptic current steps. The top row shows recordings from cell 1, the bottom row from cell 2. In the left column, cell 1 is presynaptic; in the right column, it is postsynaptic. The coupling coefficients are also given – the pair is strongly coupled. (**Middle**) Fluorescence micrograph of the same area as on the left after 40min of Lucifer Yellow injection into cell 1. Cell 1 is nicely filled, but despite strong electrical coupling, the dye did not pass into the two cells surrounding cell 1 (their location is indicated by the white arrows). Also note the luminescence of the isolated (and presumably dead) neuron to the left of cell 1.*

point of contact.

7.2.1 Attempts to localize the synapses by staining

The left part of fig. 7.15 shows a pair of A-cluster neurons from the pedal ganglia of *Lymnaea* stagnalis, embedded in a sparse network of other neurons, after two days in conventional cell culture. The two neurons have made physical contact at several locations and – as also shown in the figure – established a strong electrical synapse. To check whether this connection is restricted to a subset of all points of contact or if a synapse is present at every point of contact, we need a way to **localize the electrical synapses**.

As no antibodies to *Lymnaea* gap junctions are available, this can not be done by immunostaining. A possible alternative method, however, arises from the fact that several water-soluble fluorescent dyes are known that are small enough to pass through many types of gap junction channels [54][68][77][82][88]. If one of the two neurons is intracellularly stained with such a dye and the spreading of the dye is monitored with fluorescence microscopy, one can therefore hope to **observe where the dye passes from one cell to the other and thus to identify the sites of coupling**.

This was tried for cultured pairs of *Lymnaea* neurons with the dye Lucifer Yellow CH (MW 443g/mol, Sigma), which can pass through many different kinds of gap junction channels [82][87]. To inject the dye, it was dissolved in water at a concentration of 10%. The neuron was then impaled with a microelectrode filled with the dye solution, and the dye was driven into the cell by application of hyperpolarizing current pulses [82][86]. When the spreading of the dye was observed with fluorescence microscopy[14], however, it turned out that the impaled neuron was nicely

[14] The excitation light from a mercury lamp was filtered with a band pass (405nm for LY and 365/10nm for HCCA) and reflected by a beam-splitter (515nm for LY and 400nm for HCCA). The fluorescence signal passed the same beamsplitter and a second filter (long pass 515nm for LY and band pass 460/50nm for HCCA). Most filters were

filled within a few minutes, but that no dye could pass into the neuron coupled to it (see fig. 7.15). The approach was tested in 23 pairs of cultured *Lymnaea* neurons that had previously been demonstrated to be electrically coupled by electrophysiological measurements, but **in none of the pairs Lucifer Yellow could spread from one cell to the other**.

The ability of a dye molecule to pass through a gap junction depends on the pore diameter of the gap junction channel and the size of the dye molecule [54][88], which is about 11Å for Lucifer Yellow [88]. There are, however, smaller fluorescent molecules, one of the smallest being HCCA (hydroxycoumarin carboxylic acid, MW 206g/mol, from Sigma, [54]). To see if HCCA can pass through electrical synapses between *Lymnaea* neurons, the staining experiments described above were repeated with this dye in two pairs of electrically coupled neurons[14] , but with the same result as for Lucifer Yellow: No dye coupling was observed.

In summary, the fact that the dye molecules tested here can not pass through the electrical synapses between snail neurons means that **staining experiments can not be used to localize the sites of electrical coupling between two cells**. However, the same fact provides information about the pore size of the gap junction channels between *Lymnaea* neurons: That neither Lucifer Yellow nor the even smaller HCCA can pass through the pore suggests that the **pore size in *Lymnaea* electrical synapses is smaller** than the 16-20Å reported for mammalian gap junctions and the 20-30Å found in insect gap junctions [88]. This is also consistent with the finding that the gap junction particles in the related snail species *Helisoma* have *outer* diameters of only 10-14nm [35].

Even though staining of one cell in a pair can not reveal where the sites of electrical coupling are, it can at least be used to **determine the sites of physical contact**. In pairs like the ones discussed in the previous section – namely those with a single cable connecting the cell bodies and with a functioning electrical synapse – staining of one of the neurons can indicate where one cell ends and the other begins. Because the single point of physical contact thus determined *must* be the site of the synapse, staining with Lucifer Yellow can be used to localize the synapse in such pairs in spite of its inability to cross the synapse. This method was used to find the site of coupling for several of the pairs in section 7.1.

7.2.2 Results obtained with the isopotential model

As the attempts to localize the sites of coupling between pairs of conventionally cultured neurons by intracellular staining failed, the pairs can not be modeled according to the detailed model from section 6.3 in order to obtain the synaptic conductance from current step experiments. Instead, only the isopotential model from section 6.2 can be applied, but as we have seen in the previous section, the two models give very similar results, anyway.

Just as with the one-contact synapses, the conventionally cultured pairs were probed with current step experiments and the cell conductances $\widetilde{G}$, the cell capacitances $\widetilde{C}$ and the synapse conductances $\widetilde{G}_{syn}$ were determined from the resulting pairs of transients as in section 7.1. Altogether, this evaluation was done for three isolated pairs of randomly growing neurons and fourteen pairs that were embedded in networks of other cells. The results for all seventeen pairs are displayed in figs. 7.16 through 7.18; for completeness, all results are also listed in a table in appendix G.

[14] from AF Analysentechnik, Tübingen.

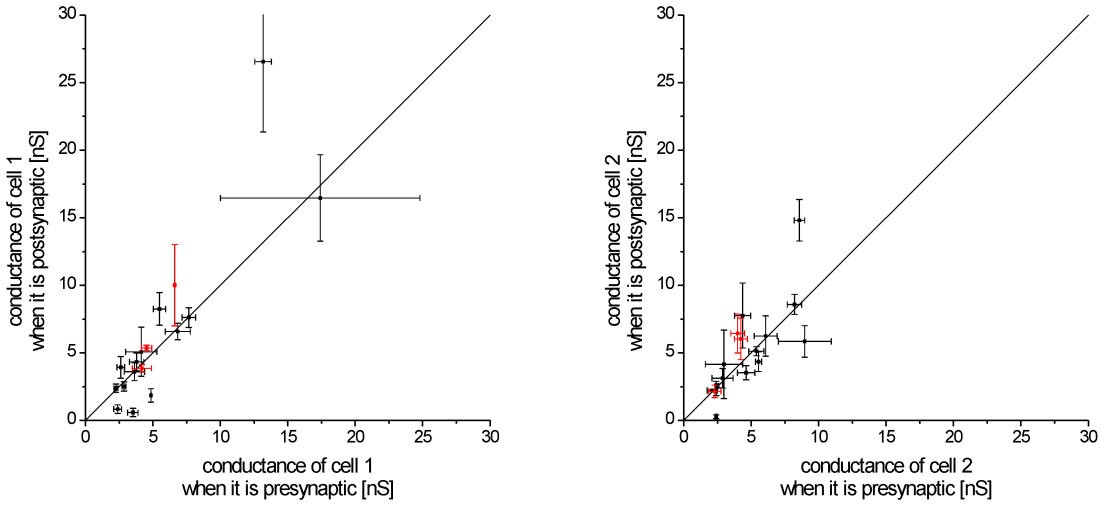

Figure 7.16: ***Results for the cell conductances of all neuron pairs with multiple contacts.*** *For cell 1 (**left**) and cell 2 (**right**) of each cell pair, these graphs plot the cell conductance value obtained when the cell is postsynaptic against the value obtained when it is presynaptic. The error bars correspond to the standard deviations of the two values. The values for the three isolated pairs are shown in red.*

Cell conductances

Fig. 7.16 shows the results for the cell conductances in the same format as in fig. 7.9. As was argued in section 6.5, the results obtained for $\widetilde{G}$ in isolated pairs if the simple model is applied are just the input conductances of the two cells. In contrast, the values of $\widetilde{G}$ obtained for embedded cell pairs depend on the conductances, resting potentials and coupling strengths of the surrounding cells. As far as one can tell from only three isolated pairs in the sample, however, the values of $\widetilde{G}$ for isolated pairs (red) and embedded pairs (black) in fig. 7.16 have rather similar distributions – while we do not know the influence of the surrounding network on the conductance values obtained for individual neurons, **being embedded in a net of other cells at least does not dramatically change the overall distribution of the conductance results**.

As with the cell conductances obtained for pairs with one contact point, we compute the mean of the two results for each cell's conductance and include it in a distribution function in fig. 7.12 (solid black symbols in the left part). Most of the values in this distribution are between 3nS and 8nS, with a minimum value of 1.3nS and a maximum value of 19.9nS. Compared to the input conductances of neurons with guided outgrowth (open black symbols), the input conductances of cells with several randomly growing neurites are thus only about 1.5 times bigger. As a small example shows, this is about the ratio we expect: With the electrical parameters from section 5.2 and with (28), a typical cell with a soma diameter of 60μm and two guided neurites of 250μm length and 5μm diameter has an input conductance of 4.94nS, and adding two or three more such neurites – which results in a primary neurite number typical for randomly growing cells – increases the input conductance by a factor of 1.54 or 1.81, respectively.

Cell capacitances

The results obtained for the cell capacitances are displayed in fig. 7.17, where the data shown in red again are the results for the three isolated cell pairs. As with the cell conductances, the results for isolated pairs and embedded pairs look very similar – being embedded in a network of neurons therefore seems to have no dramatic impact on the voltage *dynamics* in a pair of neurons,

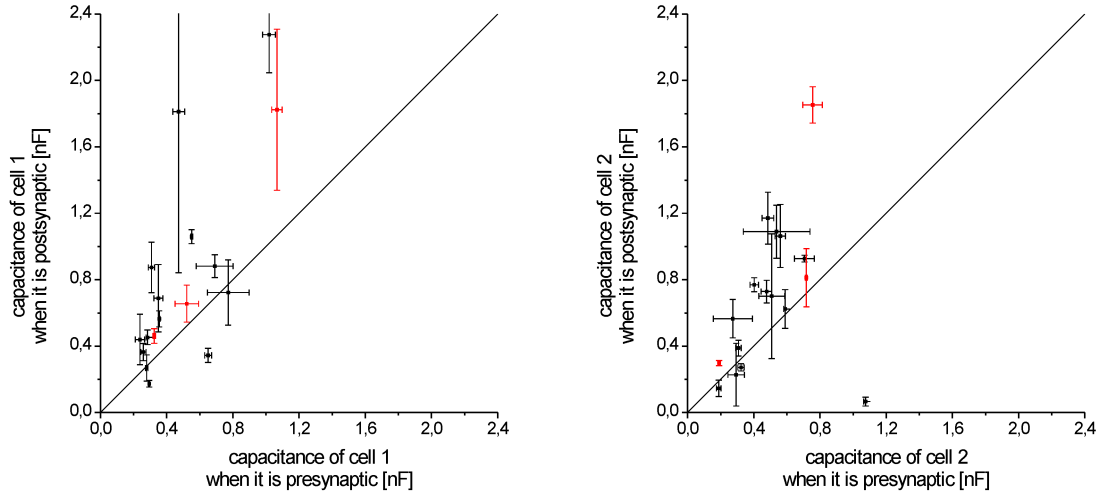

Figure 7.17: ***Results for the cell capacitances of all neuron pairs with multiple points of contact.*** *For cell 1 (**left**) and cell 2 (**right**) of each cell pair, these graphs plot the cell capacitance value obtained when the cell is postsynaptic against the value obtained when it is presynaptic. The error bars correspond to the standard deviations of the two values. The capacitance obtained from the isopotential model tends to be higher when a cell is postsynaptic than when it is presynaptic. Data for isolated pairs are shown in red.*

either. Again, the mean values of the two results for each neuron's capacitance are plotted as a distribution function in the right part of fig. 7.12 (solid black symbols); they range from 167pF to 1648pF, with most values between 300pF and 800pF. The values of $\widetilde{C}$ for the cells in multiple-contact pairs are therefore by about a factor of two larger than those for cells in single-contact pairs.

Synapse conductances

Fig. 7.18 shows the synapse conductances of all pairs with multiple contacts. According to section 6.5, the value obtained for $\widetilde{G}_{syn}$ in isolated pairs is just the total synaptic conductance between the two cells, while $\widetilde{G}_{syn}$ as determined for embedded pairs – due to additional contributions from parallel current pathways via surrounding cells – is only an upper limit for the real synaptic conductance between the two neurons. The fact that the values of $\widetilde{G}_{syn}$ for isolated pairs (red) and embedded pairs (black) are in the same range in fig. 7.18 therefore implies that this **upper limit is not too far above the actual value**. This confirms the estimations from section 6.5, which state that (at least in the sparse networks we are dealing with) the synaptic conductance obtained from current step experiments is on the same order of magnitude as the real synaptic conductance.

Again, the mean value of the synaptic conductance for each pair is included in fig. 7.12 (solid blue symbols) – typical values are between 0.5nS and 5nS, with extreme values of 0.4nS and 10.6nS. It is instructive to compare this distribution function to two of the other curves shown in the same figure, namely to that for single-point synapses (open blue) and to that for the input conductances of cells in multiple-contact pairs (solid black):

Compared to single-point synapses, the connections established by randomly growing neurons are about five to ten times more conductive. According to section 6.5, the value of $\widetilde{G}_{syn}$ obtained for pairs with multiple points of contact is equal to the sum of all single synaptic contacts between the two cells (in isolated pairs) or is an upper limit for this sum (in embedded pairs). Because the staining experiments described in section 7.2.1 failed, we do not know the number

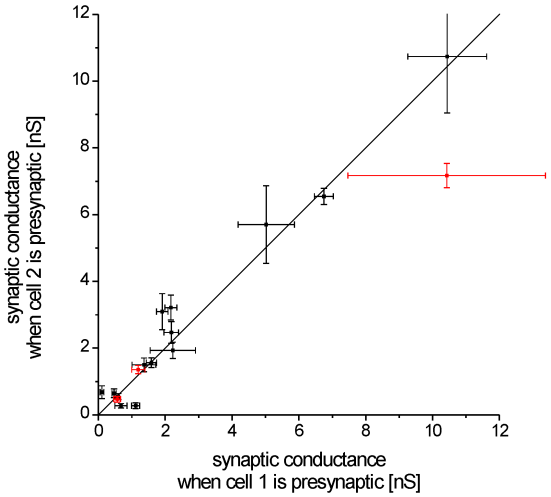

Figure 7.18: ***Results for the synapse conductances of all neuron pairs with multiple points of contact.*** *This graph plots the synapse conductance value obtained when the cell 2 is presynaptic against the value obtained when cell 1 is presynaptic. The error bars correspond to the standard deviations of the two values. Results from isolated pairs with multiple contacts are shown in red. If the detailed model is a good description of the coupled cell pair, the data points should fall on the diagonal.*

of functional synapses in such randomly growing pairs. In the rather sparse networks used for the present experiments, however, we can very roughly estimate the number of physical contacts between the neurites of the two cells in question. These numbers typically also are on the order of ten or below (see for example figs. 1.1 and 7.15), so the values of $\widetilde{G}_{syn}$ found in such pairs are consistent with the assumption that pairs of *Lymnaea* neurons – like *Helisoma* neurons [35] – probably form an electrical synapse at every point of contact. Lacking more conclusive evidence, this remains speculation, but the finding that pairs with multiple contacts have significantly stronger synaptic connections than pairs with a single contact suggests that **the strength of synaptic coupling between neurons in designed networks could be controlled in the future by pre-determining the number of contacts** between the neurons via guided outgrowth.

Compared to the input conductances of randomly growing cells, the synaptic conductances of pairs with multiple contacts are only by about a factor of three smaller. In randomly growing networks, the ratio κ (introduced on page 72) between the average synaptic conductance and the average cell conductance is therefore approximately $\kappa \approx 1/3$, compared to $\kappa \approx 1/10$ for designed networks with guided outgrowth and single-point synapses (see section 7.1). As discussed in section 6.5, the value of κ describes how well the result obtained for $\widetilde{G}_{syn}$ from current step experiments on a neuron pair reflects the actual synaptic conductance between the two cells: The smaller κ is, the better $\widetilde{G}_{syn}$ approximates the real value, while large values of κ imply that current pathways through adjacent cells can significantly increase the value of $\widetilde{G}_{syn}$. Therefore, the synapse conductance between pairs of neurons in designed networks can reliably be estimated with current step experiments as in section 7.1 in spite of the surrounding cells. The error in the synaptic conductance estimate can be larger for cell pairs in random networks, especially if the two cells in question are in touch with large numbers of other cells. But **for the sparse networks used here, $\widetilde{G}_{syn}$ is a good approximation of the actual conductance** in spite of $\kappa \approx 1/3$ – this is supported by the finding that the values obtained for embedded pairs do not significantly differ from those for isolated pairs (see fig. 7.18).

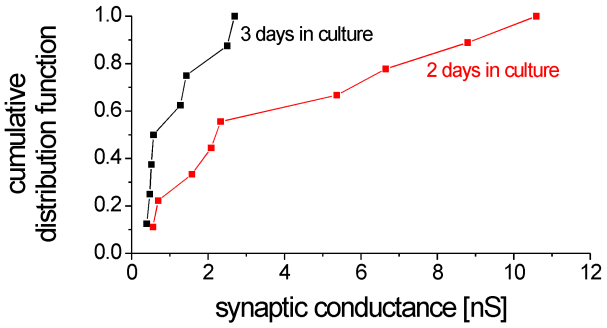

Figure 7.19: ***The conductance of multi-point synapses decreases with time in culture.*** *This graph shows the distribution functions for the conductances of multi-point synapses after two (red) and three (black) days in cell culture. Surprisingly, the synaptic conductance decreases.*

As for the single-point synapses, we compute the **coupling coefficient** for each pair and direction of signal transfer for comparison with values from the literature. The k_{12} and k_{21} are included in the left part of fig. 7.13 (solid symbols): Typical coupling coefficients for pairs with multiple contact points were between 0.2 and 0.5, with extreme values of 0.04 and 0.77. These numbers are in the same range as

- the coupling coefficients between cultured neurons from the marine mollusk *Aplysia*, where 90% of the measured coefficients are between 0.05 and 0.50 and extreme values are 0.02 and 0.80 [5].
- the coupling coefficients between cultured neurons from the snail *Helisoma*, which are 0.42±0.10 [36].
- the values found for a pair of identified neurons from *Lymnaea* in cell culture, namely 0.26±0.04 [61]. Note that these cells were not pedal A-cluster neurons.
- the *in vivo* coupling coefficients in *Lymnaea* of 0.05-0.3 between identified pairs of neurons in the parietal ganglia [62] and of 0.68 between a pair of giant neurons [1].

Compared to the coupling coefficients from pairs with a single point of contact (open symbols in the same figure), those between pairs with multiple contacts are by about a factor of four larger.

The same data are plotted against $\widetilde{G}_{syn}$ in the right part of the figure (solid symbols); as for the single-point synapses, the coupling coefficients are only weakly correlated to $\widetilde{G}_{syn}$ because they also depend on the postsynaptic cell conductance $\widetilde{G}_B$, which can vary a lot between different cells (see (66)). To illustrate how the coupling coefficient would depend on $\widetilde{G}_{syn}$ if $\widetilde{G}_B$ was less variable, the red curve in the figure shows the k_{AB} corresponding to $\widetilde{G}_B = 5$nS and different $\widetilde{G}_{syn}$. This curve was obtained by fitting (66) to the solid data points with $\widetilde{G}_B$ as fit variable; and the result of 5nS for the average postsynaptic conductance, not surprisingly, is consistent with the conductances of randomly growing neurons shown in fig. 7.12. According to (66), the coupling coefficient approaches a value of one as the synaptic conductance increases. As the red curve shows, however, the typical conductances of the neurons used here imply that the synapse conductances would have to be several tens of nS to achieve a coupling coefficient close to one.

Synapse conductances decrease with time in culture

An interesting observation related to the synaptic conductance is illustrated by fig. 7.19, where the

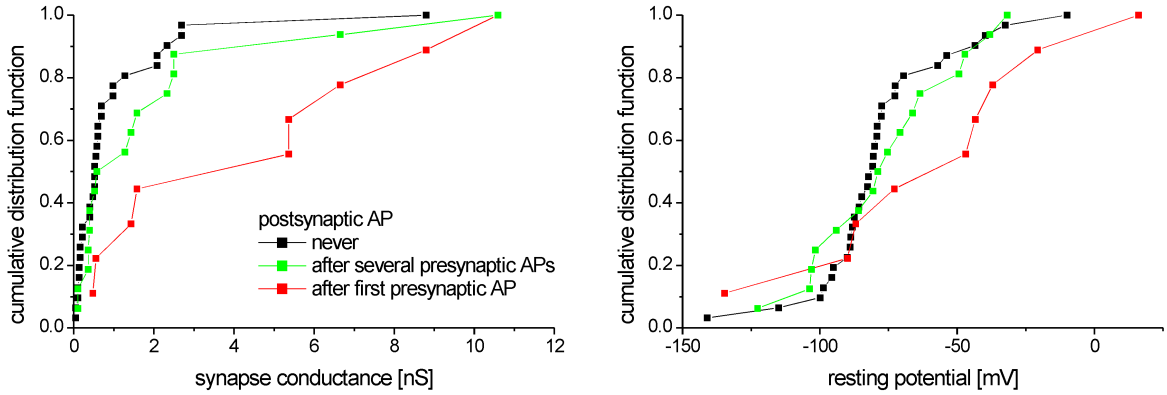

Figure 7.20: ***The efficiency of action potential transmission depends on synaptic conductance and postsynaptic resting potential.*** *For this figure, the neurons from all pairs (with single-point and multi-point synapses) were divided into three groups: Those that never fired action potentials when they were postsynaptic (black), those in which temporal summation of several presynaptic spikes could trigger a postsynaptic action potential (green) and those in which a single presynaptic spike was sufficient to ellicit a postsynaptic action potential (red). (**Left**) Synapse conductance distributions for the three groups. (**Right**) Resting potential distributions for the three groups. The legend applies to both plots. Transmission of action potentials is most efficient for high synapse conductances and if the postsynaptic neuron is close to threshold.*

conductance distribution functions of multi-point synapses measured after two days in culture and after three days in culture are plotted separately. *Lymnaea* neurons are usually still growing after two days in conventional cell culture, so the number of physical contacts between the neurites of two cells in such a culture is likely to increase between the second and third day. In contrast, the figure demonstrates that the overall coupling strength actually *decreases* during this time, indicating that **either previously established synapses are lost again, or that the conductance of existing synapses is decreasing, or both**.

For the design of neural networks, this result implies that the **synaptic strengths established in the network can not be assumed to be constant on the timescale of days**, which may complicate studies of signal processing in such networks. On the other hand, the way synaptic strengths change with time is in itself interesting, and **designed networks with single-point synapses provide an ideal system for studying such processes** and their dependence on, for example, cell type, culture conditions or network activity.

7.3 Postsynaptic action potentials

As illustrated by figs. 7.5 and 7.15, in some of the neuron pairs (with multi-point synapses as well as single-point synapses) the current transferred through the electrical synapse upon depolarization of the presynaptic neuron can be sufficient to elicit a postsynaptic action potential. To understand the **requirements for such postsynaptic action potentials**, the altogether 56 neurons from the 28 pairs studied in sections 7.1 and 7.2 were divided into **three groups**, namely

- those that never fired action potentials when they were postsynaptic
- those in which a train of several spikes in the other neuron could bring the membrane potential above threshold through temporal summation (as, for example, in fig. 7.4)
- and those in which an action potential could be triggered by a single spike in the partner

neuron.

The left part of fig. 7.20 shows the synapse conductance distributions for these three categories of cells. The result is not surprising: Most of the cells that never fired postsynaptic action potentials (black curve) were only weakly coupled to their partner cell in the pair, with typical synapse conductances below 1nS. Triggering a postsynaptic action potential via temporal summation (green curve) required slightly larger synapse conductances, with most values between 0.5nS and 2.5nS. And cells for which a single presynaptic action potential was sufficient to induce a postsynaptic spike (red curve) were strongly coupled to the presynaptic neuron, with typical synapse conductances between 1nS and 10nS. The three distributions, however, show extensive overlap, which indicates that the **synaptic conductance is not the only parameter that determines the efficiency of action potential transfer within a neuron pair**.

A likely candidate for an additional parameter that could play a role in the triggering of postsynaptic action potentials by presynaptic spikes is the **resting potential of the postsynaptic neuron**: A cell whose potential is already close to the firing threshold should require less synaptic current to make it fire an action potential than a cell with a very low resting potential. This is confirmed by the right graph in fig. 7.20, where the resting potential distributions for the same three cell categories are displayed. As expected, neurons that can not be brought above threshold by presynaptic spike trains (black curve) tend to have lower resting potentials than those that fire after several presynaptic action potentials (green curve) or even a single presynaptic action potential (red curve).

Implications for designed networks from *Lymnaea* neurons

What do these results mean for neural network design? In designed neural networks, **neither extremely weak nor very strong coupling of the cells is desirable**: If all the cells that have electrical synapses with a given neuron are coupled so weakly that they can not even trigger an action potential in the neuron if they all fire simultaneously, this neuron can not contribute much to the signal processing in the network because it is silent. If, on the other hand, a pair of cells in the net is so strongly coupled that a spike in one of the cells always elicits an action potential in the other cell, they effectively behave like a single neuron and can not perform different signal processing tasks. At least in networks that encode information in spike patterns, it is therefore desirable to have **synapse strengths that ensure that the dynamic range of all neurons is efficiently used**.

As shown in fig. 7.12, single-point synapses have conductances below 1nS, and it is therefore not surprising that 77% of the cells in pairs with single-point synapses fall into the black category in fig. 7.20 and that the rest belongs to the green category. Cells in geometrically simple designed networks will be connected via such single-point synapses – this implies that in designed networks from *Lymnaea* neurons, a single spike in just one neighboring neuron will never be sufficient to trigger an action potential in a cell, and that temporal summation of the inputs from just one neighbor will usually not be sufficient, either. However, cells in such networks will normally be connected to more than one other cell, and if just a few of those other cells fire at about the same time, their combined synaptic currents can depolarize the postsynaptic neuron above threshold. This is because the synapse conductances for the green group in the left part of fig. 7.20 – in which *temporal* summation can lead to a spike – are only by about a factor of two larger than for the black group, indicating that the *spatially* summed synaptic current from just a few firing

neighbors may also be in the right range to trigger a spike.

In summary, the **electrical single-point synapses established by *Lymnaea* neurons in designed networks have about the right conductances to enable efficient signal processing in such networks**: They are strong enough such that approximately coincident spikes in just a few presynaptic cells can bring a postsynaptic neuron above threshold, and they are not conductive enough to couple two cells so strongly that they behave like a single cell.

8
Summary

Small neural networks are difficult to study because in nervous tissue the neurons are not well accessible and can have very entangled neurites and unknown connectivity. Neural network design tries to overcome this by assembling small neural networks of simple geometry and controlled connectivity from cells with well-known electrical properties in the cell culture dish.

With neurons from the pedal ganglia of the pond snail *Lymnaea stagnalis*, the present work makes several steps toward such defined *in vitro* networks:

Through photolithographic patterning of a layer of proteins secreted by snail brains, lanes of growth-promoting factors separated by areas of inactivated protein were created. *Lymnaea* neurons, when individually isolated from the ganglion and placed on such patterns, grew neurites that followed the lanes of intact substrate – with this method, the geometry of neuritic trees in cultured neural networks can be controlled.

By guiding neurites on such patterned substrates, functioning electrical synapses localized to a single point of contact were induced: Synapses could be established between growth cones and cell bodies, between growth cones and neuritic cables, and when two growth cones met. This allows a wide variety of different network geometries.

The neurons and guided neuritic cables that are the building blocks of designed networks were characterized by recording neuritic voltage transients with the aid of voltage-sensitive dyes and by fitting these imaging data to theoretical cable models. The imaging data were crucial for determining the electrical parameters, because electrophysiological recordings at the soma alone do not provide sufficient information.

From the same imaging data, maps of signal propagation in the guided neurites were constructed – both the electrical parameters and the propagation maps show that the neurons are electrotonically very compact.

Using the electrical parameters of the neuritic cables, the conductances of the *in vitro* synapses were determined by probing electrically coupled neuron pairs with current steps and by analyzing their voltage response with theoretical models. Synapses restricted to a single point of contact were found to be weaker than multi-contact synapses. Their conductance is, however, in the right range to enable efficient signal processing in small designed networks of *Lymnaea* neurons.

With a method for guiding neural outgrowth and inducing synapses and with the electrical properties of neurons and synapses known, the present work sets the stage for systematic studies of small neural networks in the future.

9
Appendices

A. Cell culture recipes

Antibacterial solution

For the decontamination of the snail's body surface and the anesthesia of deshelled snails, a solution containing

normal saline	75%
Listerine	25%

was used [62]. Normal saline is antibiotic saline (see below) without the gentamycin and Listerine is a commercially available antibacterial mouthwash whose anesthetic effect on snails is presumably due to its menthol content [39].

Antibiotic saline

Snail dissections and brain rinsing were done in antibiotic saline, a solution containing

NaCl	51.3mM
KCl	1.7mM
$CaCl_2$	4.1mM
$MgCl_2$	1.5mM
HEPES buffer	5.0mM
gentamycin	150μg/ml

at pH 7.9 [76]. All chemicals were obtained from Sigma.

Defined medium

The cell culture medium necessary for the survival (but not sufficient for neurite extension) of *Lymnaea* neurons is called 'defined medium' and contains

NaCl	40.0mM
KCl	1.7mM
$CaCl_2$	4.1mM
$MgCl_2$	1.5mM
gentamycin	20μg/ml

and all the other ingredients of serum-free Leibovitz L-15 medium [22] at half of the standard concentration [76]. This medium, with all ingredients except gentamycin and glutamine, was obtained from PAN Systems, Aidenbach; gentamycin and glutamine (both from Sigma) were added before use. The pH of defined medium is 7.9.

High osmolarity medium

Cell isolation was done in a high osmolarity medium to make the neurons less susceptible to mechanical membrane damage during aspiration into the micropipette. This medium is defined

medium with an additional 30mM of glucose (Sigma) [76].

Enzyme cocktail

To digest the extracellular matrix between the neurons prior to cell isolation, the ganglia were treated with an enzyme cocktail consisting of

collagenase/dispase (Boehringer Mannheim)	1.33mg/ml
trypsin (T-4665, Sigma)	0.67mg/ml

in defined medium (see above) [76]. While the collagenase acts solely on collagen, the dispase and the trypsin are unspecific proteases – this is why after the enzyme treatment the ganglia were washed several times and treated with trypsin inhibitor to minimize damage to membrane proteins.

Trypsin inhibitor

The enzymatic activity of trypsin was inhibited after enzyme treatment with a solution containing soybean trypsin inhibitor (T-9003, Sigma) at a concentration of 0.67mg/ml in defined medium (see above) [76].

Micropipettes

For aspiration and positioning of the neurons, micropipettes manufactured from glass capillaries (No. 564, Assistent) were used. After pulling the capillary tubes to the desired inner diameter of about 100μm at the tip and fire-polishing (both done with a DMZ Universal Puller, Zeitz, Augsburg), the pipettes were sterilized and coated with a silicon solution (Sigmacote, Sigma) to minimize cell losses due to a sticky glass surface. Mounted on a flexible tube whose other end was connected to a mouth-piece, the pipettes were then used to aspirate cells.

Glass coverslip cleaning

Round cover glasses (⌀ 30mm, thickness 1, Assistent) for cell culture chambers were cleaned by the following procedure (modified from [28]):

- sonication at 80°C in a solution of 5% Ultrax 102 S (KLN, Heppenheim) in ultra-pure water for 60min
- 5-6 rinses with ultra-pure water
- sonication at 80°C in a solution of 5% Tickopur RP100 (Bandelin, Berlin) in ultra-pure water for 60min
- 5-6 rinses with ultra-pure water
- sonication for 60min at 80°C in ultra-pure water, changing the water every 15min
- air drying under sterile conditions

Ultra-pure water was derived from a Milli-Q water system (Millipore).

Polylysine coating

For polylysine coating, clean coverslips (see above) were attached to round silicone chambers (flexiPERM, special order from In Vitro Systems & Services, Osterode) to complete the culture dishes. These were incubated over night with a solution of 1mg/ml poly-L-lysine (Sigma) in 0.15 Tris buffer (Sigma), pH 8.4. After incubation, the dishes were washed twice with ultra-pure water (Millipore), rinsed for 20min with antibiotic saline (see above), washed two more times

with water and immediately filled with defined medium (see above) [95].

B. Staining with voltage-sensitive dyes

Dye solution

To solubilize the amphiphilic voltage-sensitive dye BNBIQ, a solution containing

cholic acid (sodium salt, Sigma)	15mM
BNBIQ	4.3mM

in defined medium (see above) was prepared [65]. Above the critical concentration of 8.4mM, cholic acid forms micelles that provide a suitable solvent for the amphiphilic dye molecules. The mixture was exposed to ultrasonic waves for several hours and subsequently centrifuged for 10min to remove undissolved dye from the solution. The supernatant was then used to stain neurons as described below.

Staining procedure

Staining of neurons with BNBIQ was done as follows:

- The culture medium was removed from the chamber containing the cells.
- 10μl of the dye solution (see above) were diluted 50-fold with defined medium and immediately added to the chamber. The dilution causes the cholic acid micelles to fall apart and frees the dye molecules that then relocate to the cell membrane or any other hydrophilic-hydrophobic interface in the dish.
- The cells were incubated in this diluted solution for 10min.
- The solution was removed from the chamber and the chamber was washed with defined medium.

These steps were repeated up to ten times, and the entire staining procedure was performed in red light to avoid any phototoxic effects of the dye on the cells prior to the measurements. Whenever the culture dish was emptied during the staining procedure, about 1mm of fluid (corresponding to 300μl) was left in the chamber to avoid damage to the cells due to strong currents, and all pipetting was done slowly.

The repeated adding of diluted dye solution and rinsing with medium allowed the accumulation of dye in the membrane without accumulating potentially damaging amounts of cholic acid in the culture chamber.

C. Analytical solutions of the cable equation

Steady state

As we need steady state solutions of the cable equation

- for neurites with sealed end boundary condition (section 4.1) and

- for neurites terminating with an electrical synapse (section 6.3),

we first find the steady state solutions for a general boundary condition and introduce the sealed end boundary condition at the end of this steady state section.

The steady state distribution of the electrotonic potential V^e in a neuron with J neurites of lengths l_j (with j running from 1 to J) is the solution of the steady state cable equation

$$\frac{\partial^2 V^e}{\partial X_j^2} = V^e \tag{115}$$

that is obtained by setting $\partial V^e/\partial T = 0$ in the time-dependent cable equation (7).

Solutions of this equation in neurite j are of the form

$$V^e(X_j) = A_j \cosh(L_j - X_j) + B_j \sinh(L_j - X_j) \tag{116}$$

where $L_j = l_j/\lambda_j$ is the electrotonic length of neurite j and A_j and B_j are two arbitrary constants [72].

At the tip of the neurite, the general boundary condition requires that

$$I_j(L_j) = -\frac{1}{\lambda_j R_j}\left(\frac{\partial V^e}{\partial X_j}\right)_{X_j = L_j} = \frac{B_j}{\lambda_j R_j} \qquad \text{or} \qquad B_j = \lambda_j R_j I_j(L_j) \tag{117}$$

where $I_j(L_j)$ is the axial current at the tip and (12) was used. This reduces the particular solution to

$$V^e(X_j) = A_j \cosh(L_j - X_j) + \lambda_j R_j I_j(L_j) \sinh(L_j - X_j)$$

The arbitrary constant A_j can be expressed in terms of the steady state electrotonic potential at the soma, V_s^e, via

$$V_s^e = V^e(X_j = 0) = A_j \cosh L_j + \lambda_j R_j I_j(L_j) \sinh L_j \tag{118}$$

$$\text{or} \qquad A_j = \frac{V_s^e}{\cosh L_j} - \lambda_j R_j I_j(L_j) \tanh L_j \tag{119}$$

which results in the final form of the steady state solution:

$$V^e(X_j) = \left[\frac{V_s^e}{\cosh L_j} - \lambda_j R_j I_j(L_j) \tanh L_j\right] \cosh(L_j - X_j) + \lambda_j R_j I_j(L_j) \sinh(L_j - X_j) \tag{120}$$

With (12), the axial current flowing along the neurite at location X_j then is

$$I_j(X_j) = \left[\frac{V_s^e}{\lambda_j R_j \cosh L_j} - I_j(L_j) \tanh L_j\right] \sinh(L_j - X_j) + I_j(L_j) \cosh(L_j - X_j) \tag{121}$$

For section 6.3, we need an expression for the amount I_j^m of current leaving the neurite through its membrane. Because of charge conservation, I_j^m is equal to the difference between the axial current entering the neurite at $X_j = 0$ and the axial current leaving it at $X_j = L_j$, so with (121) we find

$$I_j^m = I_j(X_j = 0) - I_j(L_j) \tag{122}$$

$$= V_s^e \frac{\tanh L_j}{\lambda_j R_j} + I_j(L_j) \frac{1 - \cosh L_j}{\cosh L_j} \tag{123}$$

So far, all results were derived without specifying the boundary condition at the tip of the neurite. Now, we consider the special case of a sealed end at which no axial current can leave the neurite, so $I_j(L_j) = 0$. In this case, the steady state voltage distribution (120) reduces to

$$V^e(X_j) = \frac{V_s^e}{\cosh L_j} \cosh(L_j - X_j) \tag{124}$$

and the axial current (121) simply is

$$I_j(X_j) = \frac{V_s^e}{\lambda_j R_j \cosh L_j} \sinh(L_j - X_j) \tag{125}$$

In particular, the axial current entering such a sealed end neurite at $X_j = 0$ is

$$I_j(X_j = 0) = V_s^e \frac{\tanh L_j}{\lambda_j R_j} = G_j V_s^e \tag{126}$$

which defines the input resistance $G_j = \tanh L_j/(\lambda_j R_j)$ of a sealed end neurite of normalized length L_j.

In the rest of this appendix, all solutions are derived for sealed end neurites only:

Current response for a voltage step at the soma

By separation of variables it can be shown that a particular solution of the time-dependent cable equation (7) for neurite j is

$$V^e(X_j, T) = \left[D_j \sin\left(\zeta_j X_j\right) + F_j \cos\left(\zeta_j X_j\right)\right] e^{-\left(1+\zeta_j^2\right)T} \tag{127}$$

where ζ_j is the separation constant and D_j and F_j are arbitrary constants [14]. For a somatic voltage step at time 0, $V^e(X_j = 0, T)$ has to be constant for $T > 0$. Therefore, $F_j = 0$, which reduces the particular solution to

$$V^e(X_j, T) = D_j \sin\left(\zeta_j X_j\right) e^{-\left(1+\zeta_j^2\right)T} \tag{128}$$

The sealed end boundary condition requires that the spatial derivative of the particular solution must vanish at $X_j = L_j$ (the tip of the neurite), which implies that

$$\zeta_j \cos\left(\zeta_j X_j\right) = 0 \tag{129}$$

and results in a set of constants $\zeta_{j,n}$ for neurite j with

$$\zeta_{j,n} = \frac{(2n-1)\pi}{2L_j} \qquad \text{for } n \geqslant 1 \tag{130}$$

The additional solution for $\zeta_j = 0$ is trivial because it belongs to $V^e(X_j, T) \equiv 0$. The general solution of the cable equation for a somatic voltage step from $V_{s,0}^e$ to $V_{s,\infty}^e$ at time 0 then is

$$V^e(X_j, T) = V_{s,\infty}^e \frac{\cosh(L_j - X_j)}{\cosh L_j} + \sum_{n=1}^{\infty} D_{j,n} \sin\left(\zeta_{j,n} X_j\right) e^{-\left(1+\zeta_{j,n}^2\right)T} \tag{131}$$

where the steady state voltage distribution from (124) was used.

At time zero, the potential distribution $V^e(X_j, T = 0)$ is equal to the steady state distribution prior to the voltage step, so

$$\sum_{n=1}^{\infty} D_{j,n} \sin\left(\zeta_{j,n} X_j\right) = (V_{s,0}^e - V_{s,\infty}^e) \frac{\cosh(L_j - X_j)}{\cosh L_j} \tag{132}$$

The coefficients $D_{j,n}$ in this Fourier series are

$$D_{j,n} = \frac{2}{L_j} (V_{s,0}^e - V_{s,\infty}^e) \frac{\zeta_{j,n}}{\zeta_{j,n}^2 + 1} \tag{133}$$

and the potential distribution in neurite j for a voltage step at the soma therefore is

$$V^e(X_j, T) = V_{s,\infty}^e \frac{\cosh(L_j - X_j)}{\cosh L_j} + \frac{2}{L_j} (V_{s,0}^e - V_{s,\infty}^e) \sum_{n=1}^{\infty} \frac{\zeta_{j,n}}{\zeta_{j,n}^2 + 1} \sin\left(\zeta_{j,n} X_j\right) e^{-\left(1+\zeta_{j,n}^2\right)T} \tag{134}$$

The current that has to be injected into the cell body to maintain the voltage clamp is the sum of the currents flowing across the somatic conductance and the currents flowing into the neurites; with (12), this is

$$I_{inj}(T) = G_s V^e_{s,\infty} + \sum_{j=1}^{J} I_j(X_j = 0) \tag{135}$$

$$= GV^e_{s,\infty} + (V^e_{s,\infty} - V^e_{s,0}) \sum_{j=1}^{J} \frac{2}{L_j \lambda_j R_j} \sum_{n=1}^{\infty} \frac{\zeta_{j,n}}{\zeta^2_{j,n} + 1} e^{-\left(1+\zeta^2_{j,n}\right)T} \tag{136}$$

where

$$G = G_s + \sum_{j=1}^{J} G_j \tag{137}$$

is the input conductance of the entire neuron.

Voltage response for a current step at the soma

We derive an expression for the voltage response to a somatic current step at time zero. For this derivation, it is convenient to start with a particular solution to the cable equation of the form

$$V^e(X_j, T) = \left[H_j \sin(\eta_j(L_j - X_j)) + K_j \cos(\eta_j(L_j - X_j))\right] e^{-\left(1+\eta^2_j\right)T} \tag{138}$$

where η_j, H_j and K_j are arbitrary constants. The sealed end boundary condition requires that

$$\left(\frac{\partial V^e(X_j, T)}{\partial X_j}\right)_{X_j = L_j} = 0 \qquad \text{and hence} \qquad H_j = 0 \tag{139}$$

The general solution for neurite j and a current step injected at the soma then is

$$V^e(X_j, T) = V^e_{s,\infty} \frac{\cosh(L_j - X_j)}{\cosh L_j} + \sum_{n=1}^{\infty} K_{j,n} \cos(\eta_{j,n}(L_j - X_j)) e^{-\left(1+\eta^2_{j,n}\right)T} \tag{140}$$

where $V^e_{s,\infty}$ is the steady state potential at the cell body that is reached long after the onset of the current step and where we again made use of the steady state potential distribution from (124). For a voltage distribution that is continuous at the soma, the voltages $V^e(X_j = 0, T)$ at the somatic ends of all neurites have to be equal at all times. This is the case if

$$\eta_{j_1,n} = \eta_{j_2,n} =: \eta_n \qquad \text{and} \qquad K_{j_1,n} \cos(\eta_n L_{j_1}) = K_{j_2,n} \cos(\eta_n L_{j_2}) \tag{141}$$

for all n and all combinations j_1 and $j_2 \in \{1...J\}$.

The constant injection current I_{inj} after the onset of the current step has to be equal to the sum of the currents flowing across the soma membrane and into the neurites for $T > 0$, so

$$I_{inj} = G_s \left[V^e(X_1 = 0, T) + \frac{\tau_s}{\tau} \left(\frac{\partial V^e(X_1, T)}{\partial T}\right)_{X_1 = 0}\right] + \sum_{j=1}^{J} I_j(X_j = 0, T) \tag{142}$$

where $\tau_s = c_s/g_s$ is the time constant of the somatic membrane. With (12) and (140), the right side of this equation can be expressed as the sum of a time-independent and a time-dependent term. The time-independent term is

$$V^e_{s,\infty} \left(G_s + \sum_{j=1}^{J} G_j\right) \tag{143}$$

which is exactly the clamp current corresponding to the steady state potential $V^e_{s,\infty}$ (compare to (126)). As I_{inj} is constant for $T > 0$, the time-dependent term has to vanish. This results in the transcendental equation

$$G_s \left[1 - \frac{\tau_s}{\tau}\left(1+\eta_n^2\right)\right] = \eta_n \sum_{j=1}^{J} \frac{\tan\left(\eta_n L_j\right)}{\lambda_j R_j} \tag{144}$$

that defines the coefficients η_n and therefore the time constants of the different exponentially decaying contributions to the voltage distributions $V^e(X_j, T)$ in the neurites.

At time zero, the voltage distribution $V^e(X_j, T=0)$ has to be equal to the steady state distribution prior to the current step, so

$$\sum_{n=1}^{\infty} K_{j,n} \cos(\eta_{j,n}(L_j - X_j)) = \left(V^e_{s,0} - V^e_{s,\infty}\right) \frac{\cosh(L_j - X_j)}{\cosh L_j} \tag{145}$$

where $V^e_{s,0}$ is the steady state potential at the cell body before the current step. The coefficients $K_{j,n}$ with respect to the non-orthogonal functions $\cos(\eta_{j,n}(L_j - X_j))$ in this generalized Fourier series can not be calculated with Churchill's modified orthogonality relation, because they arise from a set of boundary conditions of the wrong form [8]. Without a straightforward way to compute the $K_{j,n}$ analytically, the spatio-temporal voltage distribution $V^e(X_j, T)$ can thus only be obtained by numerically solving the cable equation under the given boundary conditions (139) and (142).

Voltage response to a brief current pulse at the soma

After a short current *pulse* of duration t^{pulse} that terminates at time zero (instead of a current *step)*, the voltage decay in neurite j is of the form

$$V^e(X_j, T) = V^e_{s,0} \frac{\cosh(L_j - X_j)}{\cosh L_j} + \sum_{n=1}^{\infty} M_{j,n} \cos(\eta_{j,n}(L_j - X_j)) e^{-\left(1+\eta^2_{j,n}\right)T} \tag{146}$$

for the same reasons that led to (140); only $V^e_{s,\infty}$ in the steady state part is replaced by $V^e_{s,0}$ (the voltage at the soma prior to the current step) because the voltage distribution very long after the termination of the current pulse will again reach the steady state from before the onset of current injection. The requirement of a continuous voltage distribution at the cell body again implies that

$$\eta_{j_1,n} = \eta_{j_2,n} =: \eta_n \qquad \text{and} \qquad M_{j_1,n} \cos(\eta_n L_{j_1}) = M_{j_2,n} \cos(\eta_n L_{j_2}) \tag{147}$$

for all n and all combinations j_1 and $j_2 \in \{1...J\}$ in complete analogy to (141); and the η_n can again be shown to be solutions of the transcendental equation (144), so the time constants of the exponential contributions for the voltage decay after a brief current pulse are the same as those for the voltage change following a current step. The coefficients $M_{j,n}$ are related to the coefficients $K_{j,n}$ for a current step via

$$M_{j,n} = K_{j,n}(1 - e^{-T^{pulse}(1+\eta_n^2)}) \tag{148}$$

where $T^{pulse} = t^{pulse}/\tau$ is the normalized pulse duration [14].

Special case of current clamp with only one neurite

In the case of $J = 1$, the index j can be dropped in all equations from above. Specifically, the two boundary conditions (139) and (142) in this case are

$$\left(\frac{\partial V^e(X,T)}{\partial X}\right)_{X=L} = 0 \tag{149}$$

and (with the use of (12))

$$I_{inj} = G_s \left[V^e(X=0,T) + \frac{\tau_s}{\tau}\left(\frac{\partial V^e(X,T)}{\partial T}\right)_{X=0}\right] - \frac{1}{\lambda R}\left(\frac{\partial V^e(X,T)}{\partial X}\right)_{X=0} \tag{150}$$

and (145) (the generalized Fourier series related to these boundary conditions) reduces to

$$\sum_{n=1}^{\infty} K_n \cos(\eta_n(L-X)) = \left(V^e_{s,0} - V^e_{s,\infty}\right) \frac{\cosh(L-X)}{\cosh L} \tag{151}$$

In contrast to the general case of arbitrarily many neurites, the form of the boundary value problem in this special case now allows the calculation of the coefficients K_n according to Churchill's modified orthogonality relation [8]. The result is

$$K_n = \left(V^e_{s,0} - V^e_{s,\infty}\right) \frac{2\eta_n \left(\tanh L + \lambda R G_s\right)}{(1+\eta_n^2)L + (1-\eta_n^2)\sin(\eta_n L) + 2\eta_n \lambda R G_s \cos(\eta_n L)} \tag{152}$$

With (148), this means that – in the case of just one neurite – we have complete analytical expressions for the voltage responses to a current step as well as to a brief current pulse.

D. Numerical solutions of the cable equation

To numerically solve the cable equation for a model neuron consisting of two unbranched neurites attached to a soma, each neurite j was divided into K_j compartments of length $\Delta x_j \approx 10\mu$m, the soma was treated as a single compartment and the compartments in neurite j were numbered starting at the soma and ending at the distal tip of the neurite.

Before the simulation, the potential distribution in the neuron was initialized by setting the membrane potential equal to the resting potential E for all compartments:

$$V_s(t=0) = E$$

where V_s is the somatic membrane potential and

$$V_{j,k}(t=0) = E \qquad \forall k \in \{1...K_j\} \text{ and } \forall j \in \{1,2\}$$

where $V_{j,k}$ is the membrane potential for compartment k of neurite j.

Starting from this initial state, the new potential distribution after each simulation time step Δt = 1μs was computed as follows:

- at the soma:

$$V_s(t+\Delta t) = V_s(t) + \left(\frac{V_{1,1}(t) - V_s(t)}{R_1 \Delta x_1} + \frac{V_{2,1}(t) - V_s(t)}{R_2 \Delta x_2} - G_s V_s(t) + I_{inj}(t)\right) \frac{\Delta t}{C_s} \tag{153}$$

- for the first compartment of neurite j:

$$V_{j,1}(t+\Delta t) = V_{j,1}(t) + \left(\frac{V_s(t) - 2V_{j,1}(t) + V_{j,2}(t)}{R_j \Delta x_j} - G_j \Delta x_j V_{j,1}(t)\right) \frac{\Delta t}{C_j \Delta x_j} \tag{154}$$

- for all compartments of neurite j with $k \in \{2...K_j - 1\}$:

$$V_{j,k}(t+\Delta t) = V_{j,k}(t) + \left(\frac{V_{j,k-1}(t) - 2V_{j,k}(t) + V_{j,k+1}(t)}{R_j \Delta x_j} - G_j \Delta x_j V_{j,k}(t)\right) \frac{\Delta t}{C_j \Delta x_j} \tag{155}$$

- and for the last compartment of neurite j:

$$V_{j,K_j}(t+\Delta t) = V_{j,K_j}(t) + \left(\frac{V_{j,K_j-1}(t) - V_{j,K_j}(t)}{R_j \Delta x_j} - G_j \Delta x_j V_{j,K_j}(t)\right) \frac{\Delta t}{C_j \Delta x_j} \tag{156}$$

where $I_{inj}(t)$ is the current injected into the soma at time t and G_s, C_s, G_j, C_j and R_j are defined by (3), (4) and (5). The above expressions were obtained by applying Euler's method to the cable

equation (6) or – for the somatic compartment – to the cable equation with an additional term for the injection current [69].

For the comparison with the experimental transient shapes $S_n^{fluo}(t)$ in section 5.2, the theoretical transients for the neuritic compartments had to be normalized; this was done via

$$S_{j,k}^{theo}(t) = \frac{V_{j,k}(t)}{|\min\left[V_{j,k}(t)\right]|} \tag{157}$$

for all j and k (compare to (2)).

The spatial resolution of the simulation was Δx = 10μm, while the spatial resolution of the imaging data varied between 3.9μm and 5.3μm (see footnote on page 19). This means that, for a given experimental transient $S_n^{fluo}(t)$, there is usually no theoretical transient $S_{j,k}^{theo}(t)$ available that was computed for the exact same location on the neurite. To overcome this, the theoretical transient expected at the site on the neurite 'seen' by a given diode was linearly interpolated between the two theoretical transients of the compartments closest to this site in the model neuron; the resulting interpolated transient for diode n is called $S_n^{theo}(t)$.

As a measure for the difference between the simulated and the experimental transients, the quantity

$$\frac{\chi^2}{D} = \frac{1}{D}\sum_n \int \left(\frac{S_n^{fluo}(t) - S_n^{theo}(t)}{\sigma_n}\right)^2 dt \tag{158}$$

was computed. Here, D is the number of data points contained in the spatio-temporal target data set and σ_n is the standard deviation of $S_n^{fluo}(t)$ as obtained from the diode's baseline signal prior to the onset of the injection current. The n-sum includes all the diodes in the target data set and the integral runs over the entire target data time window. With this definition, χ^2 is the same as the 'chi-square'-quantity usually used for least square fitting [69].

E. Hodgkin-Huxley rates

The voltage variable V_{HH} that Hodgkin and Huxley used in their original work [42] denotes the displacement of the membrane potential from its resting value, with negative values for depolarization. In terms of the variables used here, this means that $V_{HH} = -V^e = E - V$. This relation was used to translate the original expressions for the voltage dependence of the activation and deactivation rate constants, resulting in the expressions in the following table. There, all rate constants are given in units of 1/ms and V and E are in mV.

particle i	activation α_i	deactivation β_i
n	$0.01\dfrac{E-V+10}{e^{\frac{E-V+10}{10}}-1}$	$0.125e^{\frac{E-V}{80}}$
m	$0.1\dfrac{E-V+25}{e^{\frac{E-V+25}{10}}-1}$	$4e^{\frac{E-V}{18}}$
h	$0.07e^{\frac{E-V}{20}}$	$\dfrac{1}{e^{\frac{E-V+30}{10}}+1}$

F. Transient solutions of the simple synapse model

We derive solutions $V_{As}(t)$ and $V_{Bs}(t)$ of the coupled differential equations (55) and (56) in response to a step in the presynaptic injection current from $I_{inj,0} = 0$ to $I_{inj,\infty}$ at time $t = 0$. Because the two equations are inhomogeneous, we first find solutions of the corresponding homogeneous system, which is

$$\frac{dV_{As}}{dt} = -\frac{\widetilde{G}_A + \widetilde{G}_{syn}}{\widetilde{C}_A} V_{As} + \frac{\widetilde{G}_{syn}}{\widetilde{C}_A} V_{Bs} \tag{159}$$

$$\frac{dV_{Bs}}{dt} = \frac{\widetilde{G}_{syn}}{\widetilde{C}_B} V_{As} - \frac{\widetilde{G}_B + \widetilde{G}_{syn}}{\widetilde{C}_B} V_{Bs} \tag{160}$$

The system's characteristic polynomial has the two solutions

$$-\nu_{+/-} = -\frac{1}{\tau_{+/-}} \tag{161}$$

$$= -\frac{1}{2}\left[\frac{\widetilde{G}_A+\widetilde{G}_{syn}}{\widetilde{C}_A} + \frac{\widetilde{G}_B+\widetilde{G}_{syn}}{\widetilde{C}_B} \pm \sqrt{\left(\frac{\widetilde{G}_A+\widetilde{G}_{syn}}{\widetilde{C}_A} - \frac{\widetilde{G}_B+\widetilde{G}_{syn}}{\widetilde{C}_B}\right)^2 + 4\frac{\widetilde{G}_{syn}}{\widetilde{C}_A}\frac{\widetilde{G}_{syn}}{\widetilde{C}_B}}\right] \tag{162}$$

which are negative, inverse time constants. Therefore, the homogeneous system has two solutions of the form

$$\begin{aligned} V_{As-} &= A_- e^{-t/\tau_-} \\ V_{Bs-} &= B_- e^{-t/\tau_-} \end{aligned} \quad \text{and} \quad \begin{aligned} V_{As+} &= A_2 e^{-t/\tau_+} \\ V_{Bs+} &= B_2 e^{-t/\tau_+} \end{aligned} \tag{163}$$

The homogeneous differential equations relate B_1 and B_2 to A_1 and A_2 and reduce the two solutions to

$$\begin{aligned} V_{As-} &= A_- e^{-t/\tau_-} \\ V_{Bs-} &= \frac{\widetilde{G}_A+\widetilde{G}_{syn}-\widetilde{C}_A\nu_-}{\widetilde{G}_{syn}} A_- e^{-t/\tau_-} \end{aligned} \quad \text{and} \quad \begin{aligned} V_{As+} &= A_+ e^{-t/\tau_+} \\ V_{Bs+} &= \frac{\widetilde{G}_A+\widetilde{G}_{syn}-\widetilde{C}_A\nu_+}{\widetilde{G}_{syn}} A_+ e^{-t/\tau_+} \end{aligned} \tag{164}$$

To solve the inhomogeneous system with the variation of constants method, we set

$$V_{As} = V_{As-} + V_{As+} \quad \text{and} \quad V_{Bs} = V_{Bs-} + V_{Bs+} \tag{165}$$

in (55) and (56). This leads to

$$A_- = \frac{-\frac{\widetilde{G}_A+\widetilde{G}_{syn}-\widetilde{C}_A\nu_+}{\widetilde{C}_A}\frac{I_{inj}+\widetilde{G}_A\widetilde{E}_A}{\widetilde{C}_A} + \frac{\widetilde{G}_{syn}}{\widetilde{C}_A}\frac{\widetilde{G}_B\widetilde{E}_B}{\widetilde{C}_B}}{\nu_-\left(\nu_+ - \nu_-\right)} e^{t/\tau_-} + D_- \tag{166}$$

$$A_+ = \frac{-\frac{\widetilde{G}_A+\widetilde{G}_{syn}-\widetilde{C}_A\nu_-}{\widetilde{C}_A}\frac{I_{inj}+\widetilde{G}_A\widetilde{E}_A}{\widetilde{C}_A} + \frac{\widetilde{G}_{syn}}{\widetilde{C}_A}\frac{\widetilde{G}_B\widetilde{E}_B}{\widetilde{C}_B}}{\nu_+\left(\nu_- - \nu_+\right)} e^{t/\tau_+} + D_+ \tag{167}$$

with the integration constants D_- and D_+. With this, the solution of the inhomogeneous system looks like

$$V_{As} = \frac{\widetilde{G}_{syn}\widetilde{G}_B\widetilde{E}_B + \left(\widetilde{G}_B + \widetilde{G}_{syn}\right)\left(I_{inj} + \widetilde{G}_A\widetilde{E}_A\right)}{\left(\widetilde{G}_A + \widetilde{G}_{syn}\right)\left(\widetilde{G}_B + \widetilde{G}_{syn}\right) - \widetilde{G}_{syn}^2} + D_- e^{-t/\tau_-} + D_+ e^{-t/\tau_+} \tag{168}$$

$$V_{Bs} = \frac{\left(\widetilde{G}_A+\widetilde{G}_{syn}\right)\widetilde{G}_B\widetilde{E}_B+\widetilde{G}_{syn}\left(I_{inj}+\widetilde{G}_A\widetilde{E}_A\right)}{\left(\widetilde{G}_A+\widetilde{G}_{syn}\right)\left(\widetilde{G}_B+\widetilde{G}_{syn}\right)-\widetilde{G}_{syn}^2} + \frac{\widetilde{G}_A+\widetilde{G}_{syn}-\widetilde{C}_A\nu_-}{\widetilde{G}_{syn}}D_-e^{-t/\tau_-}+\frac{\widetilde{G}_A+\widetilde{G}_{syn}-\widetilde{C}_A\nu_+}{\widetilde{G}_{syn}}D_+e^{-t/\tau_+} \tag{169}$$

For $t=\infty$, we expect that $V_{As}(t=\infty)=V_{As,\infty}$ and $V_{Bs}(t=\infty)=V_{Bs,\infty}$. This requires that

$$V_{As,\infty} = \frac{\widetilde{G}_{syn}\widetilde{G}_B\widetilde{E}_B+\left(\widetilde{G}_B+\widetilde{G}_{syn}\right)\left(I_{inj}+\widetilde{G}_A\widetilde{E}_A\right)}{\left(\widetilde{G}_A+\widetilde{G}_{syn}\right)\left(\widetilde{G}_B+\widetilde{G}_{syn}\right)-\widetilde{G}_{syn}^2} \tag{170}$$

$$V_{Bs,\infty} = \frac{\left(\widetilde{G}_A+\widetilde{G}_{syn}\right)\widetilde{G}_B\widetilde{E}_B+\widetilde{G}_{syn}\left(I_{inj}+\widetilde{G}_A\widetilde{E}_A\right)}{\left(\widetilde{G}_A+\widetilde{G}_{syn}\right)\left(\widetilde{G}_B+\widetilde{G}_{syn}\right)-\widetilde{G}_{syn}^2} \tag{171}$$

With the aid of (63) and (65) one can show that both these relations hold true, proving that the above solutions are consistent with the steady state expressions from section 6.2.

For $t=0$, it is required that

$$V_{As}(t=0)=V_{As,\infty}+D_-+D_+=V_{As,0} \tag{172}$$

$$V_{Bs}(t=0)=V_{Bs,\infty}+\frac{\widetilde{G}_A+\widetilde{G}_{syn}-\widetilde{C}_A\nu_-}{\widetilde{G}_{syn}}D_-+\frac{\widetilde{G}_A+\widetilde{G}_{syn}-\widetilde{C}_A\nu_+}{\widetilde{G}_{syn}}D_+=V_{Bs,0} \tag{173}$$

This defines D_- and D_+; they turn out to be

$$D_- = -\frac{\frac{\widetilde{G}_A+\widetilde{G}_{syn}-\widetilde{C}_A\nu_+}{\widetilde{C}_A}\Delta V_{As}-\frac{\widetilde{G}_{syn}}{\widetilde{C}_A}\Delta V_{Bs}}{\nu_--\nu_+} \tag{174}$$

$$D_+ = \frac{\frac{\widetilde{G}_A+\widetilde{G}_{syn}-\widetilde{C}_A\nu_-}{\widetilde{C}_A}\Delta V_{As}-\frac{\widetilde{G}_{syn}}{\widetilde{C}_A}\Delta V_{Bs}}{\nu_--\nu_+} \tag{175}$$

where $\Delta V_{As}=V_{As,\infty}-V_{As,0}$ and $\Delta V_{Bs}=V_{Bs,\infty}-V_{Bs,0}$.

With this, the solution of the inhomogeneous system finally is

$$V_{As} = V_{As,\infty}-\left(\frac{\widetilde{G}_A+\widetilde{G}_{syn}-\widetilde{C}_A\nu_+}{\widetilde{C}_A\left(\nu_--\nu_+\right)}\Delta V_{As}-\frac{\widetilde{G}_{syn}}{\widetilde{C}_A\left(\nu_--\nu_+\right)}\Delta V_{Bs}\right)e^{-t/\tau_-} + \left(\frac{\widetilde{G}_A+\widetilde{G}_{syn}-\widetilde{C}_A\nu_-}{\widetilde{C}_A\left(\nu_--\nu_+\right)}\Delta V_{As}-\frac{\widetilde{G}_{syn}}{\widetilde{C}_A\left(\nu_--\nu_+\right)}\Delta V_{Bs}\right)e^{-t/\tau_+} \tag{176}$$

$$V_{Bs} = V_{Bs,\infty}+\left(\frac{\widetilde{G}_{syn}}{\widetilde{C}_B\left(\nu_--\nu_+\right)}\Delta V_{As}+\frac{\widetilde{G}_A+\widetilde{G}_{syn}-\widetilde{C}_A\nu_-}{\widetilde{C}_A\left(\nu_--\nu_+\right)}\Delta V_{Bs}\right)e^{-t/\tau_-} - \left(\frac{\widetilde{G}_{syn}}{\widetilde{C}_B\left(\nu_--\nu_+\right)}\Delta V_{As}+\frac{\widetilde{G}_A+\widetilde{G}_{syn}-\widetilde{C}_A\nu_+}{\widetilde{C}_A\left(\nu_--\nu_+\right)}\Delta V_{Bs}\right)e^{-t/\tau_+} \tag{177}$$

G. Tables of results from synapse experiments

For completeness, the following table lists the values and standard deviations obtained for the cell

conductances $\widetilde{\mathbf{G}}$, the cell capacitances $\widetilde{\mathbf{C}}$ and the synaptic conductances $\widetilde{\mathbf{G}}_{syn}$ from experiments on eleven neuron pairs with one-point synapses. For each parameter and pair, two values are given: The value at the top was obtained when cell 1 was presynaptic, the value at the bottom when cell 2 was presynaptic.

pair	$\widetilde{\mathbf{G}}_1$ [nS]	$\widetilde{\mathbf{C}}_1$ [pF]	$\widetilde{\mathbf{G}}_2$ [nS]	$\widetilde{\mathbf{C}}_2$ [pF]	$\widetilde{\mathbf{G}}_{syn}$ [nS]
i	2.33/0.55	133/86	4.33/3.47	527/305	0.060/0.011
	0.99/0.36	153/96	1.41/0.11	171/4	0.029/0.012
ii	2.76/0.30	222/0	7.20/1.73	280/76	0.135/0.024
	2.97/0.77	343/153	2.75/0.30	234/11	0.061/0.009
iii	2.59/0.25	166/1	9.56/1.52	751/682	0.099/0.011
	2.77/0.23	394/112	9.94/0.72	332/72	0.105/0.011
iv	1.66/0.25	154/23	7.28/6.94	2070/3378	0.136/0.124
	1.79/0.06	291/109	3.92/0.58	451/30	0.134/0.012
v	2.51/1.03	86/5	6.56/2.24	492/210	0.194/0.019
	2.81/1.16	690/113	3.40/1.06	165/6	0.129/0.041
vi	3.32/0.29	131/28	1.60/0.71	321/51	0.099/0.020
	11.37/6.25	839/875	2.20/0.17	316/13	0.329/0.142
vii	1.30/0.09	174/4	4.59/1.57	621/318	0.403/0.109
	1.69/0.69	325/104	2.81/0.36	328/54	0.324/0.095
viii	1.55/0.17	228/7	3.14/0.60	621/318	0.416/0.062
	1.57/0.36	379/74	2.99/0.37	163/6	0.387/0.074
ix	2.06/0.14	159/42	1.25/0.37	243/59	0.448/0.090
	2.67/0.25	358/35	1.60/0.17	141/5	0.594/0.047
x	4.55/0.88	448/31	4.91/1.33	478/199	0.612/0.143
	4.95/1.63	936/825	4.03/0.81	428/64	0.579/0.149
xi	5.30/1.32	315/13	2.43/1.26	310/108	0.839/0.271
	8.48/2.08	752/182	2.95/0.75	145/10	1.121/0.288

The second table lists the corresponding results for cell pairs with multiple contact points. The three isolated cell pairs are marked with asterisks; the rest of the pairs was embedded in networks of other neurons.

pair	$\widetilde{\mathbf{G}}_1$ [nS]	$\widetilde{\mathbf{C}}_1$ [pF]	$\widetilde{\mathbf{G}}_2$ [nS]	$\widetilde{\mathbf{C}}_2$ [pF]	$\widetilde{\mathbf{G}}_{syn}$ [nS]
i	3.52/0.38	651/21	0.28/0.14	65/26	0.109/0.057
	0.56/0.31	344/44	2.41/0.06	1075/11	0.679/0.190
ii	2.39/0.30	230/7	7.77/2.40	701/375	0.678/0.180
	0.84/0.32	268/79	4.37/0.60	508/78	0.273/0.067
iii*	6.62/0.01	1067/32	6.44/1.44	1853/109	0.564/0.101
	10.01/3.00	1823/485	4.00/0.51	755/59	0.468/0.085
iv	2.27/0.14	239/28	4.35/0.73	623/117	0.472/0.063
	2.52/0.35	440/151	5.55/0.23	590/10	0.643/0.129
v	2.85/0.16	356/5	2.22/0.04	388/47	0.602/0.016
	2.38/0.32	564/48	2.12/0.37	307/16	0.544/0.089
vi	4.86/0.01	295/4	14.81/1.53	1171/156	1.115/0.126
	1.86/0.49	173/20	8.58/0.39	485/36	0.272/0.087
vii*	4.54/0.38	325/8	2.16/0.46	298/16	1.196/0.197
	5.37/0.20	461/44	2.31/0.45	191/6	1.355/0.124

pair	$\widetilde{\mathbf{G}}_1$ [nS]	$\widetilde{\mathbf{C}}_1$ [pF]	$\widetilde{\mathbf{G}}_2$ [nS]	$\widetilde{\mathbf{C}}_2$ [pF]	$\widetilde{\mathbf{G}}_{syn}$ [nS]
viii	3.80/0.53 4.34/0.66	308/18 874/152	6.25/1.49 6.07/0.84	1063/190 560/31	1.366/0.356 1.498/0.206
ix	7.67/0.51 7.62/0.74	1019/39 2276/230	2.57/0.14 2.51/0.07	769/42 402/25	1.589/0.157 1.562/0.148
x	2.62/0.28 3.93/0.81	259/259 364/51	5.86/1.17 8.97/1.96	565/115 273/118	2.231/0.679 1.932/0.245
xi	6.85/0.93 6.58/0.62	285/10 453/44	5.13/0.34 5.39/0.56	728/68 477/33	2.184/0.219 2.472/0.324
xii	5.50/0.46 8.26/1.20	552/7 1059/42	3.54/0.52 4.63/0.64	927/20 706/60	1.911/0.169 3.091/0.542
xiii	13.17/0.61 26.56/5.21	473/36 1812/971	2.37/0.54 2.41/0.10	271/22 322/19	2.173/0.176 3.215/0.371
xiv	4.15/1.16 5.09/1.81	690/111 881/69	4.16/2.54 2.98/1.38	228/188 294/50	5.025/0.843 5.702/1.161
xv	3.64/0.76 3.61/0.67	350/27 688/203	8.59/0.73 8.22/0.53	1089/159 538/201	6.748/0.284 6.547/0.242
xvi*	4.19/0.72 3.85/0.27	522/71 656/111	6.04/1.54 4.24/0.48	811/176 718/6	10.422/2.958 7.166/0.363
xvii	17.41/7.39 16.47/3.20	772/126 723/197	3.12/0.73 2.88/0.78	146/49 188/14	10.439/1.180 10.737/1.687

Bibliography

[1] P.R. Benjamin and J.B. Pilkington, *The electrotonic location of low-resistance intercellular junctions between a pair of giant neurones in the snail Lymnaea*, J. Physiol. **370** (1986), 111–126.

[2] M.V.L. Bennett, *Physiology of electrotonic junctions*, Ann. New York Acad. Sci. **137** (1966), 509–539.

[3] M.V.L. Bennett, L.C. Barrio, T.A. Bargiello, D.C. Spray, E. Hertzberg, and J.C. Saez, *Gap junctions: New tools, new answers, new questions*, Neuron **6** (1991), 305–320.

[4] M.V.L. Bennett and D.C. Spray, *Gap junctions*, Cold Spring Harbor Laboratory, 1985.

[5] R. Bodmer, D. Dagan, and I.B. Levitan, *Chemical and electrotonic connections between Aplysia neurons in primary culture*, J. Neurosci. **4** (1984), no. 1, 228–233.

[6] P.R. Brink, K. Cronin, and S.V. Ramanan, *Gap junctions in excitable cells*, J. Bioenerg. Biomembr. **28** (1996), no. 4, 351–358.

[7] A.G.M. Bulloch and N.I. Syed, *Reconstruction of neuronal networks in culture*, TINS **15** (1992), no. 11, 422–427.

[8] R.V. Churchill, *Expansions in series of non-orthogonal functions*, Bulletin Amer. Math. Soc. **48** (1942), 143–149.

[9] P. Clark, S. Britland, and P. Connolly, *Growth cone guidance and neuron morphology on micropatterned laminin surfaces*, J. Cell Sci. **105** (1993), 203–212.

[10] K.S. Cole and A.L. Hodgkin, *Membrane and protoplasm resistance in the squid giant axon*, J. Gen. Physiol. **22** (1939), 671–687.

[11] J.M. Corey, B.C. Wheeler, and G.J. Brewer, *Compliance of hippocampal neurons to patterned substrate networks*, J. Neurosci. Res. **30** (1991), 300–307.

[12] A. Curtis, C. Wilkinson, and L. Breckenridge, *Living nerve nets*, In: Enabling Technologies for Cultured Neural Networks (D.A. Stenger and T.M. McKenna, eds.), Academic Press, 1994, pp. 99–120.

[13] J. DeFelipe and E.G. Jones, *Cajal on the cerebral cortex - An annotated translation of the complete writings*, Oxford University Press, 1988.

[14] D. Durand, *The somatic shunt cable model for neurons*, Biophys. J. **46** (1984), 645–653.

[15] D. Durand, P.L. Carlen, N. Gurevich, A. Ho, and H. Kunov, *Measurement of the passive electrotonic parameters of granule cells in the rat hippocampus*

using HRP staining and short current pulses., J. Neurophysiol. **50** (1983), 1080–1096.

[16] H. Ephardt and P. Fromherz, *Fluorescence of amphiphilic hemicyanine dyes without free double bonds*, J. Phys. Chem. **97** (1993), 4540–4547.

[17] R. Fechter and G. Falkner, *Weichtiere - Europäische Meeres- und Binnenmollusken*, Mosaik Verlag, 1990.

[18] Z.-P. Feng, J. Klumperman, K. Lukowiak, and N.I. Syed, *In vitro synaptogenesis between the somata of identified Lymnaea neurons requires protein synthesis but not extrinsic growth factors or substrate adhesion molecules*, J. Neurosci. **17** (1997), no. 20, 7839–7849.

[19] M.E. Finbow, *Vertebrate and invertebrate gap junctions: A common molecular basis?*, Cell Biol. Int. **21** (1997), no. 6, 329–331.

[20] M.E. Finbow, M. Harrison, and P. Jones, *Ductin - a proton pump component, a gap junction channel and a neurotransmitter release channel*, BioEssays **17** (1995), no. 3, 247–255.

[21] A.S. Finkel and S.J. Redman, *Optimal voltage clamping with single microelectrode*, In: Voltage and Patch Clamping with Microelectrodes (T.G. Smith, H. Lecar, S.J. Redman, and P.W. Gage, eds.), American Physiological Society, 1985, pp. 95–120.

[22] R.I. Freshley, *Culture of animal cells - A manual of basic technique*, 3rd ed., Wiley, 1994.

[23] P. Fromherz, K.H. Dambacher, H. Ephardt, A. Lambacher, C.O. Müller, R. Neigl, H. Schaden, O. Schenk, and T. Vetter, *Fluorescent dyes as probes of voltage transients in neuron membranes*, Ber. Bunsenges. Phys. Chem. **95** (1991), 1333–1345.

[24] P. Fromherz and A. Lambacher, *Spectra of voltage-sensitive fluorescence of styryl-dye in neuron membrane*, Biochim. Biophys. Acta **1068** (1991), 149–156.

[25] P. Fromherz and C.O. Müller, *Voltage-sensitive fluorescence of amphiphilic hemicyanine dyes in neuron membrane*, Biochim. Biophys. Acta **1150** (1993), 111–122.

[26] P. Fromherz and C.O. Müller, *Cable properties of a straight neurite of a leech neuron probed by a voltage-sensitive dye*, Proc. Natl. Acad. Sci. USA **91** (1994), 4604–4608.

[27] P. Fromherz, C.O. Müller, and R. Weis, *Neuron transistor: Electrical transfer function measured by the patch-clamp technique*, Phys. Rev. Lett. **71** (1993), no. 24, 4079–4082.

[28] P. Fromherz and G. Reinbold, *Energy transfer between fluorescent dyes spaced by multilayers of cadmium salts of fatty acids*, Thin Solid Films **160** (1988), 347–353.

[29] P. Fromherz and H. Schaden, *Defined neuronal arborizations by guided outgrowth of leech neurons in culture*, Eur. J. Neurosci. **6** (1994), 1500–1504.

[30] P. Fromherz, H. Schaden, and T. Vetter, *Guided outgrowth of leech neurons in culture*, Neurosci. Lett. **129** (1991), 77–80.

[31] P. Fromherz and T. Vetter, *Propagation of voltage transients in arborized neurites of Retzius cells of the leech in culture*, Z. Naturforsch. **46c** (1991), 687–696.

[32] P. Fromherz and T. Vetter, *Cable properties of arborized Retzius cells of the leech in culture as probed by a voltage-sensitive dye*, Proc. Natl. Acad. Sci. USA **89** (1992), 2041–2045.

[33] M.D. Ganfornina, D. Sanchez, M. Herrera, and M.J. Bastiani, *Developmental expression and molecular characterization of two gap junction channel proteins expressed during embryogenesis in the grasshopper Schistocerca americana*, Dev. Genet. **24** (1999), 137–150.

[34] R.W. Gundersen, *Sensory neurite growth cone guidance by substrate adsorbed nerve growth factor*, J. Neurosci. Res. **13** (1985), 199–212.

[35] P.B. Guthrie, R.E. Lee, V. Rehder, M.F. Schmidt, and S.B. Kater, *Self-recognition: A constraint on the formation of electrical coupling in neurons*, J. Neurosci. **14** (1994), no. 3, 1477–1485.

[36] R.D. Hadley, D.A. Bodnar, and S.B. Kater, *Formation of electrical synapses between isolated, cultured Helisoma neurons requires mutual neurite elongation*, J. Neurosci. **5** (1985), no. 12, 3145–3153.

[37] R.D. Hadley, S.B. Kater, and C.S. Cohan, *Electrical synapse formation depends on interaction of mutually growing neurites*, Science **221** (1983), 466–468.

[38] J.A. Hammarback, S.L. Palm, L.T. Furcht, and P.C. Letourneau, *Guidance of neurite outgrowth by pathways of substratum-adsorbed laminin*, J. Neurosci. Res. **13** (1985), 213–220.

[39] P.G. Haydon, W. Winlow, and A.V. Holden, *The effects of menthol on central neurons of the pond-snail, Lymnaea stagnalis (L.)*, Comp. Biochem. Physiol. **73C** (1982), 95–100.

[40] D. Higgins and G. Banker, *Primary dissociated cell cultures*, In: Culturing Nerve Cells, 2nd ed. (G. Banker and K. Goslin, eds.), MIT Press, 1998, pp. 37–78.

[41] B. Hille, *Ionic channels of excitable membranes*, 2nd ed., Sinauer, 1992.

[42] A.L. Hodgkin and A.F. Huxley, *A quantitative description of membrane current and its application to conduction and excitation in nerve*, J. Physiol. **117** (1952), 500–544.

[43] A.L. Hodgkin and W.A.H. Rushton, *The electrical constants of a crustacean nerve fiber*, Proc. R. Soc. Lond. B **133** (1946), 444–479.

[44] P. Horowitz and W. Hill, *The art of electronics*, 2nd ed., Cambridge University Press, 1989.

[45] R. Iansek and S.J. Redman, *An analysis of the cable properties of spinal motoneurons using a brief intracellular current pulse*, J. Physiol. (Lond.) **234** (1973), 613–636.

[46] S.A. John, D. Saner, J.D. Pitts, A. Holzenburg, M.E. Finbow, and R. Lal, *Atomic force microscopy of arthropod gap junctions*, J. Struct. Biol. **21** (1997), no. 6, 329–331.

[47] E.R. Kandel, J.H. Schwartz, and T.M. Jessell (eds.), *Essentials of neural science and behaviour*, Appleton and Lange, 1995.

[48] H. Kawaguchi and K. Fukunishi, *Dendrite classification in rat hippocampal neurons according to signal propagation properties*, Exp. Brain Res. **122** (1998), 378–392.

[49] M. Kawato, *Cable properties of a neuron model with non-uniform membrane resistivity*, J. theor. Biol. **111** (1984), 149–169.

[50] I. Kiss, *Electronic transmission between giant neurones indentified in the CNS of Lymnaea stagnalis*, Acta Biol. Acad. Sci. Hung. **30** (1979), no. 1-2, 103–119.

[51] D. Kleinfeld, K.H. Kahler, and P.E. Hockberger, *Controlled outgrowth of dissociated neurons on patterned substrates*, J. Neurosci. **8** (1988), no. 11, 4098–4120.

[52] D. Kleinfeld, T.D. Parsons, F. Raccuia-Behling, B.M. Salzberg, and A.L. Obaid, *Foreign connections are formed in vitro by Aplysia californica interneurone L10 and its in vivo followers and non-followers*, J. exp. Biol. **154** (1990), 237–255.

[53] C. Koch, *Biophysics of computation - information processing in single neurons*, Oxford University Press, 1999.

[54] M. Koval, S.T. Geist, E.M. Westphale, A.E. Kemendy, R. Civitelli, E.C. Beyer, and T.H. Steinberg, *Transfected connexin45 alters gap junction permeability in cells expressing endogenous connexin43*, J. Cell Biol. **130** (1995), no. 4, 987–995.

[55] B. Kuhn, *Modulation zweidimensionaler Fluoreszenzspektren durch das elektrische Feld in einer Nervenmembran*, Diploma thesis, Universität Ulm, Germany, 1996.

[56] M. Kyriakides, C.R. McCrohan, C.T. Slade, N.I. Syed, and W. Winlow, *The morphology and electrophysiology of the neurones of the paired pedal ganglia of Lymnaea stagnalis*, Comp. Biochem. Physiol. **93A** (1989), no. 4, 861–876.

[57] D.W. Laird, *The life cycle of a connexin: Gap junction formation, removal, and degradation*, J. Bioenerg. Biomembr. **28** (1996), no. 4, 311–318.

[58] A.F. Lau, W.E. Kurata, M.Y. Kanemitsu, L.W.M. Loo, B.J. Warn-Cramer, W. Eckhardt, and P.D. Lampe, *Regulation of connexin43 function by activated tyrosine protein kinases*, J. Bioenerg. Biomembr. **28** (1996), no. 4, 359–368.

[59] S.S. Lin and I.B. Levitan, *Concavalin A alters synaptic specificity between cultured Aplysia neurons*, Science **237** (1987), 648–650.

[60] C.W. Lo, *The role of gap junction membrane channels in development*, J. Bioenerg. Biomembr. **28** (1996), no. 4, 379–385.

[61] N.S. Magoski and A.G.M. Bulloch, *Trophic and contact conditions modulate synapse formation between identified neurons*, J. Neurophysiol. **79** (1998), 3279–3283.

[62] N.S. Magoski, N.I. Syed, and A.G.M. Bulloch, *A neuronal network from the mollusc Lymnaea stagnalis*, Brain Res. **645** (1994), 201–214.

[63] G. Major, A.U. Larkmann, P. Jonas, B. Sakmann, and J.J.B. Jack, *Detailed passive cable models of whole-cell recorded CA3 pyramidal neurons in rat hippocampal slices*, J. Neurosci. **14** (1994), no. 8, 4613–4638.

[64] P. Meda, *The role of gap junction membrane channels in secretion and hormonal action*, J. Bioenerg. Biomembr. **28** (1996), no. 4, 369–377.

[65] E. Meyer, C.O. Müller, and P. Fromherz, *Cable properties of dendrites in hippocampal neurons of the rat mapped by a voltage-sensitive dye*, Eur. J. Neurosci. **9** (1997), 778–785.

[66] C.O. Müller, *Spannungsprofile linearer Neurite: Messungen mit Fluoreszenzfarbstoffen an Neuronen von Hirudo medicinalis*, Ph.D. thesis, Universität Ulm, Germany, 1994.

[67] npi advanced electronic systems, Tamm, Germany, *SEC 05L/H single electrode system - Operating instructions and system description*, 1996.

[68] A. Peinado, R. Yuste, and L.C. Katz, *Extensive dye coupling between rat neocortical neurons during the period of circuit formation*, Neuron **10** (1993), 103–114.

[69] W.H. Press, S.A. Teukolsky, W.T. Vetterling, and B.P. Flannery, *Numerical recipes in C - The art of scientific computing*, 2nd ed., Cambridge University Press, 1997.

[70] A.A. Prinz, *Optische Detektion der elektrischen Signalausbreitung in Neuronen*, Diploma thesis, Universität Ulm, Germany, 1996.

[71] A.A. Prinz and P. Fromherz, *Electrical synapses by guided growth of cultured neurons from the snail Lymnaea stagnalis*, Biol. Cybern. **82** (2000), L1–L5.

[72] W. Rall, *Branching dendritic trees and motoneuron membrane resistivity*, Exp. Neurol. **1** (1959), 491–527.

[73] W. Rall, *Membrane potential transients and membrane time constant of motoneurons*, Exp. Neurol. **2** (1960), 503–532.

[74] W. Rall, *Electrophysiology of a dendritic neuron model*, Biophys. J. **2** (1962), 145–167.

[75] W. Rall, *Time constants and electrotonic length of membrane cylinders and neurons*, Biophys. J. **9** (1969), 1483–1508.

[76] R.L. Ridgway, N.I. Syed, K. Lukowiak, and A.G.M. Bulloch, *Nerve growth factor (NGF) induces sprouting of specific neurons of the snail, Lymnaea stagnalis*, J. Neurobiol. **22** (1991), no. 4, 377–390.

[77] D.M. Rup, R.D. Veenstra, H.-Z. Wang, P.R. Brink, and E.C. Beyer, *Chick connexin-56, a novel lens gap junction protein*, J. Biol. Chem. **268** (1993), no. 1, 706–712.

[78] I. Segev, M. Rapp, Y. Manor, and Y. Yarom, *Analog and digital processing in single nerve cells*, In: Single Neuron Computation (T. McKenna, J. Davis, and S. Zornetzer, eds.), Academic Press, 1992, pp. 173–198.

[79] C.T. Slade, J. Mills, and W. Winlow, *The neuronal organisation of the paired pedal ganglia of Lymnaea stagnalis (L.)*, Comp. Biochem. Physiol. **69A** (1981), 789–803.

[80] G.E. Sosinsky, *Molecular organization of gap junction membrane channels*, J. Bioenerg. Biomembr. **28** (1996), no. 4, 297–309.

[81] G.E. Spencer, N.I. Syed, K. Lukowiak, and W. Winlow, *Halothane affects both inhibitory and excitatory synaptic transmission at a single identified molluscan synapse, in vivo and in vitro*, Brain Res. **714** (1996), 38–48.

[82] W.W. Stewart, *Functional connections between cells as revealed by dye-couplin with a highly fluorescent naphthalimide tracer*, Cell **14** (1978), 741–759.

[83] N. Syed, P. Richardson, and A. Bulloch, *Ciliary neurotrophic factor, unlike nerve growth factor, supports neurite outgrowth but not synapse formation by adult Lymnaea neurons*, J. Neurobiol. **29** (1995), no. 3, 293–303.

[84] N.I. Syed, A.G.M. Bulloch, and K. Lukowiak, *In vitro reconstruction of the respiratory central pattern generator of the mollusk Lymnaea*, Science **250** (1990), 282–285.

[85] N.I. Syed, K. Lukowiak, and A.G.M. Bulloch, *Specific in vitro synaptogenesis between identified Lymnaea and Helisoma neurons*, NeuroReport **3** (1992), 793–796.

[86] N.I. Syed and W. Winlow, *Morphology and electrophysiology of neurons innervating the ciliated locomotor epithelium in Lymnaea stagnalis (L.)*, Comp. Biochem. Physiol. **93A** (1989), no. 3, 633–644.

[87] R.D. Veenstra, *Size and selectivity of gap junction channels formed from different connexins*, J. Bioenerg. Biomembr. **28** (1996), no. 4, 327–337.

[88] R.D. Veenstra, H.-Z. Wang, E.C. Beyer, S.V. Ramanan, and P.R. Brink, *Connexin37 forms high conductance gap junction channels with subconductance state activity and selective dye and ionic permeabilities*, Biophs. J. **66** (1994), 1915–1928.

[89] T.F. Weiss, *Cellular biophysics, vol. 2 - Electrical properties*, MIT Press, 1996.

[90] J.A. White, P.B. Manis, and E.D. Young, *The parameter identification problem for the somatic shunt model*, Biol. Cybern. **66** (1992), 307–318.

[91] T.W. White and R. Bruzzone, *Multiple connexin proteins in single intercellular channels: Connexin compatibility and functional consequences*, J. Bioenerg. Biomembr. **28** (1996), no. 4, 393–350.

[92] K. Willecke and S Haubrich, *Connexin expression systems: To what extent do they reflect the situation in the animal?*, J. Bioenerg. Biomembr. **28** (1996), no. 4, 319–326.

[93] W. Winlow, A.V. Holden, and P.G. Haydon, *Characterization of lymnaea neurones by determination of action potential trajectories*, J. Exp. Biol. **99** (1982), 207–221.

[94] R.G. Wong, D.L. Barker, S.B. Kater, and D.A. Bodnar, *Nerve growth-promoting factor produced in culture media conditioned by specific CNS tissues of the snail Helisoma*, Brain Res. **292** (1984), 81–91.

[95] R.G. Wong, R.D. Hadley, S.B. Kater, and G.C. Hauser, *Neurite outgrowth in molluscan organ and cell cultures: The role of condtioning factor(s)*, J. Neurosci. **1** (1981), no. 9, 1008–1021.

[96] R.G. Wong, E.C. Martel, and S.B. Kater, *Conditioning factor(s) produced by several molluscan species promote neurite outgrowth in cell culture*, J. exp. Biol. **105** (1983), 389–393.

[97] M.J. Zigmond, F.E. Bloom, S.C. Landis, J.L. Roberts, and L.R. Squire (eds.), *Fundamental neuroscience*, Academic Press, 1999.